TECHNISCHE UNIVERSITÄT WIEN
Vienna | Austria

Investigation of relaxation behaviour of individual collagen fibrils through AFM nanoindentation

DIPLOMA THESIS

submitted in partial fulfillment of the requirements for the degree of

Master of Science

in

Biomedical Engineering

by

Christian Ehrenberger, B.Sc.
Registration Number 1327085

to the Faculty for Mechanical and Industrial Engineering

at the TU Wien

Advisor: Univ.Prof. Dipl.-Ing. Dr.sc.nat. Philipp Thurner
Assistance: Univ.Ass. Dipl.-Ing. Mathis Nalbach
Univ.Prof. Dipl.-Ing. Dr.sc.nat. Philipp Thurner

Die approbierte gedruckte Originalversion dieser Diplomarbeit ist an der TU Wien Bibliothek verfügbar.
The approved original version of this thesis is available in print at TU Wien Bibliothek.
TU Bibliothek Your knowledge hub

Die approbierte gedruckte Originalversion dieser Diplomarbeit ist an der TU Wien Bibliothek verfügbar.
The approved original version of this thesis is available in print at TU Wien Bibliothek.

TECHNISCHE UNIVERSITÄT WIEN
Vienna | Austria

Untersuchung des Relaxationsverhaltens einzelner Kollagenfibrillen durch AFM-Nanoindentation

DIPLOMARBEIT

zur Erlangung des akademischen Grades

Diplom-Ingenieur

im Rahmen des Studiums

Biomaterials and Biomechanics

eingereicht von

Christian Ehrenberger, B.Sc.
Matrikelnummer 1327085

an der Fakultät für Maschinenwesen und Betriebswissenschaften

der Technischen Universität Wien

Betreuung: Univ.Prof. Dipl.-Ing. Dr.sc.nat. Philipp Thurner
Mitwirkung: Univ.Ass. Dipl.-Ing. Mathis Nalbach
Univ.Prof. Dipl.-Ing. Dr.sc.nat. Philipp Thurner

Die approbierte gedruckte Originalversion dieser Diplomarbeit ist an der TU Wien Bibliothek verfügbar.
The approved original version of this thesis is available in print at TU Wien Bibliothek.
TU WIEN Bibliothek Your knowledge hub

Die approbierte gedruckte Originalversion dieser Diplomarbeit ist an der TU Wien Bibliothek verfügbar.
The approved original version of this thesis is available in print at TU Wien Bibliothek.

Erklärung zur Verfassung der Arbeit

Christian Ehrenberger, B.Sc.

Hiermit erkläre ich, dass ich diese Arbeit selbständig verfasst habe, dass ich die verwendeten Quellen und Hilfsmittel vollständig angegeben habe und dass ich die Stellen der Arbeit – einschließlich Tabellen, Karten und Abbildungen –, die anderen Werken oder dem Internet im Wortlaut oder dem Sinn nach entnommen sind, auf jeden Fall unter Angabe der Quelle als Entlehnung kenntlich gemacht habe.

Wien, 12. Oktober 2020

Christian Ehrenberger

Die approbierte gedruckte Originalversion dieser Diplomarbeit ist an der TU Wien Bibliothek verfügbar.
The approved original version of this thesis is available in print at TU Wien Bibliothek.
TU WIEN Bibliothek Your knowledge hub

Die approbierte gedruckte Originalversion dieser Diplomarbeit ist an der TU Wien Bibliothek verfügbar.
The approved original version of this thesis is available in print at TU Wien Bibliothek.

Acknowledgements

My first acknowledgment goes to my parents, who already in younger years encouraged and inspired me to focus, even on bumpy roads, on my education. They, unselfishly, helped and supported me over many years, which allowed me to finish on this level. Especially I would like to thank my girlfriend Iris, who helped me at every phase of my academic education with her love and knowledge. Also I would like to express my deepest gratitude to Mathis Nalbach M.Sc., who gave me the chance to work on this project. He has helped me from the beginning of AFM measurements till the finish of my thesis. Also sincerest thanks goes to Prof. Philipp Thurner, who allowed me to work in his team and gave guidance for this thesis. Further my appreciation goes to Dr. Orestis Andriotis who helped me with AFM analysis and further evaluation. Furthermore I would like to thank all colleagues and team members, who provided interesting discussion and some laughs during long lab hours.

Die approbierte gedruckte Originalversion dieser Diplomarbeit ist an der TU Wien Bibliothek verfügbar.
The approved original version of this thesis is available in print at TU Wien Bibliothek.
TU WIEN Bibliothek Your knowledge hub

Die approbierte gedruckte Originalversion dieser Diplomarbeit ist an der TU Wien Bibliothek verfügbar.
The approved original version of this thesis is available in print at TU Wien Bibliothek.

Abstract

Collagen plays an integral part for the biomechanical properties of many tissues, like bones, blood vessels, ligaments and tendons. The mechanical assessment has moved, with help of technical advancements, from tendons to individual collagen fibrils. Their biomechanical properties can nowadays be analyzed under hydration with tools such as the atomic force microscopy (AFM). The effects of sample preparation and hydration itself are not well studied so far. Therefore this thesis was aimed to determine the behavior of collagen fibril (CF) in typical phosphate-buffered saline (PBS) test setups with a series of long and short incubations and intermittent drying. Collagen fibrils came from a thawed mice tail tendon. Height and mechanical properties of 27 CF and 16 reconstituted collagen protein (RCP) fibrils were assessed with AFM nanoindentation. Eight CF were incubated two times for 9 days in 37° PBS with in between testing. The mean indentation modulus (IM) was reduced significantly after both incubations (1D vs 9D $p=0.005$, 9D vs 18D $p=0.002$). Swelling was significant ($p=0$) on every individual fibril after 9D. Further incubation did not increase the observed swelling. A sequence of short incubations of 2 hours on eight CF for determining the onset of height and IM changes indicated the first 2 hours as instance of most changes. However, significant changes were only on individual fibril level. 6 of 8 CF swell ($p\leq0.01$) and 4 reduced their IM ($p\leq0.36$) significantly. RCP fibrils behaved very differently from native CF. They were generally smaller and showed neither swelling nor IM changes. Intermittent drying of native CF incubated in PBS increased their IM significantly compared to before drying ($p=0.007$) and to distilled water incubation ($p=0.002$). D-Banding spacing showed mostly no changes during incubation and drying while imprinting with force of 500-6000 nN recovered initial surface after hydration. The findings indicate combinations of tropocollagen (TC) and cross-link changes due to incubation. Debonding of cross-links and local melting of TC could explain the swelling and IM reduction due to less structural integrity. Salt concentration elevation and cross-link rigidity increase due to residual irons after washing were assumed as influencing factors for the IM increase after drying. The handling of CF in nanoindentation experiments should incorporate a preselection of similar fibrils for better statistical evaluation, protease inhibitors and avoidance of intermittent drying if testing mechanical properties.

Die approbierte gedruckte Originalversion dieser Diplomarbeit ist an der TU Wien Bibliothek verfügbar.
The approved original version of this thesis is available in print at TU Wien Bibliothek.
TU Bibliothek Your knowledge hub WIEN

Die approbierte gedruckte Originalversion dieser Diplomarbeit ist an der TU Wien Bibliothek verfügbar.
The approved original version of this thesis is available in print at TU Wien Bibliothek.

Kurzfassung

In vielen biologischen Geweben wie Knochen, Blutgefäße, Bänder und Sehnen ist Kollagen der integralste Bestandteil für deren biomechanische Eigenschaften. Mithilfe immer neuerer und verbesserter Methoden kann man mittlerweile einzelne Kollagen Fibrillen (CF) untersuchen. Heutzutage werden deren biomechanischen Eigenschaften häufig unter Hydrierung mit einem Rasterkraftmikroskop (AFM) aufgenommen. Die Effekte der Probenvorbereitung und Hydrierung ansich wurde aber soweit nicht oft untersucht. Dadurch war das Ziel dieser Arbeit das Verhalten von einzelne Kollagen Fibrillen in typischen AFM Testaufbau durch eine Reihe von Experimenten mit langen und kurzen Inkubationen sowie zeitweises trocknen zu untersuchen. Dafür wurden 27 Fibrillen von einem aufgetauten Mäuse Schwanz und 16 Rekonstituierte Fibrillen herangenommen. Acht native KF wurden zweimal für je 9 Tage in PBS bei 37° inkubiert. Der durchschnittliche Indentations Modulus wurde nach jeder Inkubation signifikant reduziert (1T vs 9T p=0.005, 9T vs 18T p=0.002). Alle individuellen Fibrillen schwollen nach 9 Tagen signifikant an (p=0), zeigten aber bei der weiteren Inkubation kein weiteres Schwellverhalten. Die kurze Inkubation von 3 x 2 Stunden mit 8 KF zeigte nur signifikante Änderungen bei einzelnen Fibrillen. 6 von 8 KF schwollen ($p \leq 00.01$) und 4 reduzierten ihren IM ($p \leq 00.36$) signifikant. Rekonstituierte Fibrillen zeigten in beiden Experimenten keine signifikanten Änderungen ihres IM und Schwellverhaltens. Das erste trocknen zwischen PBS inkubieren zeigte eine signifikante Erhöhung des IM (p=0.007), auch im vergleich zum inkubieren im destillierten Wasser (p=0.002). Es wurden nur kleine Veränderungen am D-Banding während der Inkubation und Trocknung festgestellt. Das hydrieren von eingedrückten KF mit 500-6000 nN Kraft zeigt eine vollständige Erholung der Kollagenoberflächen. Diese Resultate deuten auf verschiedene Änderungen der Quervernetzungen und Tropokollagen Moleküle während der Inkubation hin. Der Abbau von Quervernetzungen und das lokale Auflösen von Tropokollagen Moleküle kann das Aufschwellen und den reduzierte IM erklären. Für den steigenden IM nach dem Trocknen wurden zwei Effekte in Anbetracht gezogen: Steigerung des Salzgehalts und Steifigkeitserhöhung von den Quervernetzungen, aufgrund von Ionen die nicht ausgespült wurden. Zukünftige Experimente sollten eine Vorauswahl von ähnlichen Fibrillen für eine bessere statistische Auswertung vornehmen, Protease Inhibitoren einsetzen und trocknen zwischen Messungen vermeiden.

Die approbierte gedruckte Originalversion dieser Diplomarbeit ist an der TU Wien Bibliothek verfügbar.
The approved original version of this thesis is available in print at TU Wien Bibliothek.
TU Bibliothek WIEN Your knowledge hub

Die approbierte gedruckte Originalversion dieser Diplomarbeit ist an der TU Wien Bibliothek verfügbar.
The approved original version of this thesis is available in print at TU Wien Bibliothek.

Contents

Abstract **ix**

Kurzfassung **xi**

Contents **xiii**

List of Figures **xv**

List of Tables **xvii**

Acronyms **xix**

1 Introduction **1**
1.1 Thesis Aim 2
1.2 Structure of the thesis 3

2 Background **5**
2.1 Tendon 5
2.2 Collagen 6
2.3 Atomic Force Microscopy 10
2.4 Nanoindentation 22

3 Material & Methods **27**
3.1 Preface 27
3.2 Overview of Conducted Experiments 27
3.3 Sample Preparation 29
3.4 Atomic Force Microscopy 29
3.5 Height and Indentation Modulus evaluation 32
3.6 Long Incubation 33
3.7 Short Incubation 34
3.8 Drying Experiment 35
3.9 Imprint Remodeling 37
3.10 Statistics 38

Die approbierte gedruckte Originalversion dieser Diplomarbeit ist an der TU Wien Bibliothek verfügbar.
The approved original version of this thesis is available in print at TU Wien Bibliothek.
TU WIEN Bibliothek Your knowledge hub

4 Results **39**
4.1 Preface 39
4.2 Incubation induced height changes 39
4.3 Indentation Modulus changes induced by incubation 45
4.4 Drying Experiment 49
4.5 Imprint Remodeling 55

5 Discussion **59**
5.1 Conclusion 63

6 Appendix **65**
6.1 Relative Changes 65

Bibliography **69**

Die approbierte gedruckte Originalversion dieser Diplomarbeit ist an der TU Wien Bibliothek verfügbar.
The approved original version of this thesis is available in print at TU Wien Bibliothek.
TU WIEN Bibliothek Your knowledge hub

List of Figures

2.1 Tendon Overview . . . 7
2.2 Biosynthesis of a collagen fibril . . . 8
2.3 Cross-links . . . 9
2.4 STM and AFM principle . . . 10
2.5 Optical lever AFM . . . 11
2.6 Interaction forces . . . 12
2.7 Lennard-Jones Potential . . . 13
2.8 Tip geometry differences in scanning . . . 16
2.9 Simplified AFM system . . . 18
2.10 Force Distance Curve and Contact Mode . . . 19
2.11 Oscillating mode range . . . 20
2.12 Intermittent contact mode . . . 21
2.13 Measured force-distance . . . 22
2.14 Oliver-Pharr basics . . . 23

3.1 Experiment plan . . . 28
3.2 Cantilever SEM images . . . 30
3.3 Spring Constant calibration . . . 31
3.4 Tip deconvolution . . . 32
3.5 Indentation modulus computation . . . 33
3.6 Long incubation experiment . . . 33
3.7 Short incubation experiment . . . 34
3.8 Drying experiment . . . 35
3.9 D-Banding evaluation . . . 36
3.10 Imprint experiment . . . 37
3.11 Imprint spots of the two experiments . . . 37

4.1 TF height results long incubation . . . 40
4.2 RCP height results long incubation . . . 41
4.3 TF height results short incubation . . . 43
4.4 RCP height results short incubation . . . 44
4.5 TF IM results long incubation . . . 45
4.6 RCP IM results long incubation . . . 46
4.7 TF IM results short incubation . . . 47

Die approbierte gedruckte Originalversion dieser Diplomarbeit ist an der TU Wien Bibliothek verfügbar.
The approved original version of this thesis is available in print at TU Wien Bibliothek.
TU WIEN Bibliothek Your knowledge hub

4.8 RCP IM short incubation issues 48
4.9 Height result drying 50
4.10 IM result drying 51
4.11 D-Banding Results 53
4.12 FFT reconstructed fibril 54
4.13 FFT D-Banding spectrum 54
4.14 Imprint height profile of single fibril 56
4.15 Imprinting images 57

5.1 Cross-link strengthening 61
5.2 Salt concentration increase 61

Die approbierte gedruckte Originalversion dieser Diplomarbeit ist an der TU Wien Bibliothek verfügbar.
The approved original version of this thesis is available in print at TU Wien Bibliothek.
TU WIEN Bibliothek Your knowledge hub

List of Tables

3.1 Cantilever spring constants long incubation 34
3.2 Cantilever spring constants short incubation 35
3.3 Cantilever spring constants drying experiment 36

4.1 TF swelling statistics long incubation 41
4.2 RCP swelling statistics long incubation 42
4.3 TF swelling statistics short incubation 42
4.4 RCP swelling statistics short incubation 44
4.5 TF IM statistics long incubation 46
4.6 RCP IM statistics long incubation 47
4.7 TF IM statistics short incubation 48
4.8 Statistics drying experiment 52
4.9 Statistics difference PBS/Water 52
4.10 FFT frequency changes 55

6.1 Relative changes of long incubation experiment 66
6.2 Relative changes of short incubation experiment 67
6.3 Relative changes of drying experiment 68

Die approbierte gedruckte Originalversion dieser Diplomarbeit ist an der TU Wien Bibliothek verfügbar.
The approved original version of this thesis is available in print at TU Wien Bibliothek.
TU WIEN Bibliothek Your knowledge hub

Die approbierte gedruckte Originalversion dieser Diplomarbeit ist an der TU Wien Bibliothek verfügbar.
The approved original version of this thesis is available in print at TU Wien Bibliothek.

Acronyms

AFM atomic force microscopy

CF collagen fibril

PBS phosphate-buffered saline

RCP reconstituted collagen protein

IM indentation modulus

TC tropocollagen

TEM transmission electron microscopy

AA amino acid

Gly Glycin

Pro Proline

Hyp hydroxyproline

CSA cross sectional area

MTJ myotendinous junction

PTM post-translational modification

LOX lysyl oxidase

PYR Pyridinoline

AGEs advanced glycation end-products

Die approbierte gedruckte Originalversion dieser Diplomarbeit ist an der TU Wien Bibliothek verfügbar.
The approved original version of this thesis is available in print at TU Wien Bibliothek.
TU WIEN Bibliothek Your knowledge hub

SFM scanning force microscopy

STM scanning tunneling microscopy

VdW Van der Waals

DIF differential comparator

PID proportional-integral-derivative controller

SNR signal to noise ratio

SEM scanning electron microscopy

FFT Fast Fourier Transformation

px pixel

TF tendon fibril

MAD median absolute deviation

Die approbierte gedruckte Originalversion dieser Diplomarbeit ist an der TU Wien Bibliothek verfügbar.
The approved original version of this thesis is available in print at TU Wien Bibliothek.
TU Bibliothek Your knowledge hub WIEN

Die approbierte gedruckte Originalversion dieser Diplomarbeit ist an der TU Wien Bibliothek verfügbar.
The approved original version of this thesis is available in print at TU Wien Bibliothek.

CHAPTER 1

Introduction

Collagen is the most abundant protein in humans and animals. It comprises over 25% of the total protein mass in human bodies. 28 different types of collagen have, so far, been identified. Especially collagen type I is accountable for more than 80% of all collagen in humans [1, 2]. Type I collagen provides the basis of our bones, dermis, tendons and ligaments by exhibiting superior mechanical properties [3, 4, 5]. Other types such as type II for cartilage and type III, along with type I, for blood vessels are integral to the function of the corresponding tissue.
CFs of type I,II,III,V and XI form a very distinct stripe pattern, called D-Banding, which can be seen with staining, transmission electron microscopy (TEM) and AFM [6, 7, 4]. The D-banding repeats with a periodicity of 67 nm and is independent of CF diameter. The diameters of CFs range from 20 nm up to 500 nm in tendon [8, 9]. Collagen fibrils of all types are built up by three parallel polypeptide chains in a left handed helical formation. Together they form a very tightly packed right handed triple helix called tropocollagen (TC) [10], where every third amino acid (AA) has to be Glycin (Gly). The sequence of XaaYaaGly with any AA in Xaa and Yaa was already established in 1955 by M. Cowen et al. [11]. The most frequent sequence is Proline (Pro)-hydroxyproline (Hyp)-Gly [12]. The formed TC-molecule is 1.5 nm in diameter, 300 nm long and has short telopeptides on either end without the repeating sequence. In comparison . The most well known build up model of TC to fibrils is proposed by Hodge & Petruska in 1964 [13], where five TC-molecules arrange in a staggered fashion. Electron density maps of rat tail tendons were used by Orgel et al. to design a computer model of five intertwisted TC-molecules, which fit the observed x-ray scatter pattern rather closely [14]. After self-assembly, CFs are loosely interconnected only by non-covalent interactions. This loose network of molecules becomes reinforced by the formation of covalent inter- and intra-molecular xlinks. Cross-links can either be formed by action of enzymes (enzymatic cross-links) or by the addition of reducing sugars (non enzymatic cross-links). The formation of enzymatic cross-links already initiates intracellularly during biosynthesis by hydroxylation

of proline and lysine. Both of these hydroxylated AA are later involved in cross-linking between two or three TC-molecules (maturing). Non-enzymatic cross-linking was found in aged collagen due to the increased stiffness versus young collagen [15]. The advanced cross-linking happens in a milieu with glucose or aldehydes. This cross-link formation is called glycation and involves complex chemicals rearrangements of glucose with collagen AA. The stiffness increase due to glycation leads to problems often found in diabetes like membrane thickening and glomerula hypertrophy [16]. Extensive knowledge exists on macro-scale mechanics of tissues with classic tensile tests [17] or bending experiments [18], but much less is known about the tissue micro- and nano-mechanics. Yet, it is these scales where the tissue is being affected. For accomplishing measurements of tissues in the nanoscale range, the AFM is a commonly used tool [3][19][20].

The AFM is a very sensitive instrument that allows force measurements by measuring contact or interaction forces with the sample surface. A cantilever that deflects due to those interactions acts as the force sensor. These cantilever deflections can be measured by different methods. A widely used method is the optical lever, which enhances small deflections of the cantilever by reflecting a focused laser beam to a photodetector[21]. Different approaches to measure the mechanical properties of single CFs have emerged. Some are based on classical mechanical tests but on the micrometer to nanometer scales like tensile tests [3], or measuring the bending fore and deflection by laying a fibril over a grated surface and record the applied cantilever tip force [22]. Another measurements form is based on force-distance curves by indenting CFs with an AFM cantilever tip [23][19][20]. Oliver and Pharr developed a well established method to calculate the elastic modulus by nanoindentation in 1992 [24]. An exact mapping of the cantilever tip is necessary to estimate the contact area between sample and cantilever tip. One approach to map the cantilever's tip is by imaging a TGT1 spike and deconvolute the tip. Andriotis et. al [19] developed a nanoindentation protocol based on Oliver and Pharr to asses the properties of CFs. This method of assessment was used in this thesis on several single CFs in PBS and distilled water with different incubation times.

1.1 Thesis Aim

This thesis was determined to investigate possible biomechanical changes caused by sample preparation and handling on CFs in AFM test protocols through measuring diameter, indentation modulus and additional detectable structural changes of the fibril. Samples often used in such experiments, and also investigated in this thesis, are reconstituted collagen fibrils, which are made out of collagen powder and swollen in hydrochloric acid among other steps [25, 3]. Other publications dissect CFs direct from tendons of rat tail [4], sea cucumber [26] and mice [19]. The effects of sample preparation by smearing due to applied strain, used by Wenger and Andriotis [19, 4],were also tested in this thesis with a proposed hydration relaxation and D-Band spacing changes. Changes due to hydration on CFs itself were, as far as I know, insufficiently studied, although experiments are conducted under hydration [3, 20]. Therefore hydration experiment via incubation at 37 °C in PBS to simulate the temperature in vivo were done. These incubations test

Die approbierte gedruckte Originalversion dieser Diplomarbeit ist an der TU Wien Bibliothek verfügbar.
The approved original version of this thesis is available in print at TU Wien Bibliothek.
TU Bibliothek Your knowledge hub WIEN

simultaneously the stability of collagen type I as Leikina et. al found out that it should be thermally unstable at body temperature [27]. Moreover influence of intermediate drying on fibrils were tested to incorporate the possibility of fibril reusing. Imprints with high force indentations, which leave visible notches similar to Wenger et. al in 2007 [4], were tested for lasting visible damage after hydration. Furthermore statistical evaluations of the measurements were often performed by combining results of different fibrils [23][20][3] while others distinguish individual fibrils by factors like diameter [4][22]. Differences of both views were discussed to bring points up where one or the other should be used. In the end this work produced new insights and recommendations for working with single PBS hydrated CFs in an AFM environment.

1.2 Structure of the thesis

The thesis is subdivided in four additional chapters with underlying sections.

Chapter 2 describes the general background of materials and theories used in the thesis. The chapter begins with a section that describes the anatomical and hierarchical build up of tendons from the smallest unit of tropocollagen to the whole epitenon enclosed tendon. Furthermore differences of functionality between two tendon types is depicted. The subsequent section covers the structure and biosynthesis of individual CFs with the following enzymatic and non-enzymatic cross-linking. Following is a section about the used measurement technique of the atomic force microscopy (AFM). The section starts with a brief historical and principle overview before describing interaction forces like Van der Waals force and electrostatic forces. The measuring of such forces due to the interaction with the cantilever tip is described the next chapters which presents different tip forms and deflection measurement systems. Furthermore the feedback control system is briefly explained, which controls the piezodrive. Afterwards the used AFM operation modes of the thesis are described. The final background section was dedicated to the nanoindentation, which was an important part of the thesis, and the following evaluation of the indentation modulus via the Oliver-Pharr method.

Chapter 3 describes the used materials and methods. It includes an overview of the conducted experiments and detailed sections about each performed experiment. Furthermore important preparation steps of the samples and the AFM are depicted. Particularly the CF sample preparation, AFM setup and IM evaluation are written in more detail due to their importance to the thesis. At last a statistic section describes the performed analysis.

Chapter 4 represents and summarizes the findings with errorbar figures and p-value tables.

Chapter 5 discusses and concludes the findings with questions and considerations for future work with CFs.

Die approbierte gedruckte Originalversion dieser Diplomarbeit ist an der TU Wien Bibliothek verfügbar.
The approved original version of this thesis is available in print at TU Wien Bibliothek.
TU Bibliothek WIEN Your knowledge hub

Die approbierte gedruckte Originalversion dieser Diplomarbeit ist an der TU Wien Bibliothek verfügbar.
The approved original version of this thesis is available in print at TU Wien Bibliothek.

Die approbierte gedruckte Originalversion dieser Diplomarbeit ist an der TU Wien Bibliothek verfügbar.
The approved original version of this thesis is available in print at TU Wien Bibliothek.

CHAPTER 2

Background

2.1 Tendon

Tendons are connective tissues that transfer muscle contraction and resulting forces to the bones, which consequently allows the movement of body parts. Two sorts of contractions have been established, both with distinguishable tendons: the positional tendon and energy storing tendon. Energy storing tendons, as implied by the name, store energy during the elongation part of a movement with larger strains than positional tendons. A prime example of this function is the human achilles tendon with strains of 6.2 to 10.3% and a 74% release of the stored energy during the plantarflexion (push off from ground) movement [28]. The positional tendons are stiffer and undergo lower strains for more precise and exact movements. E.g. human digital flexor tendons only experience strains of around 1.2 $\pm$0.38 % [29]. Forces in tendons varies largely based on the executed motion. Achilles tendons have to withstand a maximum force of 9 kN in running or 5.5 kN in hopping [30][28]. Digitalis tendons experience a theoretical force of 50 N [29]. To prevent damage by overextending, tendons adapt to mechanical stimuli through tendon fibroblasts, which secrete collagen type I, and consequently increase the cross sectional area (CSA) [31]. Tendons connect on one end to the muscle, called myotendinous junction (MTJ), and on the other end to the enthesis or osteotendinous junction. Also the junction between bone and ligaments is called enthesis. The tendon-bone transition can be subdivided into three zones: bone, fibrocartilage and tendon [32]. Older views list four zones with a differentiation of mineralized fibrocartilage and fibrocartilage, which are seperated by a tidemark [33]. Recent studies shows the fibrocartilage has a smooth gradient of partially mineralized collagen fibrils with random mineral deposits for an effective stress transfer [32]. The transition begins from the tendon part, which has at the start the same properties and constituents of a tendon (mainly collagen type I). Across the fibrocartilage the mineralization increases and the dominant collagen type changes from type I to type II [33]. The mineralized part is the true junction with large amounts

of interlocking between calcified fibrocartilage and bone [34]. This zone is also suspected to form a barrier against bone blood vessels and intercell communication between bone and tendon cells [35]. Another form of bone-tendon junction is the fibrous one, which is connected with dense connective tissue [33]. MTJ has more direct contact with musclefibers unlike the transition in the enthesis. Several transmembrane, extracellular and intracellular proteins link the last actin filaments of musclefibers to the sarcolemma (interface muscle/tendeon)[36]. The sacrolemma is folded into a wave like form to increase the area of contact and withstand muscle forces of up to 34 $\frac{kN}{m^2}$ [36]. The tendon itself is a highly hierarchical structure over many orders of magnitude of CSA, from TC with 1.5 nm up to the tendon with 0.5 to 2 mm, as seen in the overview of Figure 2.1. A small unit of the tendon is the collagen fibril, which was investigated in this thesis. Fibrils are built from of multiple intra/inter-linked TC-molecules. Fibrils vary in diameter between 20 nm to 500 nm in tendons [8, 9]. Multiple fibrils form a fibre and multiple fibres form a fibre bundle with a visible crimp pattern under a microscope (indicated in Figure 2.1). The next level formed of fiber bundles is the fascicle, which is enclosed in a connective tissue called endotenon. Endotenons contain the blood, nerve and lymph supply [37]. Between the fibre bundles elongated tenocytes are found, which are responsible for the formation of tendons. The last hierarchical step are the bundles of fascicles, which form the final tendon. Tendons are enclosed with the epitenon, which also contains nerves and lymphs cells [37]. Around a tendon is another layer of tissue called paratenon. The space between the epitenon and paratenon is filled with a fluid to reduce friction during movements [37].

The main composition of tendons are collagens, proteoglycans and glycoproteins. Water and cells are the remaining parts [38]. Collagen type I makes the majority of tendon dry weight with around 66% and 95% of all collagen content [39]. The remaining parts consists mainly of type III collagen [39]. Proteoglycans and glycoproteins provide water stabilization [40], compression resistance [40], extracellular matrix stabilization [41] and wound healing [42].

2.2 Collagen

Collagen comprises over 25% of the total human protein mass and is the most abundant protein in human bodies. At least 28 different types of collagen have been identified so far. Up to 80% of all collagen in humans is type I [1, 2] and lays down the foundation of our bones, dermis, tendons, ligaments and exhibits superior mechanical properties [3, 3, 4, 5]. Other types such as type II for cartilage and type III for blood vessels are integral to their function of the corresponding tissue. The post-translational modification (PTM) of collagen peptides plays a critical role in forming biomechanical properties. Especially important are the inter and intramollecular cross-links between TC-moleculs. Another distinct feature of collagen fibrils types I,II,III,V and XI is the visible repeating stripe pattern every 67 nm called D-Banding, which is visible with staining, TEM and AFM [6, 7, 4].

Die approbierte gedruckte Originalversion dieser Diplomarbeit ist an der TU Wien Bibliothek verfügbar.
The approved original version of this thesis is available in print at TU Wien Bibliothek.
TU Bibliothek WIEN Your knowledge hub

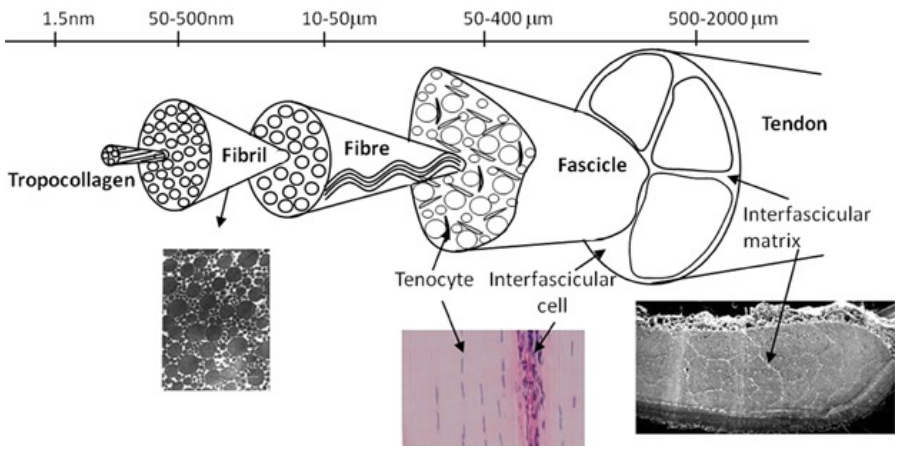

Figure 2.1: Overview of the hierarchical structure of a tendon. Example pictures below transversal cuts (black/white photos). Fascicle image is an histological picture, which highlights interfascicular cells. Copyright by [43].

2.2.1 Genesis

The biosynthesis of type I collagen starts in the endoplasmic reticulum with the translation of three peptide chains. Two $\alpha 1$ and one $\alpha 2$ chain form from the C-terminus into a tight left handed helical formation, called procollagen. The spacial arrangement was already established in 1954 by Ramachandran [10], which requires that every third AA has to be Gly (smallest AA) to tightly pack the chains. The α-chains have a typical 3 AA sequence XaaYaaGly found by M. Cowen et al. [11] with 337 to 343 repetitions [44]. The most common sequence is Pro-Hyp-Gly [12]. The hydroxylation of Pro is done before the three chains are zipped together [45] by PTM. The majority of post-translational modification is the hydroxylation of Pro and lysine. Proline is hydroxilated either by prolyl-3-hydroxylase or prolyl-4-hydroxylase, based on its Xaa,Yaa position in the XaaYaaGly triplet [44, 45]. The hydroxylation is a critical factor in stabilizing the triple helix by forming hydrogen bonds and inductive effects [46]. Lysine hydroxylation is important for further glycosylation and cross-linking. The trimerization is initiated by special AA sequences in the C-telopeptide with further help of chaperons to guide the assembly [47]. The helical region is bordered by non-helical C- and N-telopeptides, which are much shorter (20 AAs) [44]. After the trimerization is finished, the procollagen is transported in a vesicle to the Golgi complex and concentrated with other procollagen molecules before it is secreted into the extracellular space. The procollagen in the vesicles form bundles but with no apparent D-Banding [44]. In the extracellular space metalloproteinases cleave the tail-propeptides off the procollagen. More recent research suggest that the cleaving already begins in the Golgi complex [48]. Figure 2.2 shows the different steps of the biosynthesis.

Die approbierte gedruckte Originalversion dieser Diplomarbeit ist an der TU Wien Bibliothek verfügbar.
The approved original version of this thesis is available in print at TU Wien Bibliothek.
TU Bibliothek Your knowledge hub WIEN

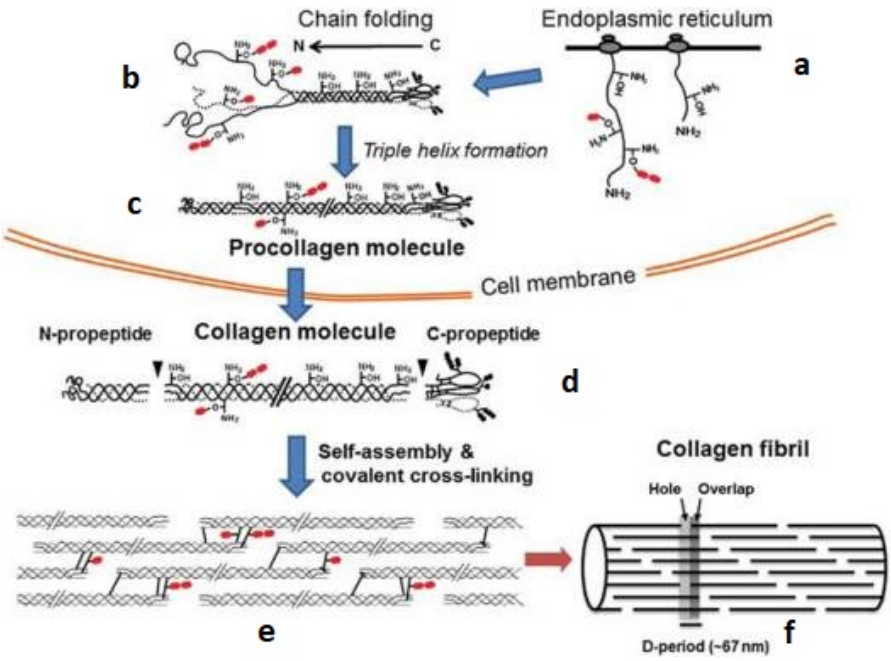

Figure 2.2: Biosynthesis of a collagen fibril. (a) The synthesis starts with the translation of the three α chains. Hydroxylation and further glycosylation takes place before the chains are combined. (b) Chains fold together starting by the C-end to form procollagen. (c) Procollagen molecules are bundled (not shown) together and are secreted into extracellular space. (d) N and C-propetides are cleaved off by metalloproteinases (e) Enzymatic inter- and intra-molecular cross-linking (f) Finished collagen fibril with D-Banding. Adapted from [45]

2.2.2 Cross-links

Cross-linking between TC molecules is thought to be the most relevant process for defining mechanical properties. The alignment of fibers varies between tissue and is based on their mechanical stress. Tendon fibrils are parallel ordered for withstanding longitudinal forces, while skin fibrils are randomly ordered to isotropically increase stiffness. Due to aging additional cross-links form, which increases their strength but also make them more brittle. Cross-linking happens in two different forms: enzymatic and non-enzymatic. Enzymatic cross-links occur on predetermined amino acids, while non-enzymatic cross-links form under the involvement of reducing sugars (glycation).

Enzymatic Cross-linking

The majority of enzymatic cross-links in collagen are based on the oxidative deamination of lysine by the enzyme lysyl oxidase (LOX) [15]. The deamination by LOX occurs only on five specific lysine and hydroxylysine sites on the C- and N-telopeptides [45], which form aldehyde residues. The formed aldehydes react with other aldehydes or lysine

Die approbierte gedruckte Originalversion dieser Diplomarbeit ist an der TU Wien Bibliothek verfügbar.
The approved original version of this thesis is available in print at TU Wien Bibliothek.
TU Bibliothek Your knowledge hub WIEN

with hydroxylysine in the helical region to form inter and intra-molecular cross-links (immature cross-linking), see Figure 2.3. Immature cross-links only occur in or between two procollagen molecules. Further cross-linking with additional AA residues is called maturing [15]. A well known mature cross-link is the Pyridinoline (PYR) cross-link, which is common in bone, cartilage and tendon [15]. It was first identified by Fujimoto in 1977 [49] and starts with the same deaminated hydroxylysine as in the immature cross-linking. The aldimine (Schiff base) cross-link is formed with a free helical region ϵ-amino hydroxylysine residue of a near procollagen molecule. The aldimine can spontaneously rearrange to a ketoamine via the Amadori rearrangement. Two of such cross-links can condense and form a cross-link with three procollagen molecules. The final cross-link releases a helical hydroxylysine residue and is considered the matured PYR.

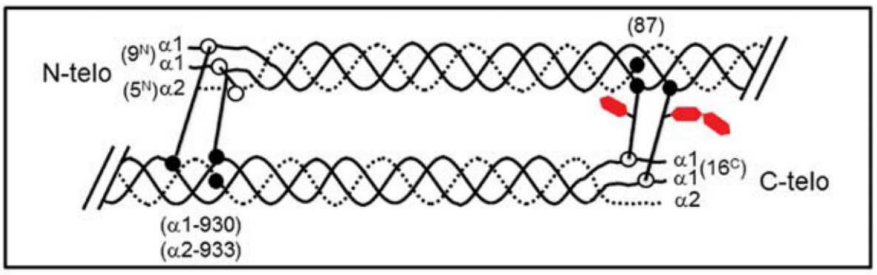

Figure 2.3: Inter and intra molecular cross-linking between two procollagen molecules. Void circles indicate telopeptide aldehyeds and filled circles helical lysine or hydroxylysine with black lines as the cross-links. Red spots are the glycoslation spots of lysine. Figure from [45].

Glycation

Further increase of stiffness with aging hinted in the direction of another non-enzymatic form of cross-linking [15]. It is now known as reaction of collagen with glucose and/or aldehydes called glycation. The reaction starts on the ϵ-amino group of lysine and forms with the involvement of glucose a Schiff-base (Maillard-reaction), the glucosyl-lysine. By Amadori rearrangement and further oxidation, dehydration and polymerization, small highly reactive sugar aldehydes develop, which are named advanced glycation end-products (AGEs) [50, 51, 52]. The cross-links are formed by a reaction of the modified lysines or arginines between collagen molecules. Two prominent lysine-arginine cross-links AGEs in human tissue are Pentosidine and Glucosepane of which the latter is the most abundant one [53]. AGEs play a fundamental role in diabetes due to the elevated glucose levels in the blood, which increases the formation of AGEs[54]. In tendons AGEs, like the aforementioned Glucosepane, increases the stiffness, which could increase the risk of damage [55].

Die approbierte gedruckte Originalversion dieser Diplomarbeit ist an der TU Wien Bibliothek verfügbar.
The approved original version of this thesis is available in print at TU Wien Bibliothek.
TU Bibliothek WIEN Your knowledge hub

2.3 Atomic Force Microscopy

2.3.1 History

Atomic force microscopy or scanning force microscopy (SFM) is an advancement of the scanning tunneling microscopy (STM) technique by Binnig, Quate and Gerber in 1982 [56]. Binning et al. imaged surfaces of Au, Si, GaAs with STM and achieved for the first time images of individual atoms. For example this high resolution helped to understand the surface structure of Si(111)-(7x7) with the combined results of transmission electron diffraction and x-ray scattering [57].
The basic principle of STM is relatively simple. A scanning metal tip is held up close above the sample surface (few Ångström) and fixed to piezodrives, which can move the tip in x, y and z direction, see Figure 2.4a. The metal tip and sample surface are two electrodes, with an applied voltage V, for the tunnel junction. If the tip is close to the surface a tunneling current J will be developed. The control unit adjusts the height of the tip via the piezodrive, thereby holding the tunneling current J constant. The surface topography is the result of the applied height changes. One major drawback of this technique is the need of conductive sample surfaces. Hence only metals and semiconductors can be scanned without preparation, due to the need of flowing electrons. Other materials must be coated with a conductive layer. Also ambient conditions, like humidity, influences the surface electron density and therefore the measurements [58]. Ideal conditions for high resolution STM are fulfilled in ultra high vacuum chambers. To circumvent these shortcomings measurements of other close surface interactions were researched. Binning et al. proposed a force microscope in 1986 which can measure ultra small forces due to detecting elastic deformations of a spring named Atomic Force Microscope [59]. The AFM measures the small and long range forces between the tip of a cantilever (spring) and the surface. Figure 2.4b shows the experimental setup of the AFM with an integrated STM. Without the need of a conductive surface, images of biological samples under physiological conditions are possible, like single DNA molecules [60] and live bacterial cells [61].

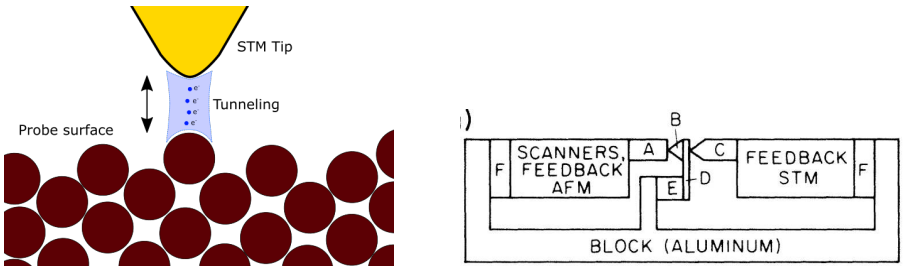

(a) STM principle (b) AFM concept

Figure 2.4: (a) STM: Metal tip is guided along the surface area and held in such a height that the tunneling current J is constant. (b) Experimental setup of the AFM which used a cantilever(D) with an diamond tip (B) as spring. The deflection was measured via an STM (C). Figure (b) adapted from [62].

Die approbierte gedruckte Originalversion dieser Diplomarbeit ist an der TU Wien Bibliothek verfügbar.
The approved original version of this thesis is available in print at TU Wien Bibliothek.
TU Bibliothek Your knowledge hub WIEN

2.3.2 AFM Principle Setup

The core of an AFM is the unit measuring the cantilever's elastic deformation. The cantilever features a sharp tip, on which the surface forces act on. With piezodrives in all three spatial dimensions, the tip is dragged (depending on the operations mode, see section 2.3.5) along the surface and the cantilever bends due to features on the surface. The bending is recognized via a sensor. The most common one is the optical lever method, where the reflection of a laser beam on the cantilever's reflective backside is recorded on a segmented photo diode. Figure 2.5 illustrates an simplified optical lever system. Other used deflection sensors are based on piezoresistance and interferometry. The output of the deflection sensor acts as an input for a control unit, which in turn controls the piezodrives.

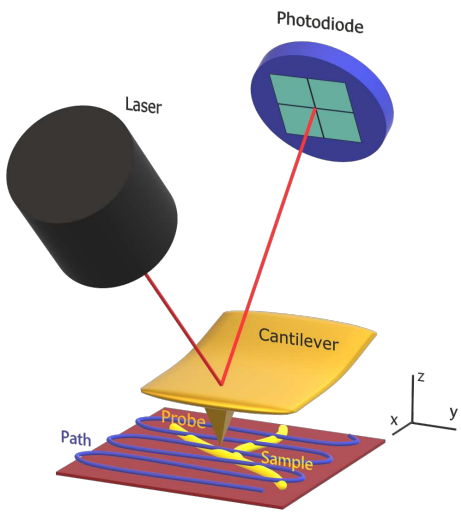

Figure 2.5: Measurement of elastic deformation from the cantilever with the deflection of an laser beam.

In the following sections the important mechanisms and parts of an AFM are described. Beginning with the surface interaction forces followed by detection methods, feedback systems, operations modes and indentation mode.

2.3.3 Interaction Forces

Interaction forces can be split into two groups, short-range and long-range. A short range force with a range of a couple nm is the interatomic potentials. Long range forces on the other hand include electrostatic, magnetic and Van der Waals forces, with hundreds of nm range.

Die approbierte gedruckte Originalversion dieser Diplomarbeit ist an der TU Wien Bibliothek verfügbar.
The approved original version of this thesis is available in print at TU Wien Bibliothek.
TU Bibliothek Your knowledge hub WIEN

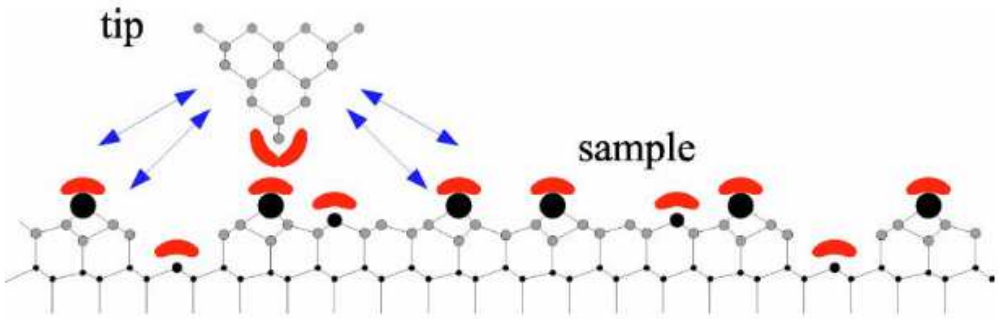

Figure 2.6: Schematics of the forces in play with a tip over a Si surface. Red orbits represents short interatomic potentials when they overlap. Blue markers indicate long-range forces of electrostatic, magnetic and Van der Waals nature. Graphic from [63].

Interatomic Potential

To calculate forces in ranges of few Ångströms between two or more atoms, an interatomic potential function can be used. This function assigns an energy to a systems of atoms within a given location in space. The force in a system between two atoms is depending on the distance r and the potential $V(r)$ [64]:

$$F(r) = -\frac{\partial V(r)}{\partial r} \tag{2.1}$$

Many versions of potential functions $V(r)$ were developed, which are all approximations and try to be as accurate as possible for different elements. Balamane, for example, compared 3 potential functions for silicon, which all have different advantages and disadvantages [65]. One finding was the relative poor modeling of small cluster, but a good description of larger silicon bulks. The real potential is a quantum mechanical problem and would require the Schrödinger equation for all electrons and nuclei to be cast into an analytical form. A simple approximation is the *Morse Potential* for diatomic molecules between an atom and a surface. Only three parameters must be fitted:

$$V(r)_{morse} = D_e(e^{-2\alpha(r-r_e)} - 2e^{-\alpha(r-r_e)}) \tag{2.2}$$

with r distance between atoms, r_e equilibrium distance, D_e the well depth and α as width of the well. The Morse equation 2.2 shows an attractive term if $r > r_e$ and an repulsive term for $r = r_e$.

Another simple approximation for two neutral atoms is the Lennard-Jones Potential:

Die approbierte gedruckte Originalversion dieser Diplomarbeit ist an der TU Wien Bibliothek verfügbar.
The approved original version of this thesis is available in print at TU Wien Bibliothek.
TU Bibliothek Your knowledge hub WIEN

$$V(r)_{LJ} = \varepsilon[(\frac{r_m}{r})^{-12} - 2(\frac{r_m}{r})^{-6}] \tag{2.3}$$

with ε as depth of the potential well, r distance between atoms and r_m minimum range for lowest potential. Lennard-Jones potential incorporates repulsive forces with the r^{-12} term and long range force such as Van der Waals forces with its r^{-6} term.

For multi body potentials the Stillinger-Weber potentials [66] is a well established function, which includes the energy of nearby neighbors. This approximation is especially good for the prediction of silicon interactons [[67][68]]. The equation is a sum of potentials equal to the number N of bodies in the problem:

$$\phi(1, ..., N) = \sum_i v_1(i) + \sum_{i,j} v_2(i,j) + \sum_{i,j,k} v_3(i,j,k) + ... + v_n(1, ..., N) \tag{2.4}$$

v_2, v_3 are the potentials for the two body and three body parts. The exact potentials of v_2, v_3 were written in the proposal of Stillinger-Weber in 1985 [66].

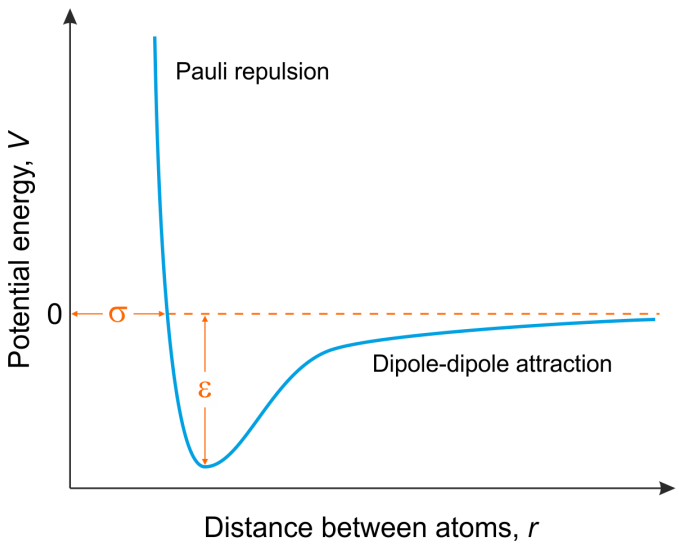

Figure 2.7: Representation of Lennard-Jones Potential. ϵ is called well depth and indicates attractive forces. σ is the radi where no potential is acting. Graphic from [69]

Van der Waals Forces

Van der Waals (VdW) attractions are weak forces, which can form from fluctuating electric dipoles. Dipoles can either occur from a fixed electron distribution in an otherwise neutral atom (positive and negative side) or from the attraction of electrons of another molecule. Even if VdW forces act in short range, they must be integrated over the

Die approbierte gedruckte Originalversion dieser Diplomarbeit ist an der TU Wien Bibliothek verfügbar.
The approved original version of this thesis is available in print at TU Wien Bibliothek.
TU Bibliothek Your knowledge hub WIEN

whole area to gain the two-object energy. This is done via a macroscopic approach by summation of each force between two pairs of atoms. The energy in a pair of atoms with distance R varies with $\frac{1}{R^6}$ [70]. For 2 spherical bodies containing a number of particles Hamaker calculated an approach for VdW forces in 1937 [71]. An assumption was made that both spheres radii $R_1 R_2$ are much larger than the distance $r, r << R_1 R_2$ between them. With that the formula can be simplified to:

$$V = -\frac{AR_1R_2}{(R_1 + R_2)6r} \tag{2.5}$$

The variable A is the *Hamaker Constant*, which is dependent on the density of both partners and their particle interactions. Giessibl calculated the corresponding forces of an etched metal tip with 100 nm width and 0.5nm gap as ≈ -10nN [63].

Electrostatic Forces

In aqueous environments the most common AFM sample support slides, which are made out of mica, graphit and Si, and the prepared biological molecules or samples are exhibiting a net surface charge due to their acidic and basic functional groups. The net charge depends on the buffer solution's pH and the pK-Values of the molecule's functional groups. The surface charge is offset by a layer of counter ions which forms an electrical double layer. The thickness of the double layer can be characterized by the Debye length λ_D (decay of electrostatic potential per unit length λ_D). [72]. If two bodies with an electrical double layer, like mica and the AFM tip, approach each other to tens of nm the layers overlap and electrostatic interactions occur. To incorporate this interaction with Van der Waals forces Derjaguin, Landau, Verwey and Overbeek developed the DLVO Theory:

$$F_{DLVO} = \frac{4\pi\sigma_s\sigma_t R\lambda_D}{\epsilon_e\epsilon_0} e^{-r/\lambda_D} - \frac{AR}{6r^2} \tag{2.6}$$

The first term in 2.6 represents the electrostatic forces with σ_s and σ_t as surface charge densities, R as sphere radius, free space permittivity ϵ_e, dielectric constant ϵ_0 and r distance between surfaces. The second term corresponds to the derivative in respect to r of the VdW Potential eq:2.5 (in accord to interatomic potentials eq:2.1), with *Hamaker Constant* A. Since the Hamaker Constant of the second term doesn't include the influence of media between the observed objects only the first term reflects them. Media with different ionic strengths affect the double layer height, with higher ionic strength the lower the double layer height [73, 74]. At ion concentrations higher than 10^{-3}M the repulsive forces of the double layer are surmounted by attractive Van der Waals forces. For even higher concentrations >1M strong short range repulsive forces were recorded [74]. This effect of media should be considered while measuring in constant force mode.

Die approbierte gedruckte Originalversion dieser Diplomarbeit ist an der TU Wien Bibliothek verfügbar.
The approved original version of this thesis is available in print at TU Wien Bibliothek.
TU Bibliothek Your knowledge hub WIEN

2.3.4 Force Detection

Cantilever and Probes

The main part of force detection is the cantilever. Therefore cantilevers were designed to only allow major deflection in one direction and be rigid in the others. Beam and V-shaped cantilevers fulfill those criteria and are the most commonly used shapes. The first cantilever from Binnig was made out of a gold foil with an attached diamond tip [59]. Other used materials were SiO_2 and Si_3N_4. Today most force sensor cantilevers and tips are made out of one piece of silicon, produced by dry and wet etching. Wolter et. al invented this procedure for cantilever production in 1991 [75]. These cantilevers typically have a very sharp tip [63], which is crucial to gain atomic-resolution. At best only a single apex atom at the tip should interact with the surface. Through special etching, tips can be produced, which come close to this goal with an curvature of lower than 1nm [76]. Other methods for sharpening are ion milling and attachment of nanotubes. Through these extra steps in production the horizontal resolution can be increased. The geometry of the probe is crucial for the correct representation of the surface. Probes with a higher aspect ratios (length to width) have a better horizontal resolution than blunter ones, see Figure 2.8 for the difference. Blunt tips cannot reach the bottom of surface pits or follow the sides of a strongly rising object. Although those special probes can produce better images, they are more prone to damage through their fragile geometry. Typically used tips are square pyramidal shaped and are more resistant to mishandling. Another important distinction in cantilever selection is the mode of operation. Basically an AFM operates in two main modes: Contact Mode and AC Mode, see Section 2.3.5. Cantilevers used in Contact Mode have a spring constant (k) lower than 1 N/m, typically 0.06 - 0.48 N/m [77]. In comparison cantilevers for AC mode usage are much stiffer with a k in the range of 10-50 N/m [78]. This is due to the fact that in contact mode the cantilever has to deflect with much lower forces than in AC Mode to gain a high signal to noise ratio. By contrast AC Mode cantilevers are excited nearly to their first resonance frequency and only have short contact (intermittent contact mode) or no contact with the sample. The higher stiffness is needed for an high enough resonance frequency to allow imaging. This behavior can be explained by simplifying the cantilever system to an dampened oscillator system, which has a resonance frequency of $\omega = \sqrt{\frac{k}{m}}$.

Die approbierte gedruckte Originalversion dieser Diplomarbeit ist an der TU Wien Bibliothek verfügbar.
The approved original version of this thesis is available in print at TU Wien Bibliothek.
TU Bibliothek Your knowledge hub WIEN

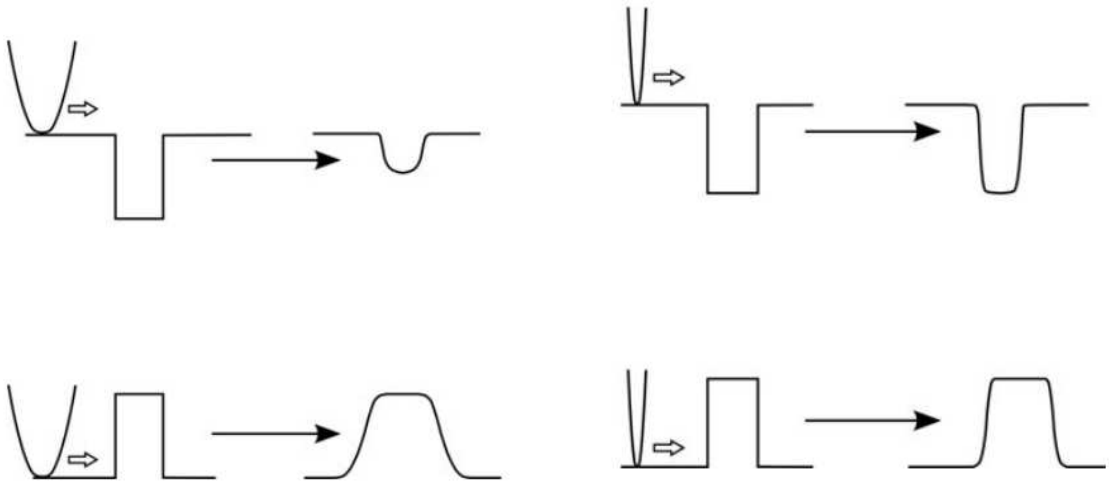

(a) Blunt probe (b) High aspect ratio probe

Figure 2.8: Difference of horizontal feature imaging with a (a) blunt and (b) high aspect ratio probe. Adapted from [79, p.37].

Cantilever Deflection

The measurement of force is performed via the deflection of the cantilever. The first AFM from Binnig used a STM for deflection detection, see Chapter History 2.3.1. Therefore the backside of the cantilever was metalized to ensure the tunneling effect. However, using the STM had two drawbacks: the tunneling current was greatly dependent on tip and material's chemical composition (influenced by ambient conditions) and the current itself exerted a force on the lever. Therefore other methods based on optical (interferometer, optical lever) and electrical (piezoeffect) effects were developed and used.

Piezoresistive Sensor

The piezoresistive sensor was developed by Tortonese et al. in order to eliminate the complex and precisely aligned optical components of an AFM [80]. The concept is a based of the varying resistance of metals by changing their geometry through bending, straining and compression. Tortonese fabricated the cantilevers with piezoresistive-sensors by etching silicon on insulator (SOI) wafers. The top layer of an silicon wafer is etched off to 2 ± 1 μm and dotted with boron to obtain an p-type piezoresistor-layer. The layer changes its resistance linearly to the deflection of the cantilever. Other research teams developed the sensor further like Minne et al., which integrated a piezioresistive sensor and piezoelectric actuators on two parallel cantilevers [81]. Although piezoresistive cantilevers a very capable for imaging, they are hard to manufacture in larger numbers, which has led to their disappearance [79, p.22].

Die approbierte gedruckte Originalversion dieser Diplomarbeit ist an der TU Wien Bibliothek verfügbar.
The approved original version of this thesis is available in print at TU Wien Bibliothek.
TU Bibliothek Your knowledge hub WIEN

Interferometer

A very sensitive method for cantilever deflection measuring introduced in 1988 by Erlandsson et al. [82]. The detection is based on a Michelson interferometer where a laser beam is split into two different paths. One path has a fixed distance and the other changes with the oscillation of the cantilever. The cantilever reflects the beam back to interfere with the other beam. Through constructive or destructive interference fringes arise, which can be correlated to the deflection of the cantilever. First applications only worked in AC-mode, due to the high influence of optical path length changes in low frequencies and static modes. Only with further improvements, like reducing interferometer cavity, beam polarization, fiber-cantilever cavity interference and more, measuring in static or low frequency modes was made possible [83, 84, 85]. Although the interferometer is very sensitive, it faded away due to fringe hopping. [79, p.22]

Optical Lever

This method was developed in 1988 by Alexander et al. [21] and is based on a laser beam, which is adjusted to reflect from the back of the cantilever. The reflected beam is then recorded by a four quadrant photodetector. Through the long distance between the cantilever and photodetector, even small deflections cause a considerable change of the laser spot on the detector, see Figure 2.5. This high sensitivity requires an precise pre-alignment of the laser beam and the photodetector position. The laser beam must be aligned to the end of the cantilever, above the tip, and be reflected to the photodetector center. This method is nowadays the defacto standard for force sensors in AFM and also used as deflection detection in this thesis [79, p.21].

Feedback Control

The feedback system begins with the vertical deflection measurement. In an optical lever AFM the deflection is measured by subtracting the signal sum of the upper part of the photodetector to the lower part e.g. (A+B)-(C+D), Figure 2.9. The outgoing signal is compared to a set point via a differential comparator (DIF), which produces the error signal. The error signal is in turn the input for the actual control, the proportional-integral-derivative controller (PID). The PID tracks the surface according to the user settings of P, I and D terms and tries to keep the error signal Z_{err} minimal in regards to the equation 2.7 [79]. Although the D-term is nowadays almost never used. The output Z_{piezo} sets the z-height of the piezodrive. Z_{piezo} and Z_{err} are typically used as image for height and error images. However, if the PID values are optimized the error image would have minimal contrast.

$$Z_{piezo} = P * V_{err} + I * \int Z_{err} dt + D * \frac{dZ_{err}}{dt} \tag{2.7}$$

Die approbierte gedruckte Originalversion dieser Diplomarbeit ist an der TU Wien Bibliothek verfügbar.
The approved original version of this thesis is available in print at TU Wien Bibliothek.
TU Bibliothek Your knowledge hub WIEN

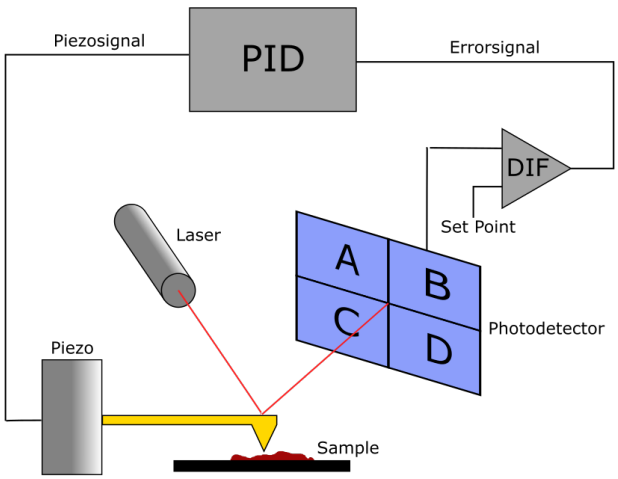

Figure 2.9: Simplified AFM system. Cantilever deflection is detected with a photodetector and compared to the desired setpoint. PID tries to reduce the error signal with height changes of the cantilever. Images can be made out of the piezo height and error signal.

2.3.5 Operation Modes

Through technical advancements more and more measurement modes were made possible beyond the topographical imaging. With special probe coating and stage material, surfaces can be probed for magnetic force (MFM), electrical-, conductive-, chemical- and force- properties [86, 87]. However, only topographical and force measurement modes were used in this thesis, which will be described in the following section.

Contact Mode

Contact mode operation was the mode with the highest accuracy in the original development of the AFM by Binnig in 1985 [59]. The principle is relative simple by measuring the deflection of the cantilever, which leads to the surface topography. At first a set point of the desired deflection has to be defined, which defines the imaging force of the cantilever. The involved forces can be visualized by a force-distance curve of Figure 2.10a. As the probe approaches the sample, the tip is attracted and snaps to the surface. This is the kink under the horizontal line of Figure 2.10a. With further approaching, the tip is acting more and more force on the surface and is repulsed. Simultaneously, the cantilever deflects in the opposite direction. By removing the the tip from the surface, often the same phenomena of attraction can be seen before enough reverse force is applied to lift the tip. The set point has to be placed in the repulsive realm, indicated with the shaded box in Figure 2.10a, to ensure permanent contact with the sample. Due to the underlying principle of contact mode various issues can arise by false configuration. For

Die approbierte gedruckte Originalversion dieser Diplomarbeit ist an der TU Wien Bibliothek verfügbar.
The approved original version of this thesis is available in print at TU Wien Bibliothek.
TU Bibliothek Your knowledge hub WIEN

example high forces can damage the tip and sample, while also leading to false images due to sample deformation. Also the lateral tip movement, as indicated in Figure 2.10b, can move or drag the sample along the surface, if it is not fixed firmly. The applied normal forces on the sample (and cantilever) can be approximated by using Hooke's law $F = k * D$ with k as the cantilever spring constant (N/m) and D as deflection.
Images in contact mode are usually generated from the z-position of the piezodrive, while cantilever deflection and error signal can be used for images to enhance surface features like slopes [79].

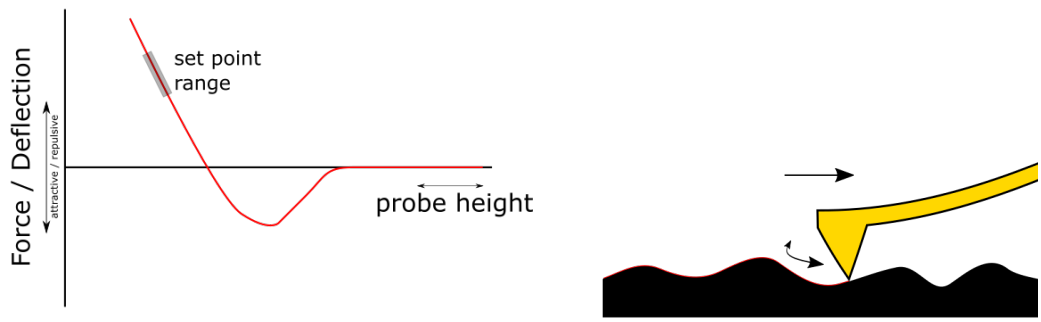

(a) Force-Distance curve

(b) Stylized contact mode operation

Figure 2.10: (a) Sample force-distance curve of an surface approach. The set point is placed in the repulsive part of the curve to ensure constant contact and cantilever tip deflection in the positive direction like in (b). (b) Stylized image of an ongoing contact mode imaging. The red line indicates the photographed area while the arrows show the lateral movement of the cantilever tip. Vertical movement is done to maintain constant force/deflection.

Oscillating Modes

Oscillating modes were proposed and tested in the original development by Binning and Quate, but were more imprecise and harder to reproduce [59] than contact mode imaging. The usage of oscillating modes spread later from better signal to noise ratio (SNR), which reduces the probe sample interaction forces and time [79].
As the name implies the cantilever oscillates during its operation. Usually a driving oscillation with a frequency close to the resonance frequency of the cantilever is chosen and monitored through the optical lever method. By approaching the surface, interaction forces arise, which damp the frequency and amplitude. The developed error signal is used by the feedback control system 2.3.4 to change the cantilever height to retain the set frequency and amplitude. The amplitude setting allows for two different operation modes distinguishable by small and large amplitudes. Small amplitude refers to the non-contact mode of the AFM, while a larger amplitude is needed in the intermittent contact mode. The need for differing amplitudes lays in their different range of operation

Die approbierte gedruckte Originalversion dieser Diplomarbeit ist an der TU Wien Bibliothek verfügbar.
The approved original version of this thesis is available in print at TU Wien Bibliothek.
TU Bibliothek Your knowledge hub WIEN

in the force-distance curve, see Figure 2.11.

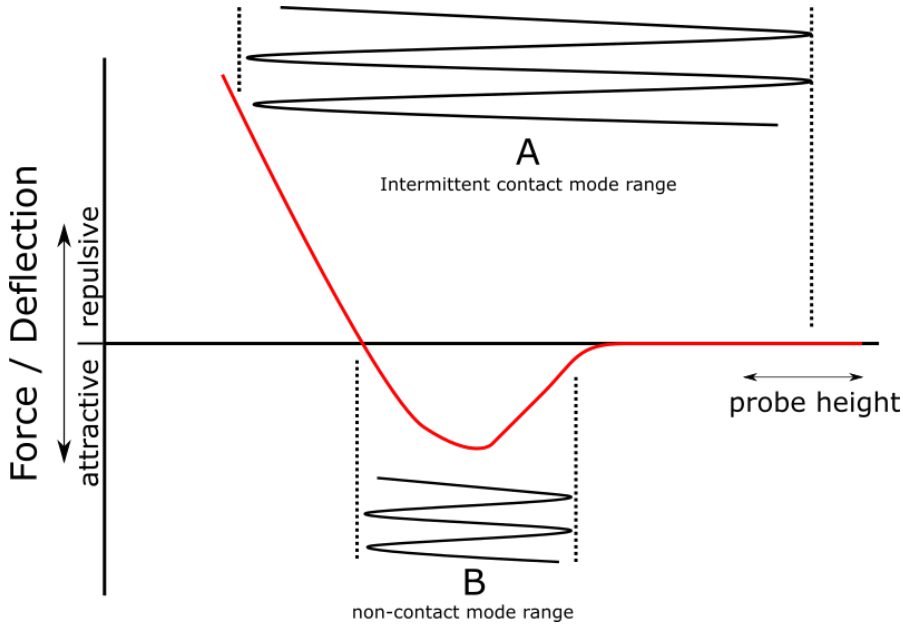

Figure 2.11: Force-distance curve with embedded range of motion for non-contact and intermittent mode. Intermittent mode (A) has a large range of motion from no-interaction force up to repulsive forces. Non-contact mode (B) can have contact with the surface but it is not possible to distinguish them from long range interaction forces. The motion range is set in the attractive regime.

Non-Contact Mode

In non-contact mode the cantilever is held in the attractive region with small amplitudes, see Figure 2.11 B, but, contrary to the name, could come into contact with the surface. However, due to the small amplitudes in the attractive region contact forces are reduced. An exact distance for surface contact can not be determined and is a matter of opinion, which interaction forces count as contact.
Generally non-contact mode can be applied for all samples where small contact forces are needed. A detrimental factor to consider while imaging under ambient condition is the contamination layer on the surface. The contamination layer is compromised of hydrocarbons and water vapor, which exercises interaction forces and dampens the oscillation. The recorded images will appear with low resolution and will not represent the actual surface topography. Although in some research it is desirable to search for water droplets on the surface [88]. With a very stiff tip and small amplitudes the cantilever can be placed inside the layer to measure the topography. However, this operation is very delicate and time consuming with the risk of a forced contact due to capillary forces [79]. Thus the intermittent contact mode is the favored mode under ambient conditions.

Die approbierte gedruckte Originalversion dieser Diplomarbeit ist an der TU Wien Bibliothek verfügbar.
The approved original version of this thesis is available in print at TU Wien Bibliothek.
TU Bibliothek Your knowledge hub WIEN

Intermittent Contact Mode

In intermittent contact mode, the amplitude range is much larger and transverses all regions in the force-distance curve, see Figure 2.11 A. Thus the tip moves from outside any interaction forces over attractive into repulsive forces. Similar to contact mode, a normal force is applied to the sample. However, force direction is always normal and no lateral forces are involved. The applied forces allow to permeate the contamination layer in ambient conditions an image the underlying surface topography. However, due to the contact force sample and tip can be damaged more easily. Figure 2.12 represents the measuring path in intermittent contact mode.

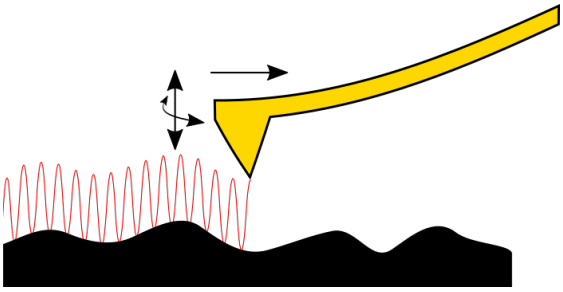

Figure 2.12: Intermittent contact mode example. Cantilever oscillation path (red line) is obstructed by the sample surface and dampens the oscillation. Only normal forces are acted on the surface.

Force Spectroscopy

Force spectroscopy is a non topography mode and records force-distance curves like Figure 2.10aa. Since the AFM is very sensitive to minimal cantilever deflections, forces in the range of pico newtons (see Results section) can be measured. Such detection capabilities can be used to record molecule-interactions [89], protein folding dynamics [90] and cell membrane behavior [91]. In this thesis force-distance curves were collected to analyze mechanical properties of collagen fibrils. Figure 2.13 shows such a force-distance curve, with a set force of of 3 μN. During the retraction, red line, a small bump can be seen, which is the attractive interaction forces of the surface.

Die approbierte gedruckte Originalversion dieser Diplomarbeit ist an der TU Wien Bibliothek verfügbar.
The approved original version of this thesis is available in print at TU Wien Bibliothek.
TU Bibliothek Your knowledge hub WIEN

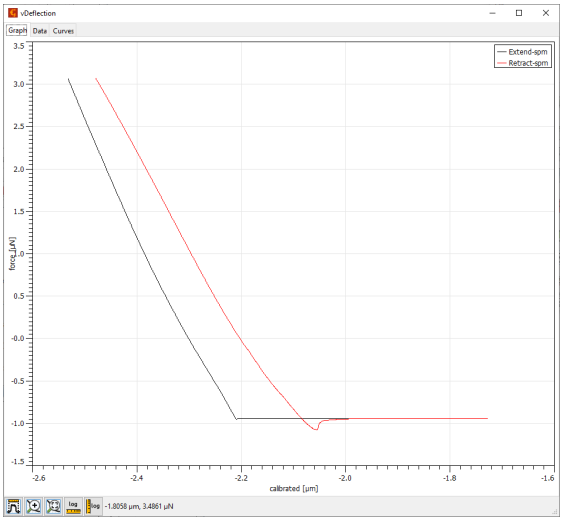

Figure 2.13: The force-distance curve on a dry collagen fibril with a maximum force of 3 μN. The red line shows the retraction with a smalll attractive force until the tip is free again. The black Line represents the extension with a clear rise in forces due to surface contact. Difference between curves can be explained by thermal drift and elastic deformation.

2.4 Nanoindentation

Nanoindentation measurements are focused on the data curves while the cantilever is in contact with the surface. By carrying out nanoindentations in a grid pattern it is possible to acquire spatial distributions of mechanical properties. On softer samples, like biological tissues, normal AFM probes can be used to indent. The collected curves must be analyzed with a contact mechanics model, e.g. Hertz or Oliver-Pharr, to determine mechanical properties.

2.4.1 Oliver-Pharr Method

A commonly used method for obtaining hardness and elastic modulus from indentation force-distance curves was originally established in 1992 by Oliver and Pharr [24]. In the paper from 1992 only self similar indenters, like the Berkovich indenter, were supposed to be used. Over the following years the method developed further with the realization that the indenter's choice is much larger than thought. Nowadays a solution exists for every axisymmetric indenter [92].
The starting point of each indentation modulus evaluation is the force-indentation curve. Figure 2.14a represents such a typical loading curve without holding the cantilever in place at max deflection. Three parameters from the curve must be measured as precisely as possible: P_{max} maximum force, h maximum indentation depth and $S = \frac{dP}{dh}$ stiffness, which is the linearized slope of the upper part of the unloading curve.

Die approbierte gedruckte Originalversion dieser Diplomarbeit ist an der TU Wien Bibliothek verfügbar.
The approved original version of this thesis is available in print at TU Wien Bibliothek.
TU Bibliothek Your knowledge hub WIEN

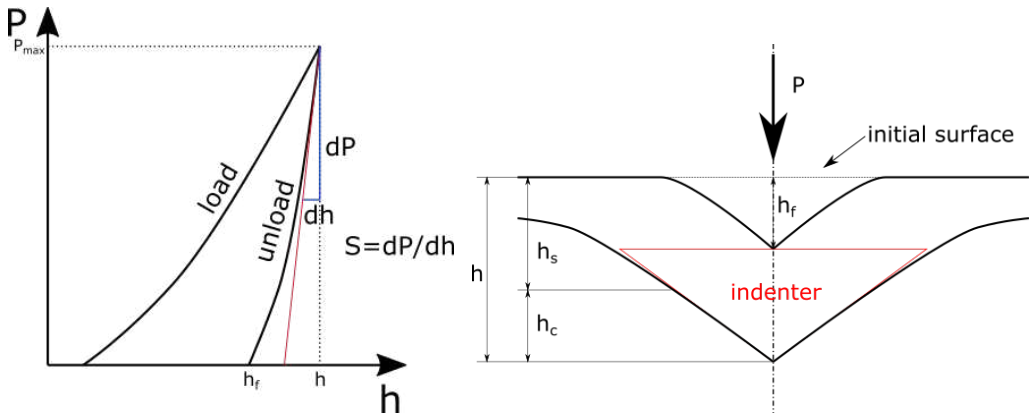

(a) Force vs indentation curve

(b) Surface imprint behavior

Figure 2.14: (a) Recorded indentation curve from which the parameters h, P_{max} and S had to be read out. (b) Schematic deformation during indentation. Note the bending material which leads to less contact area. The length of contact h_c can not be measured directly and must be assumed to determine IM.

Another important quantity, which can not be measured directly, is the length of contact between indenter and sample, h_c. Figure 2.14b shows the lifting between the sample-indenter surface during the loading process. To integrate this behavior the sample is assumed as an elastic half space. h_c can then be calculated as:

$$h_c = h - \epsilon \frac{P_{max}}{S} \tag{2.8}$$

with ϵ as a constant depending of the indenter's shape. A value of ϵ=0.75 has become the recommended choice [92]. The second term:

$$\epsilon \frac{P_{max}}{S} \tag{2.9}$$

is equal to h_s in Figure 2.14 and depicts the region with no interface contact. In experiments a clean cantilever is important, since pile up can drastically influence the real contact depth [92] and delivers false assumptions for this model. The contact depth h_c is used to calculate the area A_c, which is unique for every indenter. For this study an area function was kindly provided by Dr. Orestis Andriotis and is discussed in section 2.4.2. With a known area A_c the indentation modulus E_{eff} can be defined with the relationship between the reduced E and the stiffness S:

$$S = \beta \frac{2}{\sqrt{\pi}} E_{eff} \sqrt{A_c} \tag{2.10}$$

Die approbierte gedruckte Originalversion dieser Diplomarbeit ist an der TU Wien Bibliothek verfügbar.
The approved original version of this thesis is available in print at TU Wien Bibliothek.
TU Bibliothek Your knowledge hub WIEN

β is a dimensionless parameter used to account for deviations in stiffness due to lack of axial symmetry of the indenter. Typical values fall in the range of 1.0226 to 1.085 [92]. For this study β was set to 1, which assumes small deformation with an axisymetric punch. E_{eff} is the combined value following:

$$\frac{1}{E_{eff}} = \frac{1-\nu^2}{E} + \frac{1-\nu_i^2}{E_i} \tag{2.11}$$

which incorporates the elastic displacements of the sample and indenter. E and ν are the "samples" elastic modulus and Poisson's ratio. Indenter modulus and ratio are declared with an subscript i. Prior studies on hydrated collagen fibrils with AFM indentations have already indicated that the indentation modulus is in the one digit MPa area. The cantilever material used in this study is silicone nitride, which has a elastic modulus of 290 GPAa [93]. Thus the equation 2.11 essentially reduces to

$$\frac{1}{E_{eff}} = \frac{1-\nu^2}{E} \tag{2.12}$$

Finally by substituting eq:2.12 into eq:2.10 the indentation modulus E of the sample can be written as:

$$E = \frac{\sqrt{\pi}S}{2\beta\sqrt{A_c}}(1-\nu^2) \tag{2.13}$$

2.4.2 Contact Area Assessment A_c

Before Oliver and Pharr proposed a fitting function without the need of imaging in 1992, the common determination of A_c was imaging an indentation series on soft materials (like aluminum) [24]. The indentations were made with various depths and high quality pictures with enough contrast had to be made to precisely determine each indentation area. With the corresponding indentations depths from force-indentation curves the area function can be fitted by plotting the indentation- area vs depths. The newly developed method of Oliver and Pharr however follows the model of two springs in series with a combined compliance of C:

$$C = C_s + C_f \tag{2.14}$$

where C_s is the sample's and C_f the load frame's compliance. By inverting eq:2.10 from stiffness to compliance and incorporating C_f, C can be expressed as

$$C = C_f + \frac{\sqrt{\pi}}{2E_{eff}}\frac{1}{\sqrt{A}} \tag{2.15}$$

Die approbierte gedruckte Originalversion dieser Diplomarbeit ist an der TU Wien Bibliothek verfügbar.
The approved original version of this thesis is available in print at TU Wien Bibliothek.
TU Bibliothek WIEN Your knowledge hub

With the assumption E_{eff} is constant along all indentation depths, plottings of are possible, which is the basis of the area function. Therefore several indentations are done on a known material. Oliver and Pharr used the known area function $A(h_c)$:

$$A(h_c) = 24.5h_c^2 \tag{2.16}$$

for a Berkovich indenter on aluminum as a first estimate. C_f and E_{eff} were first estimated with the known area function and the C vs $\sqrt{A}$ plots. Other contact areas of indentations were computed with the aforementioned estimates by rearranging eq:2.15 to A:

$$A = \frac{\pi}{4}\frac{1}{E_{eff}^2}\frac{1}{(C - C_f)^2} \tag{2.17}$$

The computed A vs h_c values were then fitted into the relationship of

$$A(h_c) = 24.5h_c^2 + C_1h_c^1 + C_2h_c^{1/2} + ... + C_8h_c^{1/128} \tag{2.18}$$

The first term of eq:2.18 described the perfect Berkovich indenter while rest describes geometrical deviation from it [24].

However, the described method is used for indenters with elastic moduli of up to 1000 GPa. The cantilevers used in this study have a stiffness of 0.2 N/m to 14 N/m and cannot indent hard surfaces without damaging the tip. Furthermore a reference material with a similar elastic modulus of hydrated CFs (1-10 MPa) is not known. Thus, another method based on the convolution effect, at which the tip geometry has influence on the measured height as described in Figure 2.8, is used. By scanning a very sharp spike, which is small compared to the tip radius, the whole tip geometry can be reconstructed in one measurement. A sharp spike geometry is commonly known as a TGT1 grating. A detailed look of the reverse reconstruction is described by Keller et. al [94] and was implemented as scripts by Andriotis et al. [19].

Die approbierte gedruckte Originalversion dieser Diplomarbeit ist an der TU Wien Bibliothek verfügbar.
The approved original version of this thesis is available in print at TU Wien Bibliothek.
TU Bibliothek Your knowledge hub WIEN

Die approbierte gedruckte Originalversion dieser Diplomarbeit ist an der TU Wien Bibliothek verfügbar.
The approved original version of this thesis is available in print at TU Wien Bibliothek.

Die approbierte gedruckte Originalversion dieser Diplomarbeit ist an der TU Wien Bibliothek verfügbar.
The approved original version of this thesis is available in print at TU Wien Bibliothek.

CHAPTER 3

Material & Methods

3.1 Preface

The aim of this thesis was to determine the mechanical and geometrical behavior of collagen fibrils by repeating incubations. Properties were measured with an established nanoindenation AFM protocol [19] and a subsequent analysis in MatLabR2018b (Mathworks, USA) and Gwyddion 2.55 [1]. The experimental description, results and discussion are ordered in a way to represent the findings of each individual experiment.

3.2 Overview of Conducted Experiments

Collagen fibrils from the same thawed tail tendon of a male wild type mouse were spread over eight microscope slides and stored in a box with water absorbent silica gel. The first experiment was to determine swelling and IM changes in long term incubation at 37°C of individual collagen fibrils. This type of experiment was conducted with native and RCP fibrils. The tendon fibrils were incubated two times for 9 days with modulus and swelling testing in between, see Figure 3.1. RCP fibrils were stored only one time for 10 days due to already large differences in behavior after the 10 days. After the first set of experiments, a similar experiment was conducted. However, CFs were probed with a much higher temporal resolution to elaborate, where the onset of structural and mechanical changes were. Tendon and RCP fibrils were tested in a sequence of incubation and measurement with an incubation time of two hours at 37 °C. Subsequent AFM indentation was carried out without drying the fibrils in between. The sequence was repeated 3 times for each set of CF. The total time in incubation for individual fibrils was six hours. Thereafter, a test setup to measure the influence of drying on tendon fibrils between hydration was conducted. Two groups of tendon fibrils were hydrated and

[1] http://gwyddion.net/, David Nečas, Petr Klapetek, Czech Republic

TU Bibliothek Your knowledge hub WIEN

dried. One grouped was hydrated in PBS the other one as comparison in distilled water. At last a different experiment was done to examine remodeling effects of fibrils after deep indentation with cantilever tips.
Figure 3.1 presents an overview of of the four experiments.

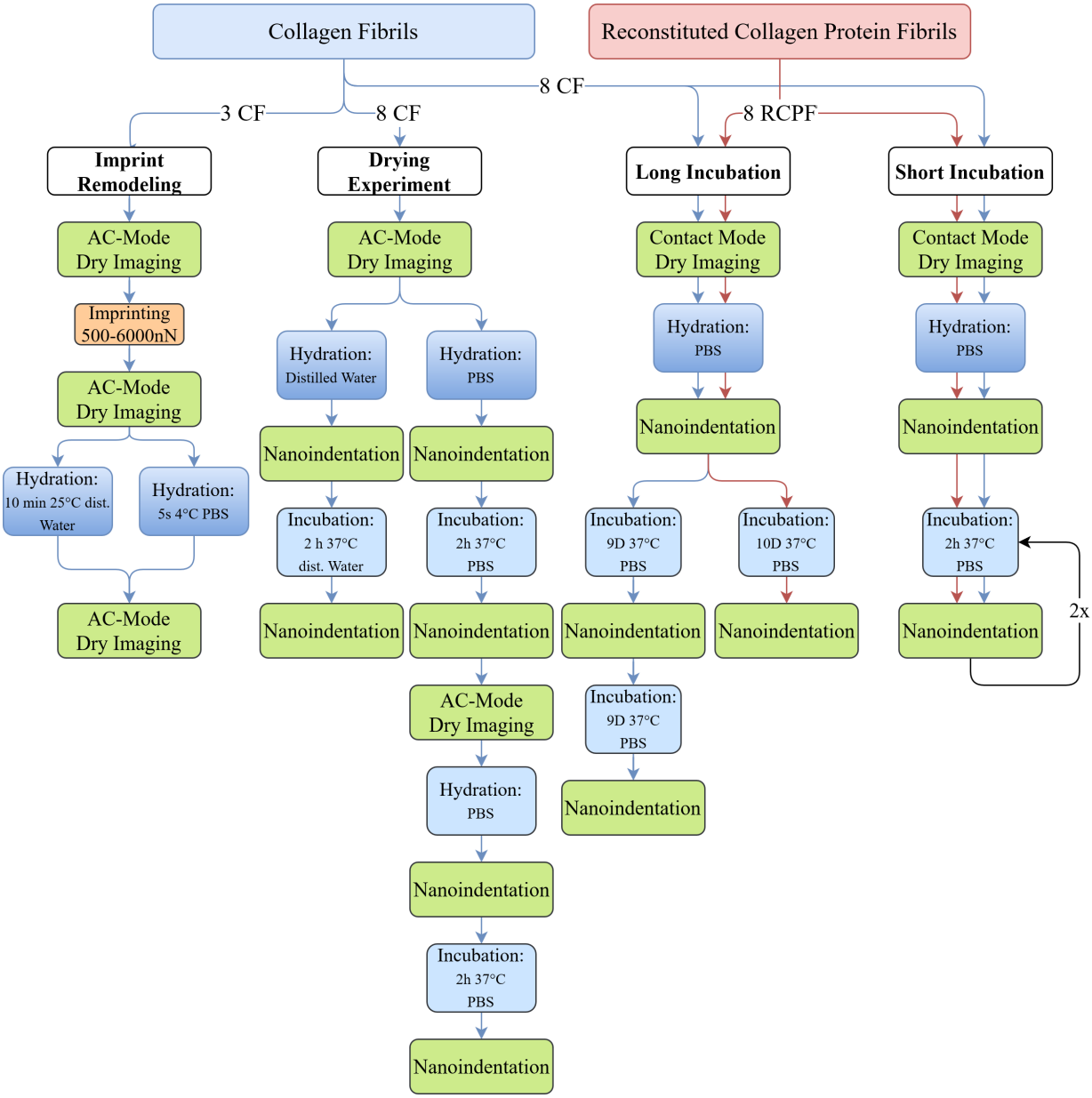

Figure 3.1: Plan of the conducted experiments.

Die approbierte gedruckte Originalversion dieser Diplomarbeit ist an der TU Wien Bibliothek verfügbar.
The approved original version of this thesis is available in print at TU Wien Bibliothek.
TU Bibliothek Your knowledge hub WIEN

3.3 Sample Preparation

Collagen Fibrils

Several fascicles of the same thawed tail-tendon of a 5 month old male wild type mouse (control fibrils in the drying experiment came from another thawed tail-tendon), are spread with tweezers and a drop of distilled water over the surface of microscope slides, according to the established method used by Andriotis et al. and Wenger et al. [19, 4]. On the microscope slide surface, individual CFs are easily accessible for an AFM tip. Each slide was thoroughly rinsed with distilled water to clean the sample from non-collagenous extracellular components proteins (COMP), proteoglycans, salts and enzymes, which inhibit clear images, indentation and prevent enzymatic decomposition. Microscope slides were stored with moisture absorption silica gel until their usage. On each slide, a ring of Polymethylmethacrylat (PMMA) was glued on using two component silicon glue to make a fluid cell. The rings were placed off-center from the fibrils to ensure enough space for the AFM chip holder and free glass surface for measuring reference slopes.

Reconstituted Collagen Proteins RCP

RCP fibrils were kindly provided from a previous work supervised by Andreas Rohatschek. They were subdivided in time of precipitation, which differentiate them in the quantity of fibrils on the slide's surface.

3.4 Atomic Force Microscopy

Experiments have been conducted on a NanoWizard NanoOptics AFM (JPK Instruments, Berlin, Germany) mounted on an inverted optical microscope (Axio Observer.D1, Zeiss).

Cantilevers

For each set of experiments, new cantilevers were used. Although, in the sequence of indentation experiments the exact same cantilever was used to minimize potential systematic error. For this work, two types of cantilevers were employed: Contact mode cantilevers and AC-mode cantilevers. Contact mode cantilevers, as said in Section 2.3.4, have a lower force constant to deflect more with lower contact forces, which also protects the samples from physical damage. These cantilevers were PNP-DB (NANOWORLD AG, Switzerland) and were used in the long/short incubation and drying experiment. The PNP-DB [2] cantilevers are beam shaped, gold coated and have four pyramidical tips per chip, two of the same type. The two tips have different lengths, which influences their force constant. The shorter cantilever (A) has a beam length of 100 μm with c=0.48 N/m (nominal stiffness) and the longer one (B) has 200 μm and a c=0.06 N/m (nominal stiffness). Cantilever A (stiffer) was used on tendon fibrils while cantilever B was used on RCP due to their lower stiffness experienced in previous tests, see Figure 3.2a

[2] https://www.nanoworld.com/pyrex-nitride-rectangular-silicon-nitride-cantilever-afm-tip-pnp-db

Die approbierte gedruckte Originalversion dieser Diplomarbeit ist an der TU Wien Bibliothek verfügbar.
The approved original version of this thesis is available in print at TU Wien Bibliothek.
TU WIEN Bibliothek Your knowledge hub

On the imprinting experiment, an AC-mode cantilever AC200TN(Olympus[3], Japan) was used to gain better image resolution for imaging of the indentations. AC-mode cantilevers typically have a higher c, which was also helpful for indenting the fibrils with high forces of up to 6000 nN. The used cantilever had manufacturer specifications of c=9 N/m, f_0=150 kHz and a length of 200 μm. The tip is tetrahedral, sharpened and located at the end of the cantilever, see Figure 3.2b.

(a) PNP-DB (b) AC200TN

Figure 3.2: Micro graphs of the applied cantilevers. (a) PNP-DB cantilever with two hard and soft beams. The shorter ones were used on tendon fibrils while the long cantilevers were used on RCP fibrils. Images kindly provided by NanoWorld. (b) scanning electron microscopy (SEM) image of a sharpend probe for AC-mode used in the imprinting experiment. The tip is located at the end of the beam. Image from footnote 3.

Spring Constant and Sensitivity Calibration

Before each experiment, the spring constant of the applied cantilever has to be determined. Since the manufacturer specifications are based on cantilever dimensions and material density, they are an estimation and cannot be taken as the true cantilever stiffness. Therefore, the Sader method [95], which is built into the JPK Software package, was used to determine the cantilever stiffness before each experiment. Correction factor of 0.817 was used, which is typically selected for the first mode of resonance frequency in air [96]. The first mode of resonance frequency was determined via thermal noise by Fast Fourier Transformation (FFT) of contact-less vibration, see Figure 3.3a. The first mode is manually selected and the spring constant, among others, is fitted to match the oscillation, see Figure 3.3b of the fitted curve.

The conversion ratio from Volts to the deflection in nm is called sensitivity and is necessary for nanoindentation to set force or amplitude in AC-mode. Sensitivity was evaluated by performing 16 force spectroscopies on a 300 x 300 μm empty slide side with a set point of 0.4V. The empty slide side should fulfill the assumption that the measured cantilever deflection Δz is equal to cantilever deflection Δd: $\Delta z = \Delta d$. Retraction curves of the spectroscopies were analyzed with a preconfigured routine which requires 3 steps:

[3] http://probe.olympus-global.com/en/product/omcl_ac200ts_r3/

Die approbierte gedruckte Originalversion dieser Diplomarbeit ist an der TU Wien Bibliothek verfügbar.
The approved original version of this thesis is available in print at TU Wien Bibliothek.
TU Bibliothek WIEN Your knowledge hub

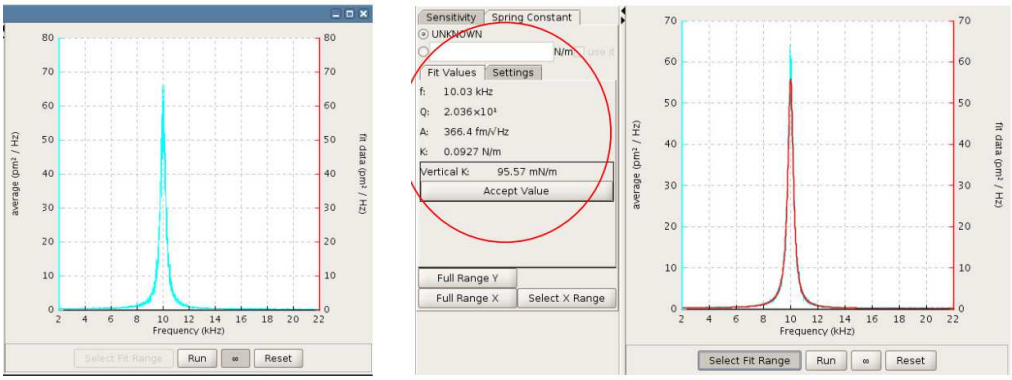

(a) Thermal noise spectrum after FFT with an peak at 10kHz

(b) The red line is the fitted harmonic oscillator of the thermal noise. The fitted parameters includes the quested spring constant(red circle)

Figure 3.3: Spring Constant calibration with JPK software. Images taken from [97, p.100].

- Set the baseline of voltage deflection (vDeflection) to zero based on the non deflected line while approaching
- Select a range on the linear upper part of the curve. A red line is linearly fitted on the selected range.
- The selection of the previous step is used as input for the remaining 15 curves. The average gradient of fitted linear lines is picked.

The picked value is converted to nm/volts and used as sensitivity.

AC Mode Calibration

For images in intermittent contact mode the frequency, at which the cantilever should be driven, must be selected. At first, a target amplitude in nm or volts has to be chosen, which the control unit tries to achieve over a selected range of frequencies. Typically the optimal driving frequency is obtained just below the resonance frequency. The used cantilever had a resonance frequency of 15 kHz and the set point was placed to around 70% of the maximum amplitude. In experiments the set point was further refined to around 90% on test fibrils to get the best trade off between image quality and contact forces.

TGT 1

Contact area A_c estimation of the used cantilever tips were needed for the computation of IM. Therefore the cantilevers used were brought in contact with a TGT1 slide and

Die approbierte gedruckte Originalversion dieser Diplomarbeit ist an der TU Wien Bibliothek verfügbar.
The approved original version of this thesis is available in print at TU Wien Bibliothek.
TU Bibliothek Your knowledge hub WIEN

images in contact mode were recorded. After an overview image was recorded a well-conditioned spike was chosen for a higher resolution image. A single spike was imaged with a resolution of 512 pixel (px) x 512 px and no scanning artifacts should be present. A scan line rate of 1 Hz, Setpoint of 0.3V and IGain of 170 Hz yielded the best results. More details on the contact area assessment can be found in section 2.4.

3.5 Height and Indentation Modulus evaluation

The height and indentation modulus were computed with several matlab scripts provided by Dr. Orestis Andriotis. Both properties are calculated from the same force-map-files, which result from force spectroscopy measurements. Additionally the indentation modulus evaluation requires the deconvoluted cantilever tips for the contact area A_c. After outlining the used tip manually, Figure 3.4a, the script computed a 3D plot of the tip with the projected Area A_c, Figure 3.4b.

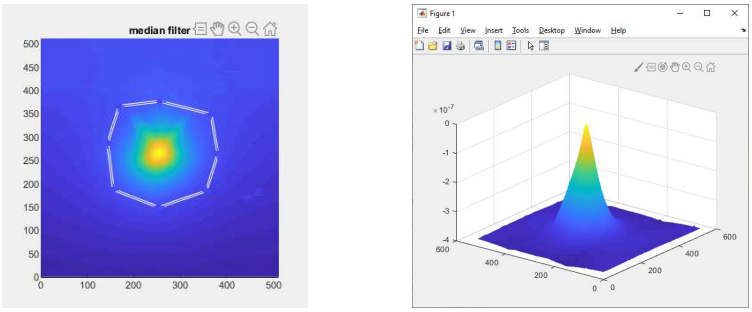

(a) Manually selected outline on the TGT1 contact mode image

(b) 3D representation of the tip after deconvolution

Figure 3.4: Deconvolution process with a matlab script from Dr. Orestis Andriotis.

This procedure has to be repeated for each cantilever, which was used for nanoindentation experiments. In this work, a total of six cantilevers were used for nanoindentation and therefore deconvoluted. After tip deconvolution the indentation modulus routine can be started by loading the tip into the matlab workspace and by selecting the file folder with the corresponding jpk-force-map-files. Afterwards a reference slope needs to be entered for each fibril indentation, which was calculated beforehand. Reference slopes were the mean linearized slopes of the upper part of the unloading curve in a force-distance curve, Figure 2.10a. The used force distance curves were from the surface of the microscope slide around each fibril. Afterwards each fibril was outlined, Figures 3.5a, and the force curves were reviewed for correct contact point assumption Figure 3.5b.

The same steps are needed to determine the height of the fibrils but without the prerequisite of a deconvoluted tip and without reviewing of the first contact point.

Die approbierte gedruckte Originalversion dieser Diplomarbeit ist an der TU Wien Bibliothek verfügbar.
The approved original version of this thesis is available in print at TU Wien Bibliothek.
TU Bibliothek Your knowledge hub WIEN

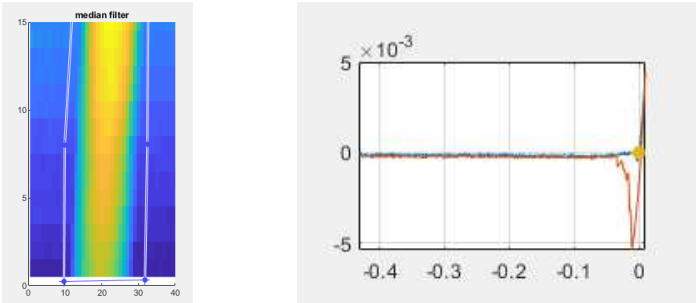

(a) Manually selected outline of each force spectroscopy fibril image.

(b) Review of the automatically chosen contact point (yellow circle). Circle should be at the start of the gradient to mark the contact point, if not the curve is rejected. Red Line: Retraction; Blue Line: Extention.

Figure 3.5: Indentation modulus computation steps.

3.6 Long Incubation

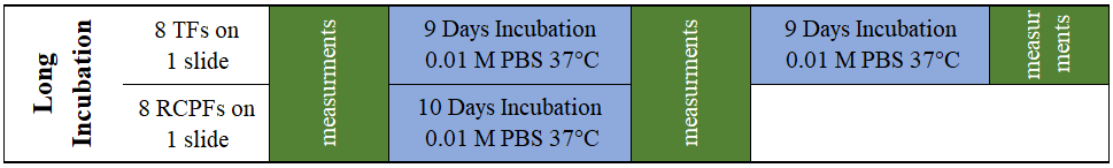

Figure 3.6: Long incubation experiment overview of tendon fibril (TF) and RCP.

In this first experiment, a slide with accessible tendon fibrils was inspected with a light microscope to find distinctive fibril intersections. On the site, eight fibrils with distinct D-Banding were chosen and imaged in dry condition. Typically the images were 1 μm x 2 μm in area with an resolution of 60 px x120 px. Afterwards the eight fibrils were immersed with 0.01 M PBS at 25°C room temperature. Nanoindentation was carried out with a force of 1 nN. The force value was chosen to not indent them deeper than 10% of their height. Thus no detectable damage and influence of the hard slide surface is ensured [19]. The area of each force spectroscopy experiment was chosen as 1/3 mica surface, 1/3 fibril and 1/3 mica surface, see Figure 3.5a. The measurements of the surface are needed for reference slope calculation, as explained in Height and Indentation Modulus evaluation section. The areas of measurements were 1.4-1.5 μm x 2.1 μm large with 40 x 14 indentation spots. It was assured that at least 10 line spots lie on the fibril. After the first round of force spectroscopy, the slide was incubated with 0.01 M PBS at 37°C in a thermally controlled incubator. Nine days later the slide was extracted from the incubator and rinsed with distilled water to prevent crystallization on the surface from the PBS. Thereafter the force spectroscopy was repeated in PBS with the same parameters as in the first round and subsequently incubated for nine days. The last

Die approbierte gedruckte Originalversion dieser Diplomarbeit ist an der TU Wien Bibliothek verfügbar.
The approved original version of this thesis is available in print at TU Wien Bibliothek.
TU Bibliothek Your knowledge hub WIEN

round of force spectroscopy was done in PBS after a final rinsing. Figure 3.6 shows the experimental plan.

The same experimental setup was performed on RCP fibrils. Dry images with a size of 1-1.5 x 2μm were done to confirm typ I collagen with D-Banding. The force set point was reduced to 0.4 nN to take into account the smaller and softer fibrils. Still the stiffer cantilever of PNP-DB was used to reduce methodical errors. The size of the force spectroscopy map was reduced to have the same 1/3,1/3,1/3 distribution between surface and fibril area. The image dimensions ranged between 0.6-0.8 μm x 1-1.4 μm with 40x17-20 indentation spots. Thereafter the slide was incubated and measured again. A second incubation was considered, but abandoned due to focusing more on tendon fibrils.

The recorded force curves of tendon fibrils and RCP were statistically evaluated, see Section 3.10 , for changes between incubation and inter group differences. Three cantilever tips on three different chips were used in this experiment, see Table 3.1.

Table 3.1: Cantilever spring constants of PNP-DB A. Evaluated with Sader method and used in long incubation experiment. Manufacture's specifications listed a 0.48 N/m spring constant.

Cantilever	K (Sader) [N/m]
PNP-DB 7A	0.2129
PNP-DB 15A	0.2473
PNP-DB 17A	0.2320

3.7 Short Incubation

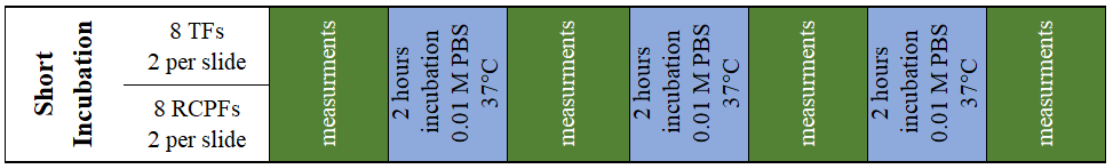

Figure 3.7: Short incubation experiment overview.

The second experiment increased the frequency of incubation by reducing the incubation time from several days to 2 hours, see Figure 3.7. Two fibrils per slide with D-Banding were selected for measurements. Subsequently 0.01 M PBS was added and force spectroscopy with a force of 1 nN was done. The fibrils were indented on the same spots with a force map size of 40 x 15 indentation spots. Afterwards the slides were incubated at 37 °C in 0.01 M PBS for two hours. Force Spectroscopy area was 0.6-1.5 μm x 1-2 μm based on the size of the fibril. This procedure was repeated until the fibrils were for 6 hours

Die approbierte gedruckte Originalversion dieser Diplomarbeit ist an der TU Wien Bibliothek verfügbar.
The approved original version of this thesis is available in print at TU Wien Bibliothek.
TU Bibliothek Your knowledge hub WIEN

incubated and four times indented. The stiffer cantilever PNP-DB 17A, Table 3.2 was used.

The same setup was done with four slides of RCP fibrils, but with a softer cantilever tip to gain a better SNR ratio, see Table 3.2 for cantilevers. The area of Force Spectroscopy was between 0.7-1.2 μm x 1-1.5 μm with 0.3 nN indentation force.

Table 3.2: Cantilever spring constants of PNP-DB.

Cantilever	K (Sader) [N/m]
PNP-DB 17A	0.2320
PNP-DB 31B	0.047

3.8 Drying Experiment

Figure 3.8: Drying experiment overview.

Based on the results of previous measurements this experiment was designed to look for the influence of drying and rehydration on collagen fibrils with two different solutions, distilled water and 0.01 M PBS. Furthermore D-Banding spacing was analyzed for a presumed prestraining of the CF application method. Therefore, 2 microscope slides with tendon fibrils were used. The eight fibrils per slide were imaged in dry state in AC mode. For better D-Banding spacing evaluation a resolution of 512 px x 768 px for an area of 1 μm x 1.5 μm per fibril was chosen. The first slide was hydrated with 0.01 M PBS and force spectroscopy with 1 nN indentation force was conducted with a resolution of 40 px x 15 px over an area of 0.8-1.2 μm x 1.7 μm. After the first round the slide was incubated for 2 hours in PBS at 37°C similar to the short incubation. Then a second round of force mapping with the same parameters was done in PBS. The fibrils were rinsed with distilled water and stored with humid absorbent silica for 8 days. Following dry images were made again with the same parameters in AC mode for D-Banding changes. Lastly the fibrils were force mapped again in PBS with 1 nN set point force. This whole process was repeated with the same parameters one more time on the same fibrils to confirm or negate changes seen in the first cycle. To measure the influence of the used hydration solution a second slide with CF, from another thawed mouse tail, was evaluated. Instead of PBS, distilled water was utilized and only one round of incubation was done. The used cantilevers are listed in Table 3.3.

Die approbierte gedruckte Originalversion dieser Diplomarbeit ist an der TU Wien Bibliothek verfügbar.
The approved original version of this thesis is available in print at TU Wien Bibliothek.
TU Bibliothek WIEN Your knowledge hub

Table 3.3: Cantilever spring costants used in drying experiment. PNP ones were utilized in force mapping and AC 200TN in AC-mode imaging with higher pixel resolution.

Cantilever	K (Sader) [N/m]
PNP-DB 38A	0.2000
PNP-DB 42A	0.2222
AC 200TN	13.68

3.8.1 D-Banding Evaluation

The distance between two D-Bands was evaluated with a custom written script in MATLAB R2018b. The raw images from AC-mode scanning were handed over to the script. Additionally two settings have to be commited: the length of the images (slow axis) and the pixel size of the moving average filter, which allows better peak detection. A value of 3 pixels yielded a sufficient result without smoothing too much. Afterwards the highest pixel in the first and last line were selected as the start and end points for the height profile, see Figure 3.9a. A linear trend curve was subtracted to remove the general slope, which is inherent to the measurement. Peaks in the profile were located with a build in matlab function findpeaks(). A minimum peak distance of 40 nm was selected to avoid over fitting. Lastly horizontal distances between each peak were calculated. Figure 3.9b shows the height line with located peaks.

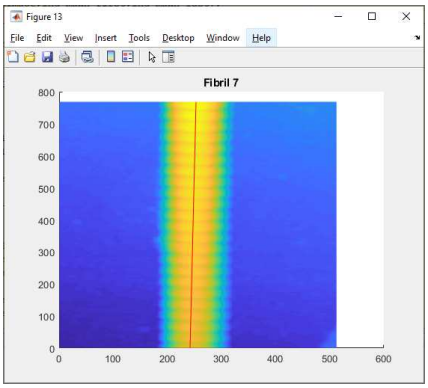

(a) Height Image with selected line for evaluation.

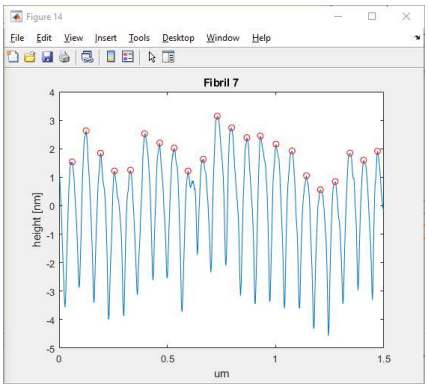

(b) Analysed height profile of a fibril.

Figure 3.9

Furthermore a FFT was done on the height profile. In the resulting spatial frequency spectrum, the three highest peaks were chosen for inspection. By inverting peak frequencies wavelength λ changes can be seen. FFT was performed on each dry image.

Die approbierte gedruckte Originalversion dieser Diplomarbeit ist an der TU Wien Bibliothek verfügbar.
The approved original version of this thesis is available in print at TU Wien Bibliothek.
TU Bibliothek Your knowledge hub WIEN

Figure 3.10: Imprint experiment overview.

3.9 Imprint Remodeling

A recognizable site of collagen fibrils with three intertwined CFs was located and imaged under dry conditions in AC-mode. The image area was 6 μm x 6 μm with a resolution of 1024 px x 1024 px, Figure 3.11a. Images of individual fibrils were the size of around 1 μm x 1 μm with 256 x 256 px - 332 px. The imprints were carried out with forces between 500 to 6000 nN. An hold time of 10 seconds after reaching the maximum force was introduced to ensure lasting imprints. Figure 3.11a shows the spots of indentation on the three fibrils. After indentation 4μl of 25°C warm distilled water was added to the fluid cell. After 10 minutes the fluid was removed and the fibrils were imaged after drying under ambient conditions. A second imprinting experiment was done on fibril no. 3 (f3, Figure 3.11b) with higher forces of 5000 to 6000 nN, which was the maximum force applicable due to range limitation of the photo multiplier and used cantilever. Figure 3.11 indicates the spots of imprints for the second experiment. Afterwards the sample was immersed in 4°C PBS (Sigma, 1mM, 7.4pH) for 5 seconds before drying and imaging.

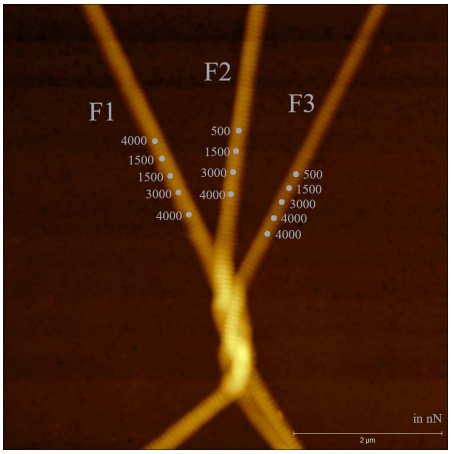

(a) Overview of intertwined collagen fibrils with marked imprint spots.

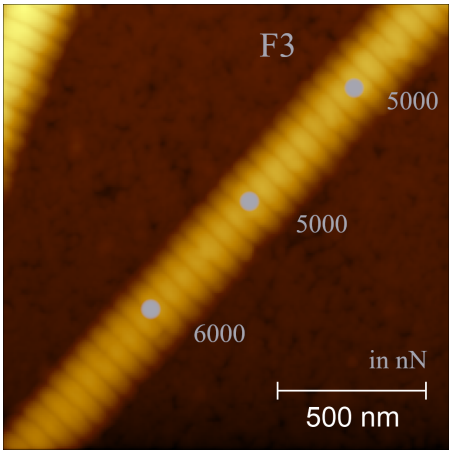

(b) Second imprints on fibril no. 3 (same fibril as in the first experiment) with higher forces.

Figure 3.11: Imprint spots of the two experiments

Die approbierte gedruckte Originalversion dieser Diplomarbeit ist an der TU Wien Bibliothek verfügbar.
The approved original version of this thesis is available in print at TU Wien Bibliothek.
TU Bibliothek Your knowledge hub WIEN

3.10 Statistics

Statistical evaluation was performed with MATLAB's implemented statistics and machine learning toolbox. Each set of height and indentation modulus data points for a fibril was analyzed for outliers, which were defined as values greater than ±3 median absolute deviation (MAD) and removed. The adjusted data sets were tested against normal distribution via a One-sample Kolmogorov-Smirnov test. As a test for significance Welch's t-test for two sided independent samples with unequal variances was chosen. Significance level was set to 5% with different tail settings to test for greater, lesser or unequal means of population. Furthermore, to combine individual results for each fibril at different time points into a representative fibril the means and standard deviations were pooled according to following equations 3.1

$$\mu_{pooled} = \frac{\sum_i n_i \mu_i}{\sum_i n_i} \qquad \sigma_{pooled} = \sqrt{\frac{\sum_i (n_i - 1)\sigma_i^2}{\sum_i (n_i - 1)}} \tag{3.1}$$

with n sample size, μ mean, σ standard deviation and i pool group.

Die approbierte gedruckte Originalversion dieser Diplomarbeit ist an der TU Wien Bibliothek verfügbar.
The approved original version of this thesis is available in print at TU Wien Bibliothek.
TU Bibliothek Your knowledge hub WIEN

Die approbierte gedruckte Originalversion dieser Diplomarbeit ist an der TU Wien Bibliothek verfügbar.
The approved original version of this thesis is available in print at TU Wien Bibliothek.

CHAPTER 4

Results

4.1 Preface

In this chapter results for incubation and drying experiments are presented and compared in two forms: absolute and relative values. Outcomes of the first two experiments, long and short incubation, were combined in sections regarding height and indentation modulus changes. The appearance of significance on the pooled relative change between the first two instances of time is based on the calculation for retrieving relative change and is debated in the discussion chapter. All relative changes are written in Chapter: Appendix 6.

4.2 Incubation induced height changes

4.2.1 Long Incubation Results

The first experiment was performed to verify previous observed swelling of tail tendon collagen fibrils by incubating them for 9 days. The first measurements assessed a mean height of 218 nm with a range of 150 nm to 287 nm Figure 4.1b. After the first incubation period of 9 days all individual fibrils were swollen significantly by testing absolute values. However, by combining the means of each fibril into an absolute pooled mean fibril the swelling was non significant, see statistic table 4.1. Relative changes showed a mean swelling of 7% with the biggest growth of 13% from fibril 8. No further swelling was observed after the second incubation for relative and absolute pooled values. On individual fibril level, fibril 1 and 3 swoll significantly for the second time. However, most other fibrils even shrank, but not to the initial height. This behavior can be seen in both graphs 4.1a and b. The pooled mean height (bold black line) rose after the first incubation and then receded a bit for subsequent incubation on the same level.
RCP height measurements yielded a different result. The mean height was 62 nm with a

TU WIEN Bibliothek Your knowledge hub

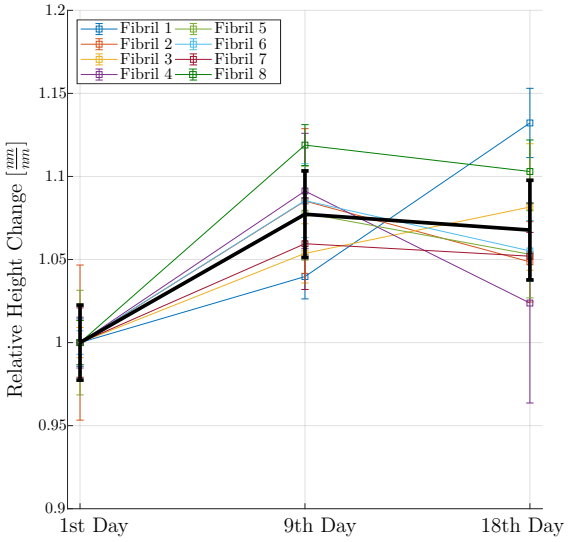

(a) Relative fibril swelling with pooled mean fibril.

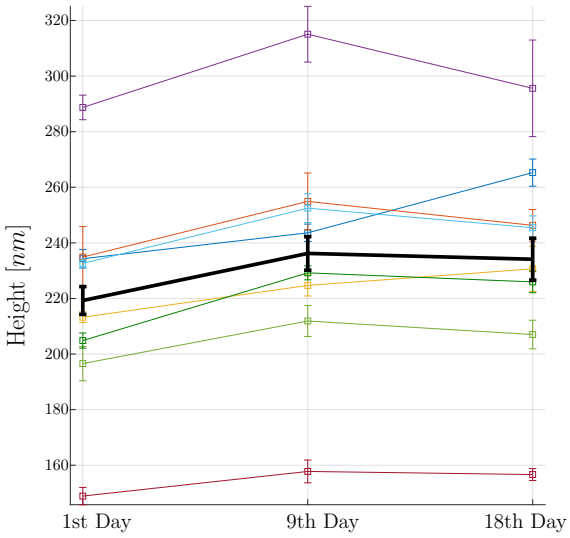

(b) Fibril height with pooled mean fibril.

Figure 4.1: Error bars of TF height measuring from long incubation swelling experiment. Line marks are the means of each fibril. Whiskers represent the Standard Deviation σ. (a) Relative height changes with an average swelling of 7% after the first incubation. Second incubation did not lead to further swelling. (b) Absolute fibril height, which gives an overview of the difference in fibril diameter. Most Fibrils were in the range of 200 to 240nm.

range from 48 nm to 72 nm Figure 4.2, which is considerable smaller than the native CF. After the first incubation no swelling behavior was visible and only one fibril, f1, swell significantly, see table 4.2 for the statistical evaluation. Some fibrils decreased its height after incubation (fibrils 3,5), see Figure 4.2. Further incubation was deemed unnecessary due to already different behavior after the first round.

Die approbierte gedruckte Originalversion dieser Diplomarbeit ist an der TU Wien Bibliothek verfügbar.
The approved original version of this thesis is available in print at TU Wien Bibliothek.
TU Bibliothek WIEN Your knowledge hub

Table 4.1: P-Values of Welch test (5% significance, left tail, test for swelling) of TF height measurements. Values < 0.05 are highlighted for significance. Individual fibrils display uniformly a significant swelling after the first 9 days incubating(0* indicates p-values lower than 0.001). The next 9 days show only 2 fibrils with further swelling. By combining all fibrils into a pooled mean fibril (one value per fibril) no significant swelling is seen.

Time/Fibrils	**1**	**2**	**3**	**4**	**5**	**6**	**7**	**8**
1D vs 9D	**0***	**0***	**0***	**0***	**0***	**0***	**0***	**0***
9D vs 18D	**0***	0.992	**0.014***	0.999	0.984	1	0.799	0.991
1D vs 18D	**0***	0.002	**0***	0.095	**0***	**0***	**0***	**0***
Mean Fibril 1D vs 9D	0.218							
Mean Fibril 1D vs 18D	0.238							
Mean Fibril 9D vs 18D	0.538							

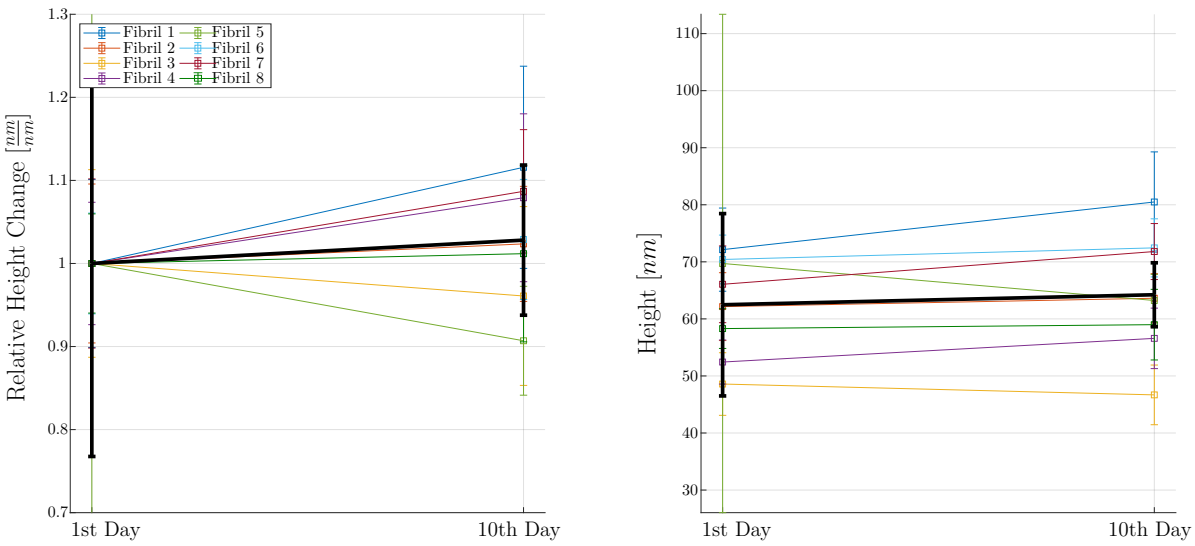

(a) Relative fibril swelling with pooled mean fibril

(b) Individual RCP fibril height with pooled mean fibril

Figure 4.2: Error bars of RCP fibrils height measuring from long incubation swelling experiment. Line marks are the means of each fibril. Whiskers are Standard Deviation σ. (a) Relative swelling behavior with no visible swelling after incubation. (b) RCP measured height which show much smaller diameters of RCP in comparison to tail tendon fibrils.

Die approbierte gedruckte Originalversion dieser Diplomarbeit ist an der TU Wien Bibliothek verfügbar.
The approved original version of this thesis is available in print at TU Wien Bibliothek.
TU Bibliothek Your knowledge hub WIEN

Table 4.2: P-Values of Welch test (5% significance, left tail, test for swelling) of RCP. Significant values are highlighted in bold. Only one fibril swell significantly. Mean fibril comparison also shows no significant swelling.

Time/Fibrils	**1**	**2**	**3**	**4**	**5**	**6**	**7**	**8**
1D vs 10D	**0.002***	1	1	1	1	0.442	0.564	1
Mean Fibril 1D vs 10D	0.218							

4.2.2 Short Incubation Results

Short incubation had the premise to measure the time frame in which the majority of swelling in fibrils occur. TF had a mean initial height of 123 nm, which rose to 127.9 nm, a 4% increase, after the first 2h of incubation. The statistical test provided a similar result like the long incubation. Six out of the eight tested fibrils did swell significantly, and the non-significant ones were close to significance with p-values of 0.05 and 0.06, see Table 4.3. However, by testing absolute pooled mean fibrils after the first incubation no significance was prevalent, see table 4.3. In the next two sets of incubation only fibril 1 and 5 showed another significant swelling. The pooled mean fibrils did not exhibit any extra swelling, see Figure 4.3b for visual representation. The relative height chart of Figure 4.3a shows the swelling after 2h. Although the first 2 hours present the majority of swelling, the mean swelling was lower than in long incubation, 4% vs 7%. Further swelling may likely occurs after 6h.
With RCP only two fibrils showed significant swelling in the first two hours, Table 4.4b. Further incubation didn't show any swelling, see Figure 4.4. The absolute and relative pooled mean fibrils swell around 4% after 2 hours but came back down to the initial height. However, the σ is too large to see a significant increase in diameter, see whiskers in Figure 4.4 . The RCP mean height was 66.4 nm, around the half of native fibrils, which is similar to the set of RCP fibrils from long incubation.

Table 4.3: P-Values of Welch test (5% significance, left tail, test for swelling) of TF. Significant values are highlighted in bold.

Time/Fibrils	**1**	**2**	**3**	**4**	**5**	**6**	**7**	**8**
0h vs 2h	**0.01***	**0***	0.05	**0***	**0.01***	**0***	0.06	**0***
2h vs 4h	0.99	0.55	0.21	0.57	0.91	0.38	0.25	1
4h vs 6h	**0.01***	0.15	0.3	0.98	**0***	0.06	0.09	0.9
Mean Fibril 0h vs 2h	0.420							
Mean Fibril 2h vs 4h	0.439							
Mean Fibril 4h vs 6h	0.419							

Die approbierte gedruckte Originalversion dieser Diplomarbeit ist an der TU Wien Bibliothek verfügbar.
The approved original version of this thesis is available in print at TU Wien Bibliothek.
TU Bibliothek WIEN Your knowledge hub

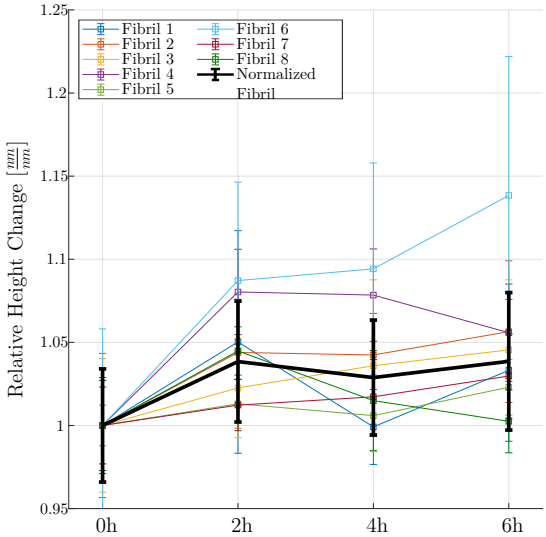

(a) Relative TF swelling with overlayed pooled fibril.

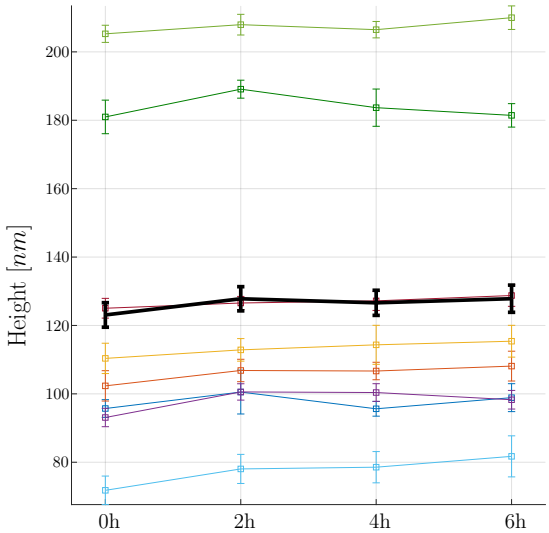

(b) Individual measured fibril height and pooled mean fibril.

Figure 4.3: Short incubation height error bars of TF. (a) Relative fibril height shows the largest swelling after 2h of incubation. Following incubations show a small decline and recover after the final incubation. (b) Representation of the fibrils heights, with a large height spectrum from 75 nm up to 220 nm.

Die approbierte gedruckte Originalversion dieser Diplomarbeit ist an der TU Wien Bibliothek verfügbar.
The approved original version of this thesis is available in print at TU Wien Bibliothek.
TU Bibliothek Your knowledge hub WIEN

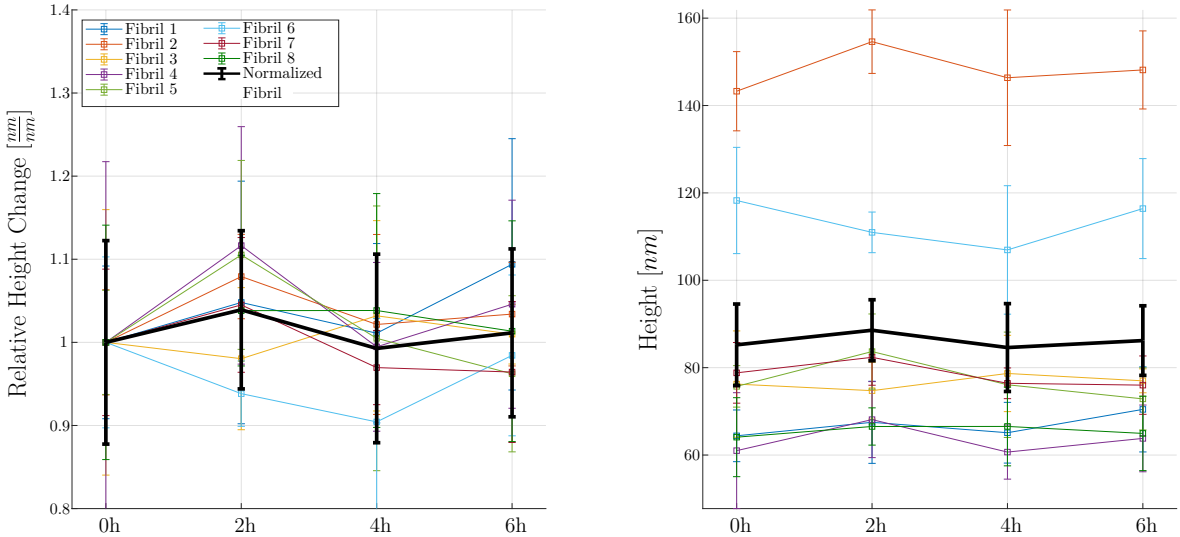

(a) RCP fibril swelling with pooled fibril

(b) Individual measured RCP fibril height

Figure 4.4: Short incubation height error bars of RCP. (a) Relative fibril height with no clear swelling behavior after incubation. (b) Measured fibrils height of RCP. Comparing them to Figure 4.3 shows the smaller diameter.

Table 4.4: P-Values of Welch test (5% significance, left tail, test for swelling) of RCP. Significant values are highlighted in bold.

Time/Fibrils	**1**	**2**	**3**	**4**	**5**	**6**	**7**	**8**
0h vs 2h	0.16	**0***	0.66	0.06	**0***	0.97	0.09	0.19
2h vs 4h	0.77	0.95	0.09	0.99	0.97	0.83	0.99	0.5
4h vs 6h	0.05	0.36	0.75	0.13	0.8	**0.04***	0.58	0.68
Mean Fibril 0h vs 2h	0.424							
Mean Fibril 2h vs 4h	0.6							
Mean Fibril 4h vs 6h	0.46							

Die approbierte gedruckte Originalversion dieser Diplomarbeit ist an der TU Wien Bibliothek verfügbar.
The approved original version of this thesis is available in print at TU Wien Bibliothek.
TU Bibliothek Your knowledge hub WIEN

4.3 Indentation Modulus changes induced by incubation

4.3.1 Long Incubation Results

The first 9D incubation showed a 50% reduction of the indentation modulus. The second 9D incubation led to another 24% decrease of the indentation modulus, see Figure 4.1. The initial fibrils had a mean IM of 3.4 MPa. Fibril 4 exhibited a higher IM, x1.6 the mean, but decreased to 38% after the first incubation, which brought its IM into similar range like the other fibrils. Unfortunately, three fibrils, initially 6,7 and f1 after the second round, could not be evaluated due to unexpected file writing errors of the corresponding .jpk files. Statistical evaluation concluded a significant decrease in indentation modulus after 9 days for individual fibrils and also the pooled mean fibril. Furthermore the second incubation also saw a significant decrease, but with the caveat of only 5 evaluable datapoints in the pooled mean fibril, see table 4.5.

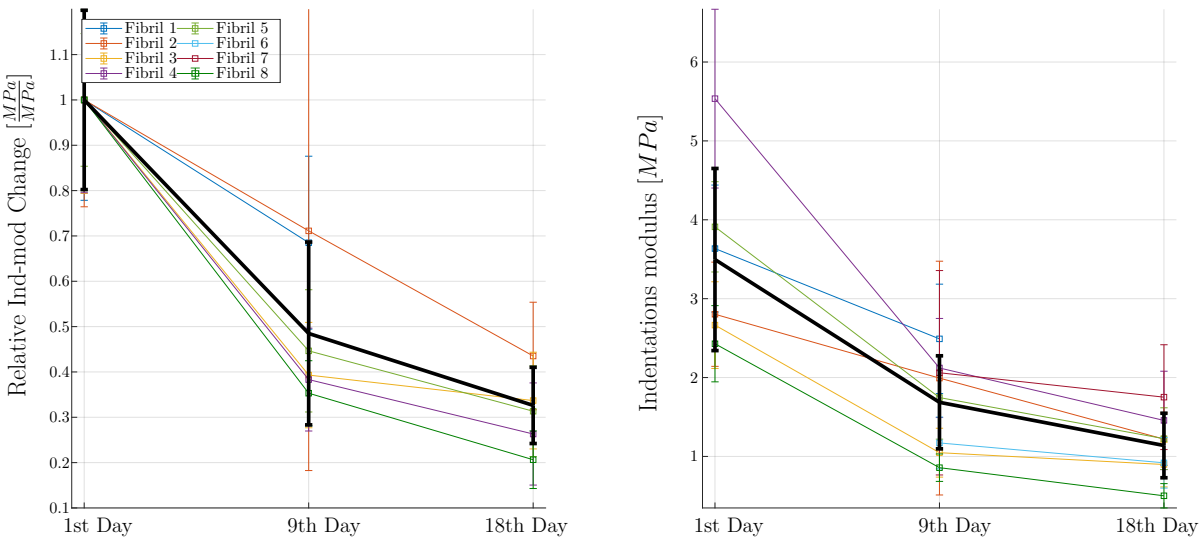

(a) Relative TF indentation modulus with pooled mean

(b) Indentation modulus

Figure 4.5: (a) The relative values show a significant decline in indentation modulus after the first incubation. The stiffness fell to around 50% of the initial value. Further incubation showed another decline, but with less softening. (b) The initial indentation modulus was relatively (expect fibril 4) homogeneous around 3.4 MPa and remained homogeneous also after two incubations.

Die approbierte gedruckte Originalversion dieser Diplomarbeit ist an der TU Wien Bibliothek verfügbar.
The approved original version of this thesis is available in print at TU Wien Bibliothek.

Table 4.5: P-Values of Welch test (5% significance, right tail, test for softening) of TF. Significant values are highlighted in bold.

Time/Fibrils	1	2	3	4	5	6	7	8
1D vs 9D	**0***	**0.05***	**0***	**0***	**0***	**-**	**-**	**0***
9D vs 18D	-	0.051	0.1	**0.006***	**0.004***	**0.029***	0.23	**0***
1D vs 18D	-	**0***	**0***	**0***	**0***	-	-	**0***
Mean Fibril 1D vs 9D	**0.005***							
Mean Fibril 1D vs 18D	**0.002***							
Mean Fibril 9D vs 18D	**0.04***							

RCP fibrils exhibited a different incubation behavior. The initial IM was already considerably lower than TF with a mean of 1.5 MPa vs. 3.5 MPa. The incubation presented also no softening but rather a increase in their IM. Although, the relative changes, Figure 4.6a, present an irregular IM behavior.

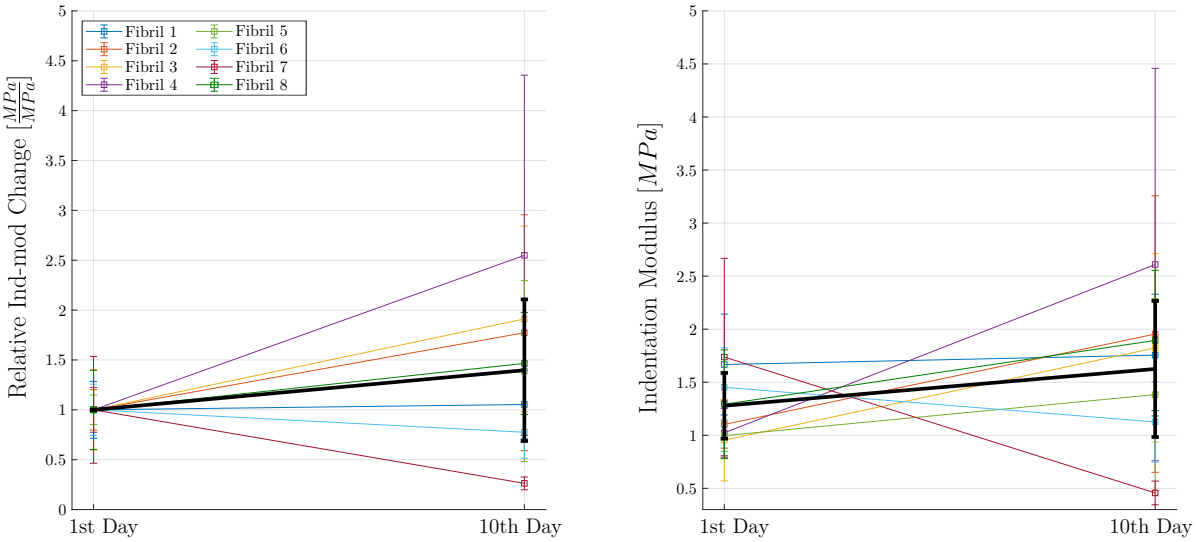

(a) Relative RCP indentation modulus

(b) Measured indention modulus of RCP fibrils

Figure 4.6: RCP indentation modulus of long incubation.

Die approbierte gedruckte Originalversion dieser Diplomarbeit ist an der TU Wien Bibliothek verfügbar.
The approved original version of this thesis is available in print at TU Wien Bibliothek.

Table 4.6: P-Values of Welch test (5% significance, left tail, test for softening) of RCP. Significant values are highlighted in bold. Two significant IM decreases were observed on individual fibril level, but no significant change was seen on pooled mean fibril.

Time/Fibrils	**1**	**2**	**3**	**4**	**5**	**6**	**7**	**8**
1D vs 10D	0.68	0.99	0.99	0.99	0.87	**0.012***	**0***	0.99
Mean Fibril 1D vs 10D	0.90							

4.3.2 Short Incubation Results

The IM of TF did not drop significantly like in the first test with 9 days of incubation. Four out of seven fibrils (f1,2,3,6) softened significantly after two hours. Two of those fibrils increased the IM again (f1,f2) while still being under the initial IM, Figure 4.7. The next 2 incubations did not lead to any overall significant softening behavior, see Table 4.7. Unfortunately, the data for fibril 3 was not analyzable due to a file error.

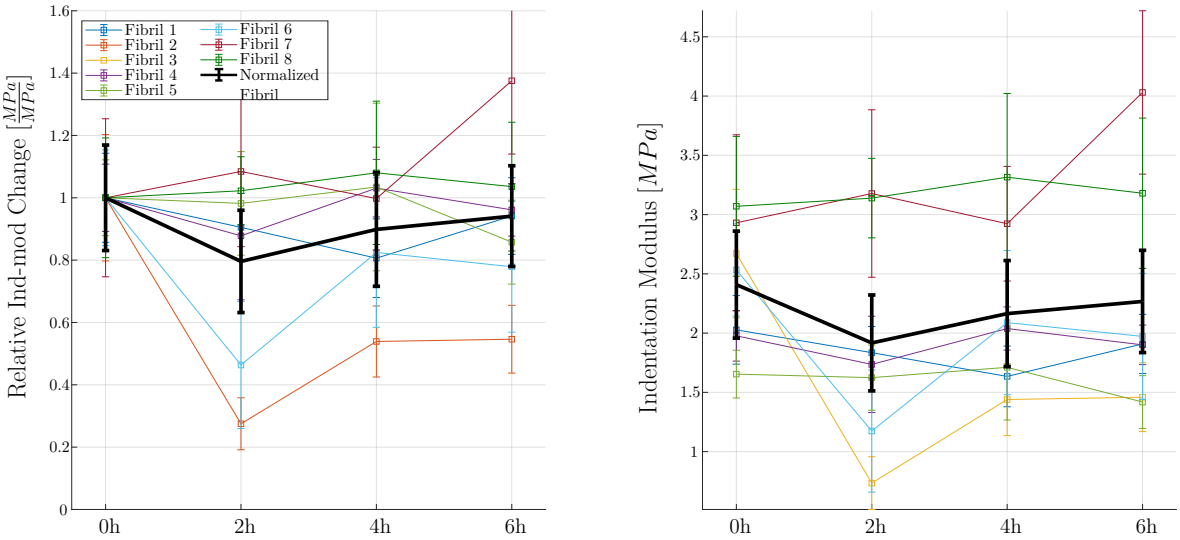

(a) Relative indentation modulus changes.

(b) Indentation modulus with pooled mean

Figure 4.7: Indentation modulus errorbars of short incubation from TF.

The IM of RCP fibrils could not be evaluated due to several problems, which culminated

Die approbierte gedruckte Originalversion dieser Diplomarbeit ist an der TU Wien Bibliothek verfügbar.
The approved original version of this thesis is available in print at TU Wien Bibliothek.

Table 4.7: P-Values of Welch test (5% significance, right tail, test for softening) of TF. Significant values are highlighted in bold.

Time/Fibrils	1	2	3	4	5	6	7	8
0h vs 2h	**0.036***	**0***	-	**0.031***	0.377	**0***	0.808	0.645
2h vs 4h	**0.029***	1	-	0.99	0.73	1	0.14	0.794
4h vs 6h	0.994	0.566	-	0.037	**0.020***	0.301	1	0.299
Mean Fibril 0h vs 2h	0.126							
Mean Fibril 2h vs 4h	0.708							
Mean Fibril 4h vs 6h	0.588							

in non usable values. The surface around RCP fibrils was sticky due to the production process and therefore the reference slopes were not accurate. Outlining the original height images displayed large gradient changes, which shouldn't occur, see Figure 4.8a, and the automatic contact point determination was difficult to perform due to low SNR, see Figure 4.8b.

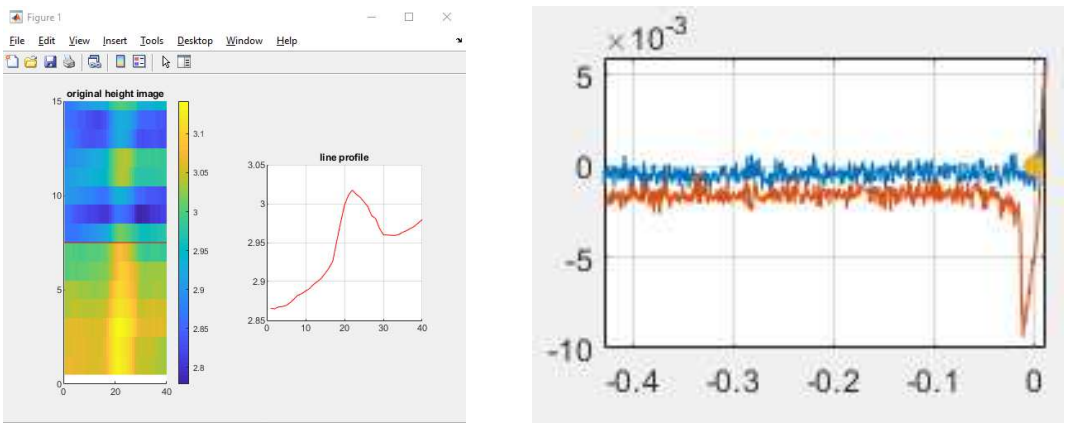

(a) Original height image issues

(b) Contact point determination issues

Figure 4.8: Two issue of the indentation modulus evaluation of RCP fibrils in the short incubation experiment, which led to non usable values and exclusion. (a) Original height images with large difference along the slow axis. (b) Contact point couldn't be accurately decided due to low SNR.

Die approbierte gedruckte Originalversion dieser Diplomarbeit ist an der TU Wien Bibliothek verfügbar.
The approved original version of this thesis is available in print at TU Wien Bibliothek.
TU Bibliothek Your knowledge hub WIEN

4.4 Drying Experiment

The aim of this stage was to measure the influence of drying on the mechanical and structural properties of TF by comparing them between PBS and distilled water.

4.4.1 Height influence

The first 2h incubation in PBS represent the same part as in the short incubation experiment. Likewise an increase of the mean height, albeit a lower one (1%), can be observed in Figure 4.9a. However, the swelling is not significant if tested as a pooled mean fibril, see Table 4.8. This result corresponds to the short incubation tests. After drying a reduction of the height can be seen but is not statically significant. The repetition of the sequence did not change the fibril height in a significant way. The control sequence with distilled water did not lead to any difference in fibril height.

4.4.2 Indentation Modulus changes

Indentation modulus tests provided more significant changes than height measurements. In contrast to short incubation, the IM appears to rise after the first 2 hours in PBS, see Figure 4.10, albeit not significantly. However, after drying and rehydration the modulus rose significantly, p=0.007, to 1.7x of the value before drying. The raise remained on this level after the second incubation and additional drying. It seems to rise further, but no additional significant change was observed, see Table 4.8 IM PBS softening/stiffening. The repetition of the first half of the experiment with distilled water saw no rise in stiffening, instead it remained on the same level.

4.4.3 PBS vs Distilled water

The pooled mean fibrils of PBS/distilled water were tested against each other. The distilled water fibrils saw a significant smaller relative height change after 2h incubation, p=0.012 Figure 4.9, than in PBS. Indentation modulus was also significantly lower in water, p=0.002, see Figure 4.10. This test had to be done with normalized changes due to large difference of the initial IM of the fibrils between the two test. The mean IM of PBS incubation was 2.7 MPa compared to 7.8 MPa of the distilled ones. This is a 2.8x difference of IM, see Figure 4.10b.

Die approbierte gedruckte Originalversion dieser Diplomarbeit ist an der TU Wien Bibliothek verfügbar.
The approved original version of this thesis is available in print at TU Wien Bibliothek.
TU Bibliothek WIEN Your knowledge hub

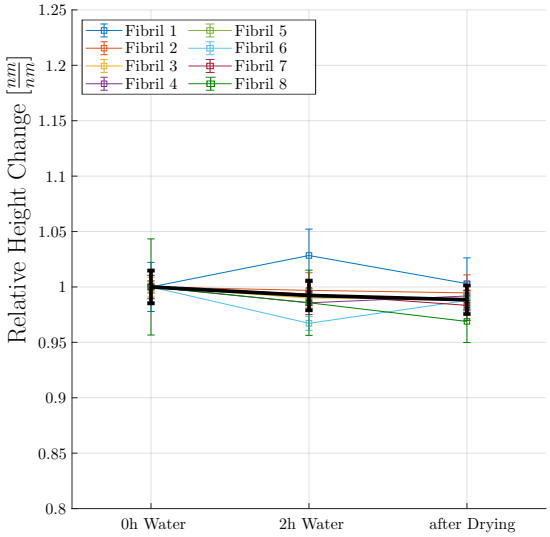

(a) Relative swelling behavior with H_2O incubation

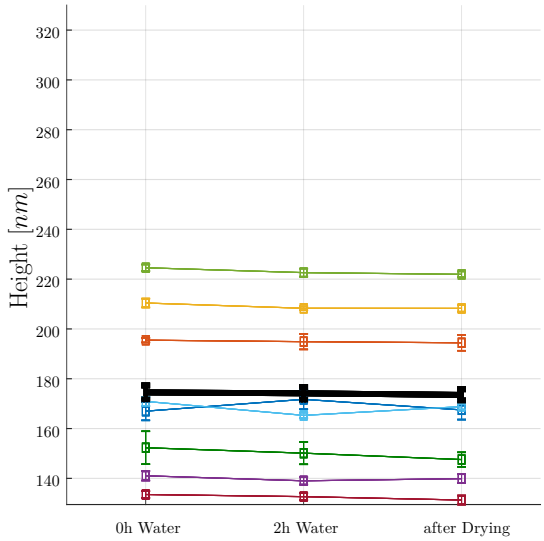

(b) Height of fibrils in H_2O

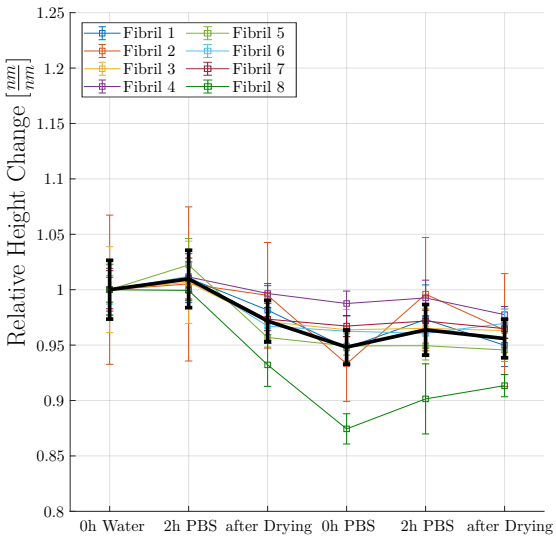

(c) Relative swelling behavior with PBS incubation

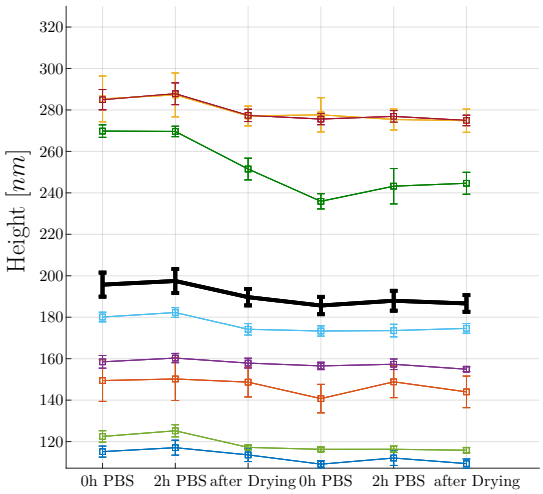

(d) Height of fibrils in PBS

Figure 4.9: Error bars of the fibril height in the drying experiment. (a) Relative height changes in H_20, which look like a decrease of height after incubation and drying. Although, it is not significant. (b) Height of H_20 fibrils. The range is smaller than PBS fibrils. (c) Height increases after first incubation, but recede during the next drying and incubation. (d) Height decrease over the span of the experiment, especially fibril 8.

Die approbierte gedruckte Originalversion dieser Diplomarbeit ist an der TU Wien Bibliothek verfügbar.
The approved original version of this thesis is available in print at TU Wien Bibliothek.
TU Bibliothek Your knowledge hub WIEN

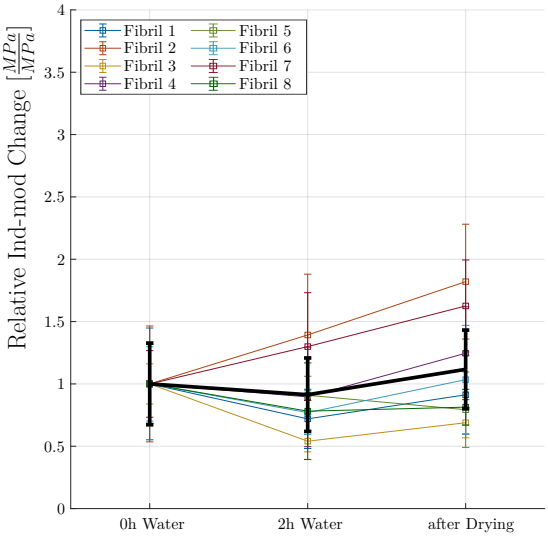

(a) Relative IM changes during H_2O incubation

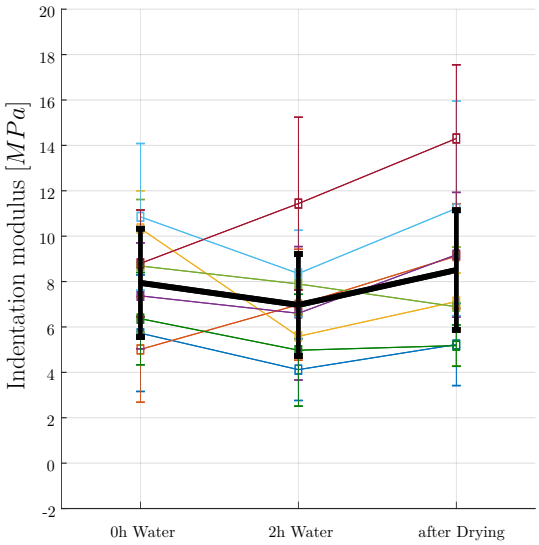

(b) IM of fibrils in H_2O

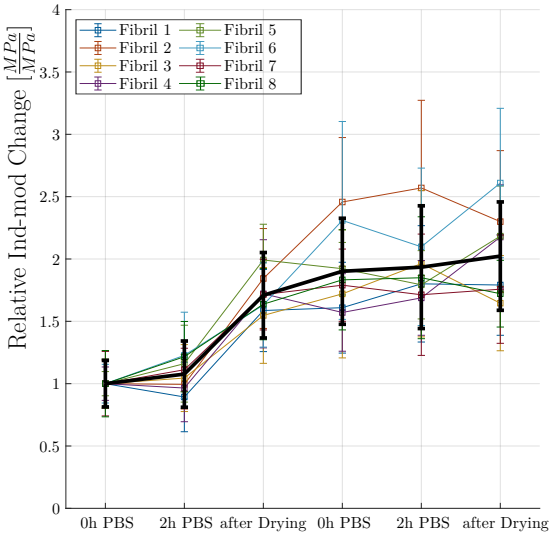

(c) Relative IM changes during PBS incubation

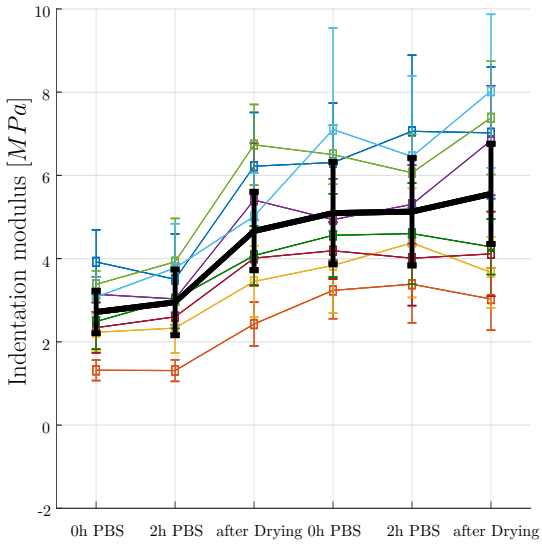

(d) IM results of PBS drying

Figure 4.10: Error bars of the IM in the drying experiment. (a) Relative IM change in H_20, which shows an mean increase after drying. (b) Absolute IM values of fibrils. They have a higher IM than the set of fibril tested in PBS, see (d). (c) Large and lasting relative IM increase after the first drying and rehydration. (d) IM which shows the absolute increase after drying and rehydration.

Die approbierte gedruckte Originalversion dieser Diplomarbeit ist an der TU Wien Bibliothek verfügbar.
The approved original version of this thesis is available in print at TU Wien Bibliothek.
TU Bibliothek Your knowledge hub WIEN

Table 4.8: P-Values of Welch test (5% significance) of the drying experiment. Significant values are highlighted in bold. IM=Indentation Modulus

Mean Fibrils				
Time	**Swelling PBS**	**Shrinking PBS**	**IM PBS Softening**	**IM PBS Stiffening**
0h vs 2h	0.482	0.518	0.681	0.319
2h vs post drying	0.585	0.415	0.993	**0.007***
post drying vs 0h repeat	0.551	0.449	0.716	0.284
0h vs 2h repeat	0.469	0.531	0.542	0.458
2h vs post drying repeat	0.512	0.488	0.677	0.323

Table 4.9: P-Values of Welch test (5% significance) of the drying experiment by testing difference between PBS and distilled water. Significant values are highlighted in bold*. IM=Indentation Modulus

PBS vs Water		
	Height	**IM**
0h	0.5	0.5
2h	**0.012***	0.088
post drying	0.966	**0.002***

4.4.4 D-Band spacing

Peak Detection

Measurement of D-Band spacing after the first PBS incubation yielded a significant contraction, p=0.0006. The mean distance was reduced from 69.4 nm to 64 nm after the first incubation, but increased significantly, p=0.023 postPBS vs prePBS rep., before the incubation was repeated (rep.), see the boxplots of Figure 4.11. Between postPBS and prePBS rep. the fibrils were in PBS to measure force maps after drying. The repeated 2h incubation led to no statistical changes. Likewise the other set of fibrils, which were incubated in distilled water, did not undergo significant changes.

Die approbierte gedruckte Originalversion dieser Diplomarbeit ist an der TU Wien Bibliothek verfügbar.
The approved original version of this thesis is available in print at TU Wien Bibliothek.
TU Bibliothek Your knowledge hub WIEN

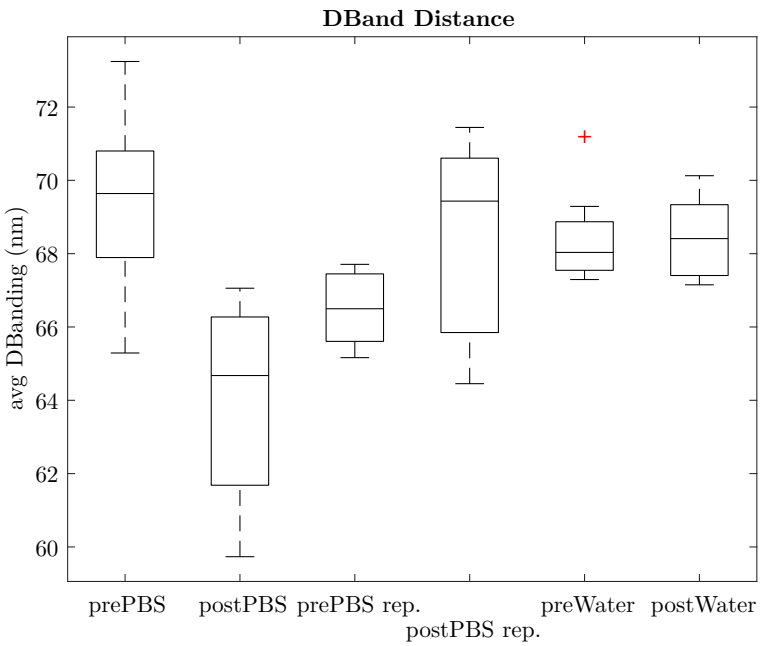

Figure 4.11: Boxplots of average d-banding length measured before and after the fibrils were incubated in water or PBS.

FFT Analysis

FFT of height profiles revealed 3 distinct peaks in the their frequency spectrum as seen in Figure 4.13. A reconstruction with the three highest peaks of one fibril was done to compare it to the original profile. The comparison can be seen in Figure 4.12. The reconstructed profile helped to analyze the 3 peaks, which can be concluded as:

- one peak at a low frequencies (LF, 2 to 3 $\frac{1}{1.5\mu m}$) with a high amplitude of 5 to 6, which contributes to the overall slow up and down to include the not straight surface.
- peak in the middle frequencies, first harmonic, (MF, 22-24 $\frac{1}{1.5\mu m}$) with a lower amplitude of 2 to 3, which corresponds to the prominent D-Banding feature (prominent sinus wave in the reconstructed profile)
- high frequency peak, second harmonic, (HF, 43 to 47 $\frac{1}{1.5\mu m}$) with the lowest amplitude of around 0.5. This peak shapes the prominent sinus wave to be steeper.

See Figure 4.13a and b for the 3 marked high peaks.

Therefore the D-Band spacing can be contributed to the middle peak. The change from frequency to spatial domain was done by inverting the frequency. The frequency means

Die approbierte gedruckte Originalversion dieser Diplomarbeit ist an der TU Wien Bibliothek verfügbar.
The approved original version of this thesis is available in print at TU Wien Bibliothek.
TU Bibliothek Your knowledge hub WIEN

the sinus has n periods in 1.5 μm, eg.: MF has 22 periods in 1.5 μm length with a wavelength λ of $\frac{1.5\mu m}{22} = 68nm$. Thus the middle peak corresponds to the staggering of D-Banding. If the frequency shifts to a higher value the wavelength shortens. This can be seen by comparing prePBS MF peak to postPBS MF. The MF peak shifts from 22 to 24 $\frac{1}{1.5\mu m}$, which is a λ change from 68.18 nm to 62.5 nm, see Table 4.10 and the comparison Figure 4.13 a and b. This D-Banding reduction corresponds with the peak detection result. The continuation leaded to one further MF shift of 23 to 24 $\frac{1}{1.5\mu m}$ from postPBS to prePBS repeat. This increased the spacing, but was not significant in the peak detection chapter. Afterwards no further changes of MF was observed.

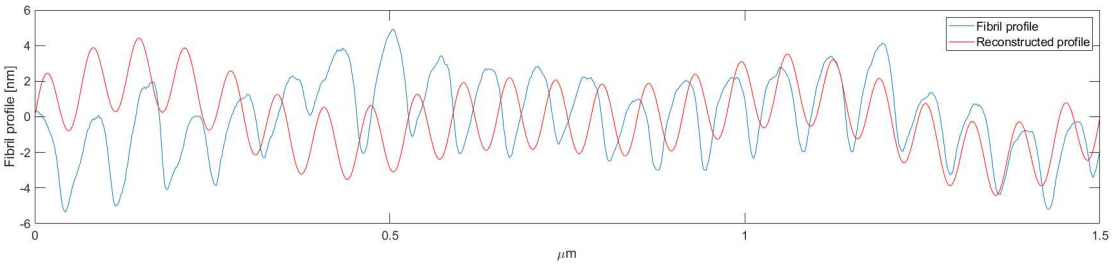

Figure 4.12: Example of an reconstructed fibril profile from the first 3 peaks of the frequency spectrum in comparison to the measured fibril profile.

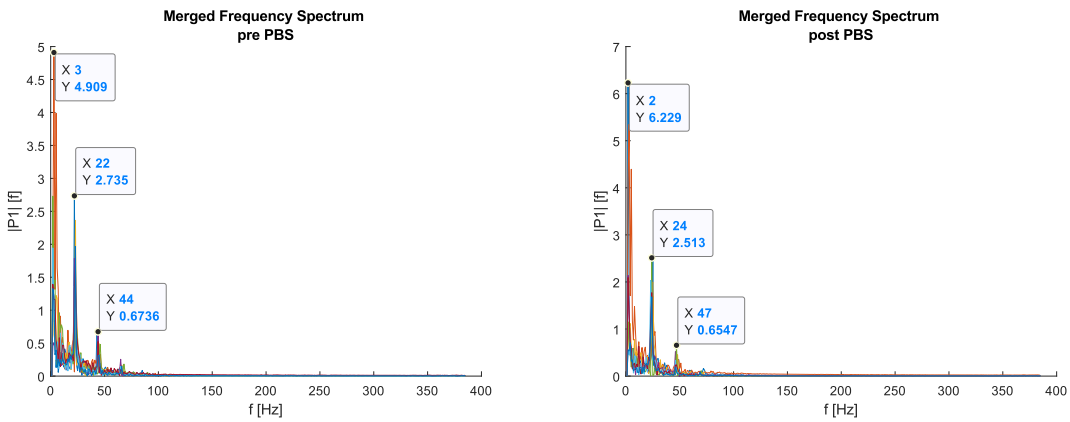

(a) Frequency Spectrum of 8 fibrils prePBS

(b) Frequency Spectrum of 8 fibrils postPBS

Figure 4.13: Frequency spectra of 8 fibril FFTs before and after incubation in PBS (5 pixel moving average filter). It indicates that the fibrils profile is largely dependent of 3 frequency peaks. One low underlying frequency of around 2/3 $\frac{1}{1.5\mu m}$, middle frequency which corresponds to the D-Banding with 22/24 $\frac{1}{1.5\mu m}$ and the second harmonic with 44 $\frac{1}{1.5\mu m}$.

Die approbierte gedruckte Originalversion dieser Diplomarbeit ist an der TU Wien Bibliothek verfügbar.
The approved original version of this thesis is available in print at TU Wien Bibliothek.
TU Bibliothek Your knowledge hub WIEN

Table 4.10: Values of the 3 peaks form merged frequency spectra, like Figure 4.13. λ is the wavelength by inverting frequency f. LF=Low Frequency, MF=Middle frequency, HF=High frequency

Peak	**LF Peak**		**MF Peak**		**HF Peak**	
[Unit]	**f** $\frac{1}{1.5\mu m}$	λ **[nm]**	**f** $\frac{1}{1.5\mu m}$	λ **[nm]**	**f** $\frac{1}{1.5\mu m}$	λ **[nm]**
prePBS	3	500	22	68.18	44	34.09
postPBS	2	750	24	62.5	47	31.91
prePBS repeat	3	500	23	65.22	46	32.61
postPBS repeat	2	750	23	65.22	43	34.88
preWater	2	750	23	65.22	45	33.33
preWater	3	500	23	65.22	45	33.33

4.5 Imprint Remodeling

Indentation on the apex of a fibril were difficult due to thermal drifting and switching of operation modes, but were close enough to leave notches, see Figure 4.15d with multiple notches off center. With faster switching of modes and more experience for positioning the notches became more well positioned.
Images of indentations show that not all marked spots lead to a visible notch. Indentations with 500 nN does not exhibit an notch, see Figure 4.15c. From 1500 nN onward, fibrils exhibit a lasting notch. Figure 4.15d displays several high force indentations, with more than the three original planned due to bringing them more closer to the apex. The upper right notch of fibril no. 3 was highlighted with an height line across the indent, see Figure 4.14b. This was an indentation with 6000 nN, which lead to a notch depth of about a third of its height and a length of around 150 nm. The length of the notches seems to be the same regardless of the indentation forces.

Die approbierte gedruckte Originalversion dieser Diplomarbeit ist an der TU Wien Bibliothek verfügbar.
The approved original version of this thesis is available in print at TU Wien Bibliothek.
TU Bibliothek Your knowledge hub WIEN

Hydration

Both experiments with 25°C distilled water and 4°C PBS led to the same outcome. All indentations have receded and the fibril surfaces look undamaged. This can qualitatively and visibly assessed by comparing Figures 4.15a and 4.15b (before hydration) with Figures 4.15e and 4.15f (after hydration). The height profile across a former high force indentation also shows no sign of an residual imprint, Figure 4.14b. The height (parallel to the Mica surface) remains unchanged of around 300 nm for fibril 3, even with an deep indentation.

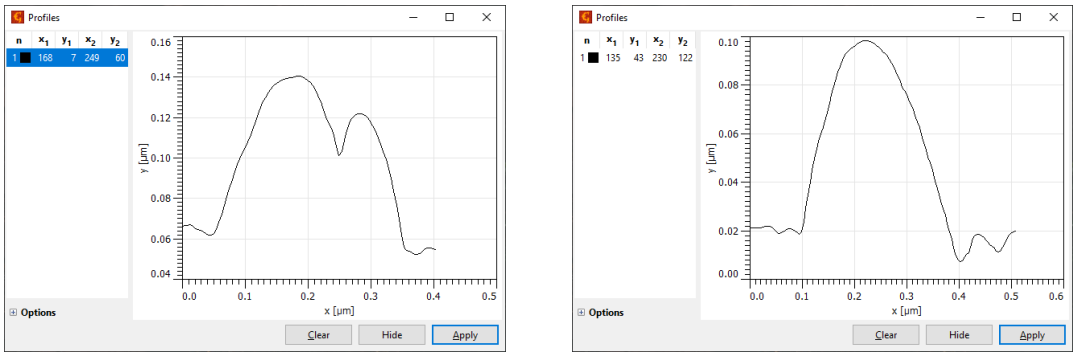

(a) Heihtline across 6000 nN indentation from line in Figure 4.15d

(b) Heihtline across same spot after seconds in PBS from line in Figure 4.15f

Figure 4.14: Height profile of damaged and undamaged fibril no. 3.

Die approbierte gedruckte Originalversion dieser Diplomarbeit ist an der TU Wien Bibliothek verfügbar.
The approved original version of this thesis is available in print at TU Wien Bibliothek.
TU Bibliothek Your knowledge hub WIEN

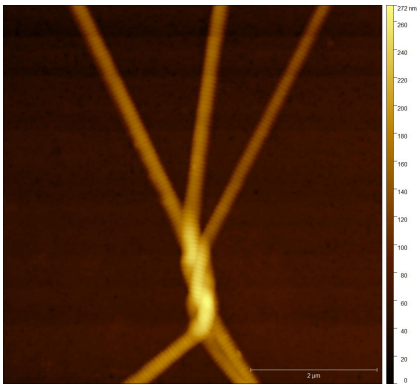

(a) Region of collagen fibrils before indentations.

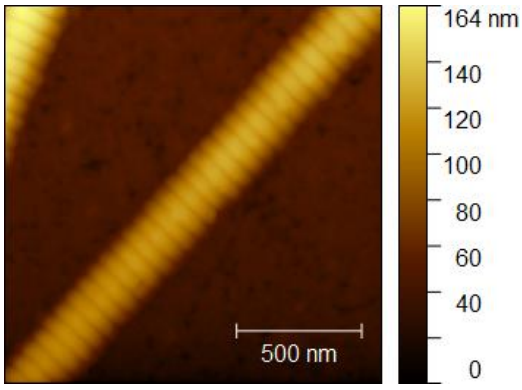

(b) Fibril before high force indentations.

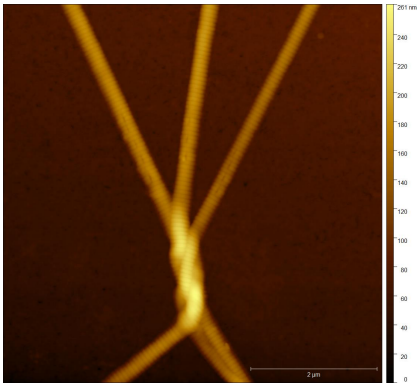

(c) Fibrils after indentations according to Figure 3.11. Lowest indentations force is not visible.

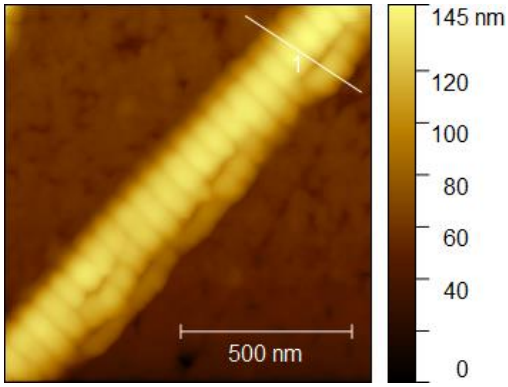

(d) Fibrils after six 5000-6000 nN indentations. Height profile in Figure 4.14a.

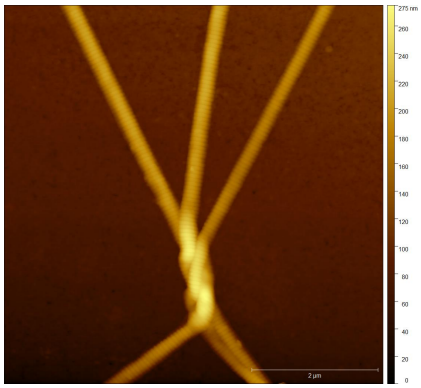

(e) Dry image with reversal of indentations spots after 10 minutes in 25°C distilled Water. No visible changes in comparison to unindented fibrils of Figure 4.15a.

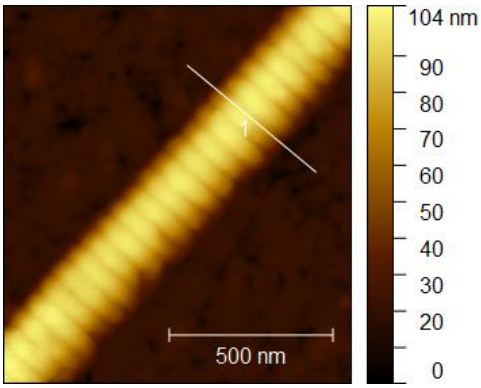

(f) Dry image after few seconds in 4°C PBS with no visible indentations left.

Figure 4.15

Die approbierte gedruckte Originalversion dieser Diplomarbeit ist an der TU Wien Bibliothek verfügbar.
The approved original version of this thesis is available in print at TU Wien Bibliothek.
TU Bibliothek Your knowledge hub WIEN

Die approbierte gedruckte Originalversion dieser Diplomarbeit ist an der TU Wien Bibliothek verfügbar.
The approved original version of this thesis is available in print at TU Wien Bibliothek.

Die approbierte gedruckte Originalversion dieser Diplomarbeit ist an der TU Wien Bibliothek verfügbar.
The approved original version of this thesis is available in print at TU Wien Bibliothek.

CHAPTER 5

Discussion

The series of experiments on collagen fibrils from mouse tails and reconstitution presented in this thesis delivered important insights in possible artifacts of collagen fibril structure and mechanics measurements, which must not be falsely interpreted in studies attempting to influence and test collagen fibril behavior. Tendon fibrils in incubation and drying experiments swell with a mean of 5% after 9 days (long incubation) compared to 4% after 2 hours, though fibrils of the drying experiment, swell only by a mean of 1% after 2 hours. The first results of the incubation experiments suggests that the majority of swelling occurs in the first two hours of incubation. However, the results of the drying and other incubation experiments show large standard deviations on the pooled mean fibril, bold black line on Figures 4.1a, 4.9a and 4.9a, which lead to an underlying problem of combining individual fibrils for a general statement of CF behavior. As an illustration, fibrils in this thesis were nanoindented and evaluated by 15 data points per instant of time. The 15 points are enough to test them statistically with a Welch-test for swelling or shrinking, but the test works only for two points in time of the same fibril. Hence an statement for individual fibril changes can be made. For general statements of fibril changes a norm fibril for relative and absolute values is needed. This normalization was done to the mean of the first measurement, due to the impossibility of indenting the exact same spot 4 times. Unfortunately, this methods leads to a value of 1 for all relative changes in the first measurement. Hence statistical evaluation is only meaningful for absolute and their derived pooled values. Comparison of relative changes can be made by excluding the first instace. A difficulty of interpretation arose due to different statistical outcomes of individual fibrils vs. pooled ones, like in two incubation experiments of tail tendon. All fibrils in the long incubation swelled significantly after 9D by testing them individually, Table 4.1, but no significance occurs in the pooled fibril. Which one is now correct ? I would argue it is better to look at individual fibrils and overall behavior. If $> \frac{3}{4}$ of the fibrils show significant swelling than the argument should be for fibril swelling after long incubation. The problem with using the pooled mean (not normalized) for

statistical testing are the large height differences between each fibril, which increases the σ of the sample pool. A possible solution would be to pre-select fibrils with similar diameters. Results for the short incubation experiment looked similar, 6 out of 8 fibril swelled significantly, but not the pooled one. In the drying experiment 3 fibrils swelled significantly. Following incubation in all experiments led to no further swelling. In total 17 out of 27 fibrils show a significant swelling after their first incubation, albeit different lengths. Along with swelling, the fibrils underwent mechanical changes during incubation. The long incubation of TF resulted in a 60% reduction of the IM, with further decrease to around 30% of the initial value after the second incubation. In short incubation, 4 out of 7 fibrils had a significant decline of IM after 2 hours, which did not decline further for the next incubations. A major contributor to the mechanical strength of collagen fibrils are the cross-links [98], which could explain the changes. Incubation in 37° PBS could lead to a debonding of immature cross-links, which reduces the IM and creates the possibility of more free movement between each TC molecule. The swelling is hereby a consequence of debonding. Another possibility are proteases which proteolyse tropocollagen mocules and therefore compromise the whole structure of fibrils. An analysis of the medium for metabolites could indicate proteases activity. Furthermore the instability of collagen type I monomers under body temperature reported by Leikina [27] could play a role. Although Leikina experimented only with monomers, TC-molecules could locally melt during incubation and refold in the lower temperature of the fluid cell. The complete unfolding is inhibited due to the structural design of the fibril, but with more incubation time more unfolding seems reasonable, which could explain the IM difference between long and short incubation.

Unexpected and very interesting in the domain of mechanical properties are the results of the drying experiment. The first round of hydration and drying resulted in a 1.7x significant increase of IM, which remained for the following repetition. The control experiment with distilled water did not exhibit this behavior. Since the difference is the used media, and fibrils were from the same species, ions could be the deciding factor. Cross-links play a major part of mechanical properties, but an increase of cross-links without enzymatic activity can only happen through glycation and PBS doesn't contain any reducing sugars for AGEs. A deeper indentation was also excluded by controlling the depth of the force curves and the same cantilever was used for both water and PBS measurements. PBS contains ions which could in theory be aggregated between TC molecules. α 1 and 2 chains have an theoretical isoelectric point of 9.88 [1] which means at the ph of 7.4 the molecule is positively charged. Chloride ions have a negative charge and could therefore be attracted to the chains. Potassium and sodium, also contained in PBS as salt, are positively charged and could enter the fibril through hydration. Two hypothetical effects of the ions were considered:

- Ions accumulate on the cross-links to strengthen them since TC molecules are too tight for ions and the intermolecular space was cleansed with distilled water after

[1] https://web.expasy.org/compute_pi/, α-chain 1: P02452, α-chain2: P08123

Die approbierte gedruckte Originalversion dieser Diplomarbeit ist an der TU Wien Bibliothek verfügbar.
The approved original version of this thesis is available in print at TU Wien Bibliothek.
TU Bibliothek WIEN Your knowledge hub

measurements, see Figure 5.1. Collagen mineralization in bones is supposed to start in the gaps between TC [99], which was the origin of this idea.

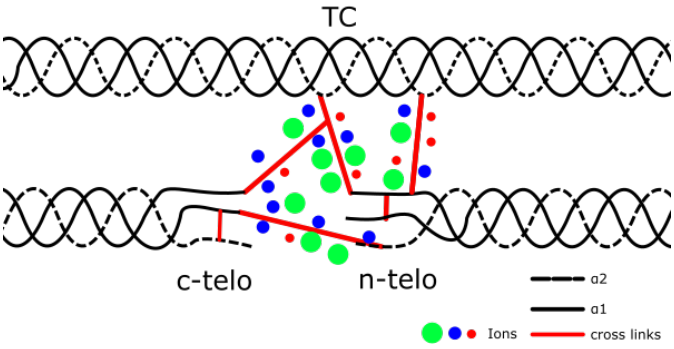

Figure 5.1: Putative strengthening of cross-links during drying. Ions attach to cross-links which reduces the cross-links flexibility.

- Chloride ions accumulate due to their charge in the intermolecular space and were not washed off after measurement. Left over N^+ and K^+ ions build with chloride their respective salt inside the fibril. After rehydration the salt concentration in the fluid cell is increased, which according to [23] increases the IM. See Figure 5.2.

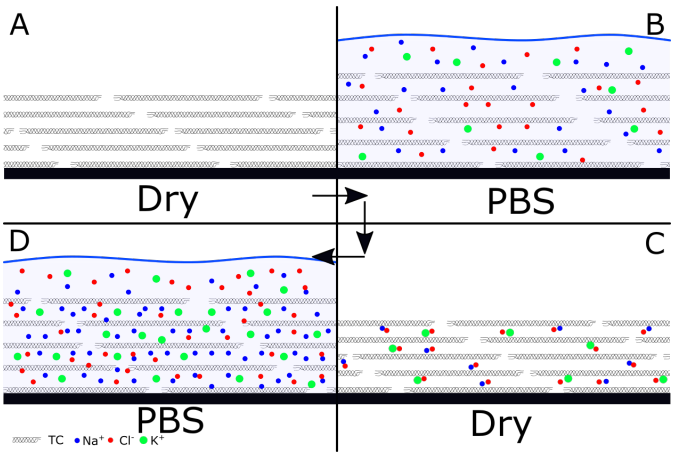

Figure 5.2: Assumed drying behavior (A)Dry fibril on the surface. (B) First hydration with PBS. Chloride is attracted to TC molecules and aggregates. Other ions flew into the fibril. (C) Chloride is not washed off and combines with leftover N^+ and K^+ into salts. (D) Salt is dissolved in second hydration and increase the concentration, which increases the IM.

Die approbierte gedruckte Originalversion dieser Diplomarbeit ist an der TU Wien Bibliothek verfügbar.
The approved original version of this thesis is available in print at TU Wien Bibliothek.
TU Bibliothek Your knowledge hub WIEN

The first effect could be tested by increasing the cross-links with glutaraldehyde and compare if the IM increases in PBS even more than in distilled water. The second effect can be tested by measuring the salt concentration of the fluid cell before and after drying by rehydration with PBS.

The observation for changes in D-Banding spacing with peak detection for a potential prestraining of fibrils due to the application on the microscope slides revealed a significant decrease after the first PBS measurements, Figure 4.11. Although the decrease couldn't be verified with the repetition on the same fibrils. The spacing after the repetition looked similar to the initial one. However, FFT analysis showed a lasting decrease in the MF and HF peak after the first 2hours in PBS, Table 4.10, which could indicate a potential relaxation of prestrain on the fibrils. Although, the repetition on another sample of fibrils with water instead of PBS showed no lasting changes of D-Band spacing. A statement for the existence of prestraining is therefore insufficiently proved, but I think with a combination of peak detection and FFT-analysis alterations can be detected.

RCP fibrils, which were designated as a control group, showed no swelling, stiffening or softening behavior and their width and mechanical properties were quite different than the fibrils from the tail of a mice. Generally RCP assembled much thinner fibrils with a maximum height of 150 nm. Mean width was under 100 nm in comparison to the mean of 220 nm and 120nm from tail fibrils. Indentation modulus was also significantly lower, 1.25 vs 3.5 MPa, in RCP fibrils. The lower modulus indicates a low concentration of cross-links, which possibly couldn't form after preparation from collagen powder. Therefore a direct comparison between RCP and native collagen could not be conducted.

The last experiment demonstrated a large behavior difference between dry and hydrated collagen fibrils. Dry fibrils showed a plastic deformation with an indentation orientation parallel to their fibril axis. Due to a fixed tip orientation and same notch alignments on fibrils with 70° orientation difference between them(fibril 1 to fibril 3), one possible explanation is the displacement and packing of tropocollagen. This observation goes along with the findings of M.Wenger et al. [4] who concluded that the elongated notches are due to high anisotropy of collagen fibrils.
An explanation of the observed indentation receding after hydration could be consequence of the more freely movable TC-moluces inside the fibrils. Grant and colleagues observed an twofold increase of fibril diameter between dry and hydrated state [23]. This means a 4x increase in area, which should mostly be filled with the added solution. TC-molecules can therefore align themselves back to the lower energy conformation with equal distance. However, we only have theories of the structural order of fibrils with the most common one of Hodge & Petruska with the parallel aligned TC-molecules. My results suggests rather flexible TC-molecules with low bending strength and no plastic deformation.
Other aspects and further questions arise for further studies. How long are indentations lasting in a dry environment and are the fibrils and corresponding subunits damaged ? In this experiment indentations were only observed for few minutes before hydration. Damages of TC-molecules and cross-links could probably be analyzed by comparing IM before and after indentation.

Die approbierte gedruckte Originalversion dieser Diplomarbeit ist an der TU Wien Bibliothek verfügbar.
The approved original version of this thesis is available in print at TU Wien Bibliothek.
TU Bibliothek WIEN Your knowledge hub

5.1 Conclusion

In this study a few points and insights emerged which should be considered for further studies with collagen fibrils:

- Preselect more than 8 fibrils of similar height for comparison of height changes. The method of combining them into one mean fibril has many shortcomings, as said in the discussion, which could be prevented by using more fibrils.
- In statistical evaluation both individual and combined fibril results should be considered equally for a discussion.
- In long term studies, application of protease inhibitors may prevent the proteolysis of collagen fibrils, which impairs the fibrils' structure. In this study a large reduction of stiffness was observed after long incubation (on the order of 10 days) in PBS.
- Test the mechanical properties of RCP fibrils beforehand to ensure similar features to native CFs. Otherwise, the same structural composition and behavior can not be assured.
- Measurements of fibrils in PBS should be performed without an intermittend drying period. Fibrils in this study increased their IM significantly after drying, which could distort studies of influences.
- Collagen fibrils have a completely different behavior between wet and dry conditions. A wet setting with an physiological buffer represents the natural environment which enables more realistic in-situ testing.

Die approbierte gedruckte Originalversion dieser Diplomarbeit ist an der TU Wien Bibliothek verfügbar.
The approved original version of this thesis is available in print at TU Wien Bibliothek.
TU Bibliothek Your knowledge hub WIEN

Die approbierte gedruckte Originalversion dieser Diplomarbeit ist an der TU Wien Bibliothek verfügbar.
The approved original version of this thesis is available in print at TU Wien Bibliothek.

CHAPTER 6

Appendix

6.1 Relative Changes

The following tables show the relative changes on individual and pooled fibril level.

Die approbierte gedruckte Originalversion dieser Diplomarbeit ist an der TU Wien Bibliothek verfügbar.
The approved original version of this thesis is available in print at TU Wien Bibliothek.
TU WIEN Bibliothek Your knowledge hub

Table 6.1: Relative changes of long incubation experiment

Long Incubation

Relative height changes TF $\left[\frac{nm}{nm}\right]$			
Fibril	**1st Day**	**9th Day**	**18th Day**
1	1.00	1.04	1.13
2	1.00	1.09	1.05
3	1.00	1.05	1.08
4	1.00	1.09	1.02
5	1.00	1.08	1.05
6	1.00	1.09	1.06
7	1.00	1.06	1.05
8	1.00	1.12	1.10
pooled	1.00	1.08	1.07

Relative height changes RCP $\left[\frac{nm}{nm}\right]$		
Fibril	**1st Day**	**10th Day**
1	1.00	1.12
2	1.00	1.02
3	1.00	0.96
4	1.00	1.08
5	1.00	0.91
6	1.00	1.03
7	1.00	1.09
8	1.00	1.01
pooled	1.00	1.03

Relative IM changes TF $\left[\frac{MPa}{MPa}\right]$			
Fibril	**1st Day**	**9th Day**	**18th Day**
1	1.00	0.71	NaN
2	1.00	0.58	0.44
3	1.00	0.41	0.33
4	1.00	0.38	0.26
5	1.00	0.45	0.31
6	NaN	NaN	NaN
7	NaN	NaN	NaN
8	1.00	0.35	0.21
pooled	1.00	0.47	0.33

Relative IM changes RCP $\left[\frac{MPa}{MPa}\right]$		
Fibril	**1st Day**	**11th Day**
1	1.00	1.05
2	1.00	1.77
3	1.00	1.91
4	1.00	2.55
5	1.00	1.39
6	1.00	0.77
7	1.00	0.26
8	1.00	1.47
pooled	1.00	1.40

Die approbierte gedruckte Originalversion dieser Diplomarbeit ist an der TU Wien Bibliothek verfügbar.
The approved original version of this thesis is available in print at TU Wien Bibliothek.
TU Bibliothek Your knowledge hub WIEN

Table 6.2: Relative changes of short incubation experiment

Short Incubation

	Relative height changes TF $\left[\frac{nm}{nm}\right]$			
Fibril	**0h**	**2h**	**4h**	**6h**
1	1.00	1.05	1.00	1.03
2	1.00	1.04	1.04	1.06
3	1.00	1.02	1.04	1.05
4	1.00	1.08	1.08	1.06
5	1.00	1.01	1.01	1.02
6	1.00	1.09	1.09	1.14
7	1.00	1.01	1.02	1.03
8	1.00	1.04	1.01	1.00
pooled	1.00	1.04	1.03	1.03

	Relative height changes RCP $\left[\frac{nm}{nm}\right]$			
Fibril	**0h**	**2h**	**4h**	**6h**
1	1.00	1.05	1.01	1.09
2	1.00	1.08	1.02	1.03
3	1.00	0.98	1.03	1.01
4	1.00	1.12	0.99	1.05
5	1.00	1.11	1.00	0.96
6	1.00	0.94	0.90	0.98
7	1.00	1.05	0.97	0.96
8	1.00	1.04	1.04	1.01
pooled	1.00	1.02	1.01	1.01

	Relative IM changes TF $\left[\frac{MPa}{MPa}\right]$			
Fibril	**0h**	**2h**	**4h**	**6h**
1	1.00	0.91	0.81	0.94
2	1.00	0.27	0.54	0.55
3	NaN	NaN	NaN	NaN
4	1.00	0.88	1.03	0.96
5	1.00	0.98	1.03	0.86
6	1.00	0.46	0.82	0.78
7	1.00	1.08	1.00	1.38
8	1.00	1.02	1.08	1.04
pooled	1.00	0.79	0.90	0.94

Die approbierte gedruckte Originalversion dieser Diplomarbeit ist an der TU Wien Bibliothek verfügbar.
The approved original version of this thesis is available in print at TU Wien Bibliothek.
TU Bibliothek Your knowledge hub WIEN

Table 6.3: Relative changes of drying experiment

Drying Experiment

	Relative height changes PBS $\left[\frac{nm}{nm}\right]$					
Fibril	**0h PBS**	**2h PBS**	**after drying**	**0h PBS repeat**	**2h PBS repeat**	**after drying repeat**
1	1.00	1.02	0.99	0.95	0.97	0.95
2	1.00	1.01	0.99	0.94	1.00	0.96
3	1.00	1.01	0.97	0.97	0.97	0.96
4	1.00	1.01	1.00	0.99	0.99	0.98
5	1.00	1.02	0.96	0.95	0.95	0.95
6	1.00	1.01	0.97	0.96	0.96	0.97
7	1.00	1.01	0.97	0.97	0.97	0.96
8	1.00	1.00	0.93	0.87	0.90	0.91
pooled	1.00	1.01	0.97	0.95	0.96	0.96

	Relative IM changes PBS $\left[\frac{MPa}{MPa}\right]$					
Fibril	**0h PBS**	**2h PBS**	**after drying**	**0h PBS repeat**	**2h PBS repeat**	**after drying repeat**
1	1.00	0.89	1.59	1.61	1.80	1.79
2	1.00	0.99	1.84	2.46	2.57	2.30
3	1.00	1.04	1.55	1.72	1.96	1.65
4	1.00	0.97	1.72	1.57	1.69	2.18
5	1.00	1.16	1.99	1.92	1.79	2.18
6	1.00	1.23	1.63	2.31	2.10	2.61
7	1.00	1.11	1.71	1.79	1.71	1.76
8	1.00	1.22	1.64	1.83	1.85	1.72
pooled	1.00	1.08	1.71	1.90	1.93	2.02

	Rel. height changes Water $\left[\frac{nm}{nm}\right]$		
Fibril	**0h Water**	**2h Water**	**after drying**
1	1.00	1.03	1.00
2	1.00	1.00	0.99
3	1.00	0.99	0.99
4	1.00	0.99	0.99
5	1.00	0.99	0.99
6	1.00	0.97	0.99
7	1.00	0.99	0.98
8	1.00	0.99	0.97
pooled	1.00	0.99	0.99

	Relative IM changes Water $\left[\frac{MPa}{MPa}\right]$		
Fibril	**0h Water**	**2h Water**	**after drying**
1	1.00	0.72	0.91
2	1.00	1.39	1.82
3	1.00	0.54	0.69
4	1.00	0.90	1.25
5	1.00	0.91	0.79
6	1.00	0.77	1.03
7	1.00	1.30	1.63
8	1.00	0.78	0.81
pooled	1.00	0.91	1.12

Die approbierte gedruckte Originalversion dieser Diplomarbeit ist an der TU Wien Bibliothek verfügbar.
The approved original version of this thesis is available in print at TU Wien Bibliothek.
TU Bibliothek Your knowledge hub WIEN

Bibliography

[1] Matthew D. Shoulders and Ronald T. Raines. Collagen Structure and Stability. *Annual Review of Biochemistry*, 78(1):929–958, 2009.

[2] Gary B Smejkal and Cody Fitzgerald. Revised Estimate of Total Collagen in the Human Body-International Journal of Proteomics & Bioinformatics. *International Journal of Proteomics & Bioinformatics*, 2(1):002–003, 2017.

[3] Joost A.J. Van Der Rijt, Kees O. Van Der Werf, Martin L. Bennink, Pieter J. Dijkstra, and Jan Feijen. Micromechanical testing of individual collagen fibrils. *Macromolecular Bioscience*, 6(9):699–702, 2006.

[4] Marco P.E. Wenger, Laurent Bozec, Michael A. Horton, and Patrick Mesquidaz. Mechanical properties of collagen fibrils. *Biophysical Journal*, 93(4):1255–1263, 2007.

[5] Laurent Bozec and Michael Horton. Topography and mechanical properties of single molecules of type I collagen using atomic force microscopy. *Biophysical Journal*, 88(6):4223–4231, 2005.

[6] Karl E. KADLER, David F. HOLMES, John A. TROTTER, and John A. CHAPMAN. Collagen fibril formation. *Biochemical Journal*, 316(1):1–11, may 1996.

[7] Yoshiko Komai and Tarsuo Ushikif. The Three-Dimensional Organization of Collagen Fibrils in the Human Cornea and Sclera. 32(8), 1991.

[8] Robert D. NIMNI, Marcel E.; HARKNESS. Molecular structures and functions of collagen. In *Collagen Volume I Biochemistry*. 1988.

[9] Kheng Lim Goh, Jennifer Hiller, J. Louise Haston, David F. Holmes, Karl E. Kadler, Ann Murdoch, Judith R. Meakin, and Timothy J. Wess. Analysis of collagen fibril diameter distribution in connective tissues using small-angle X-ray scattering. *Biochimica et Biophysica Acta - General Subjects*, 1722(2):183–188, 2005.

[10] G. N. RAMACHANDRAN and G. KARTHA. Structure of Collagen. *Nature*, 174(4423):269–270, aug 1954.

[11] PAULINE M. COWAN, STEWART McGAVIN, and A. C. T. NORTH. The Polypeptide Chain Configuration of Collagen. *Nature*, 176(4492):1062–1064, dec 1955.

[12] John A.M. Ramshaw, Naina K. Shah, and Barbara Brodsky. Gly-X-Y tripeptide frequencies in collagen: A context for host-guest triple-helical peptides. *Journal of Structural Biology*, 1998.

[13] J. A. PETRUSKA and A. J. HODGE. a Subunit Model for the Tropocollagen Macromolecule. *Proceedings of the National Academy of Sciences of the United States of*, 51:871–876, 1964.

[14] J. P. R. O. Orgel, T. C. Irving, A. Miller, and T. J. Wess. Microfibrillar structure of type I collagen in situ. *Proceedings of the National Academy of Sciences*, 103(24):9001–9005, 2006.

Die approbierte gedruckte Originalversion dieser Diplomarbeit ist an der TU Wien Bibliothek verfügbar.
The approved original version of this thesis is available in print at TU Wien Bibliothek.
TU WIEN Bibliothek Your knowledge hub

[15] N.C. Avery and A.C. Bailey. Chapter 4 Restraining Cross-Links Responsible for the Mechanical Properties of Collagen Fibers: Natural and Artificial. In *Collagen*, pages 81–110. 2008.

[16] H Vlassara, L J Striker, S Teichberg, H Fuh, Y M Li, and M Steffes. Advanced glycation end products induce glomerular sclerosis and albuminuria in normal rats. *Proceedings of the National Academy of Sciences of the United States of America*, 91(24):11704–8, nov 1994.

[17] Karol Miller and Kiyoyuki Chinzei. Mechanical properties of brain tissue in tension. *Journal of Biomechanics*, 35(4):483–490, 2002.

[18] Jiaping Xie, Jianbo Zhou, and Y. C. Fung. Bending of blood vessel wall: Stress-strain laws of the intima-media and adventitial layers. *Journal of Biomechanical Engineering*, 117(1):136–145, 1995.

[19] Orestis G Andriotis, Wiparat Manuyakorn, Jurgita Zekonyte, Orestis L Katsamenis, Sebastien Fabri, Peter H Howarth, Donna E Davies, and Philipp J Thurner. Nanomechanical assessment of human and murine collagen fi brils via atomic force microscopy cantilever-based nanoindentation. *Journal of the Mechanical Behavior of Biomedical Materials*, 39:9–26, 2014.

[20] Colin A. Grant, David J. Brockwell, Sheena E. Radford, and Neil H. Thomson. Effects of hydration on the mechanical response of individual collagen fibrils. *Applied Physics Letters*, 92(23), 2008.

[21] S. Alexander, L. Hellemans, Marti O., J. Schneir, V. Elings, P. K. Hansma, Matt Longmire, and John Gurley. Microscope Implemented Using an Optical Lever. *Journal of Applied Physics*, 65(July 1988):164–167, 1989.

[22] Lanti Yang, Kees O. Van Der Werf, Carel F.C. Fitié, Martin L. Bennink, Pieter J. Dijkstra, and Jan Feijen. Mechanical properties of native and cross-Linked type i collagen fibrils. *Biophysical Journal*, 2008.

[23] Colin A. Grant, David J. Brockwell, Sheena E. Radford, and Neil H. Thomson. Tuning the elastic modulus of hydrated collagen fibrils. *Biophysical Journal*, 97(11):2985–2992, 2009.

[24] W.C. Oliver and G.M. Pharr. An improved technique for determining hardness and elastic modulus using load and displacement sensing indentation experiments. *Journal of Materials Research*, 7(6):1564–1583, jun 1992.

[25] Lucas Novaes Teixeira, Christian Ravagnani, Oscar Peitl, and Edgar Dutra Zanotto. In vitro osteogenesis on a highly bioactive glass-ceramic. pages 2–10, 2006.

[26] August J. Heim, Thomas J. Koob, and William G. Matthews. Low strain nanomechanics of collagen fibrils. *Biomacromolecules*, 8(11):3298–3301, 2007.

[27] E. Leikina, M. V. Mertts, N. Kuznetsova, and S. Leikin. Type I collagen is thermally unstable at body temperature. *Proceedings of the National Academy of Sciences*, 99(3):1314–1318, 2002.

[28] G. A. Lichtwark and A. M. Wilson. In vivo mechanical properties of the human Achilles tendon during one-legged hopping. *Journal of Experimental Biology*, 208(24):4715–4725, 2005.

[29] Samuel R. Ward, Gregory J. Loren, Scott Lundberg, and Richard L. Lieber. High stiffness of human digital flexor tendons is suited for precise finger positional control. *Journal of Neurophysiology*, 96(5):2815–2818, 2006.

[30] P V Komi, S Fukashiro, and M Järvinen. Biomechanical loading of Achilles tendon during normal locomotion. *Clinics in sports medicine*, 11(3):521, 1992.

[31] Henning Langberg, Lars Rosendal, and Michael Kjær. Training-induced changes in peritendinous type I collagen turnover determined by microdialysis in humans. *Journal of Physiology*, 534(1):297–302, 2001.

[32] Guy M. Genin and Stavros Thomopoulos. The tendon-to-bone attachment: Unification through disarray. *Nature Materials*, 16(6):607–608, 2017.

Die approbierte gedruckte Originalversion dieser Diplomarbeit ist an der TU Wien Bibliothek verfügbar.
The approved original version of this thesis is available in print at TU Wien Bibliothek.
TU Bibliothek Your knowledge hub WIEN

[33] John Apostolakos, Thomas J.S. Durant, Corey R. Dwyer, Ryan P. Russell, Jeffrey H. Weinreb, Farhang Alaee, Knut Beitzel, Mary Beth McCarthy, Mark P. Cote, and Augustus D. Mazzocca. The enthesis: A review of the tendon-to-bone insertion. *Muscles, Ligaments and Tendons Journal*, 4(3):333–342, 2014.

[34] M Benjamin and J R Ralphs. Entheses–the bony attachments of tendons and ligaments. *Italian journal of anatomy and embryology = Archivio italiano di anatomia ed embriologia*, 106(2 Suppl 1):151–7, 2001.

[35] M Benjamin, Kumai T., Milz S., Boszczyk B.M., Boszczyk A.A., and Ralphs J.R. The skeletal attachment of tendons - Tendon 'entheses'. *Comparative Biochemistry and Physiology - A Molecular and Integrative Physiology*, 133(4):931–945, 2002.

[36] Benjamin Charvet, Florence Ruggiero, and Dominique Le Guellec. The development of the myotendinous junction. A review. *Muscles, Ligaments and Tendons Journal*, 2(2):53–63, 2012.

[37] J. Kastelic, A. Galeski, and E. Baer. The Multicomposite Structure of Tendon. *Connective Tissue Research*, 6(1):11–23, jan 1978.

[38] James H.-C. Wang. Mechanobiology of tendon. *Journal of Biomechanics*, 39(9):1563–1582, 2006.

[39] G. P. Riley, R. L. Harrall, C. R. Constant, M. D. Chard, T. E. Cawston, and B. L. Hazleman. Glycosaminoglycans of human rotator cuff tendons: Changes with age and in chronic rotator cuff tendinitis. *Annals of the Rheumatic Diseases*, 53(6):367–376, 1994.

[40] Preethi L Chandran and Ferenc Horkay. Aggrecan, an unusual polyelectrolyte: review of solution behavior and physiological implications. *Acta biomaterialia*, 8(1):3–12, jan 2012.

[41] Sean P Giblin and Kim S Midwood. Tenascin-C: Form versus function. *Cell adhesion & migration*, 9(1-2):48–82, 2015.

[42] B Wojciak and J F Crossan. The accumulation of inflammatory cells in synovial sheath and epitenon during adhesion formation in healing rat flexor tendons. *Clinical and experimental immunology*, 93(1):108–14, jul 1993.

[43] Hazel R.C. Screen, David E. Berk, Karl E. Kadler, Francesco Ramirez, and Marian F. Young. Tendon functional extracellular matrix. *Journal of Orthopaedic Research*, 33(6):793–799, 2015.

[44] D.J.S. Hulmes. Chapter 2 Collagen Diversity, Synthesis and Assembly. In *Collagen*, pages 15–48. 2008.

[45] Mitsuo Yamauchi and Marnisa Sricholpech. Lysine post-translational modifications of collagen. *Essays in Biochemistry*, 52:113–133, may 2012.

[46] Barbara Brodsky and Anton V. Persikov. Molecular Structure of the Collagen Triple Helix. pages 301–339. 2005.

[47] M Tasab, M R Batten, and N J Bulleid. Hsp47: a molecular chaperone that interacts with and stabilizes correctly-folded procollagen. *The EMBO journal*, 19(10):2204–11, may 2000.

[48] Elizabeth G Canty, Yinhui Lu, Roger S Meadows, Michael K Shaw, David F Holmes, and Karl E Kadler. Coalignment of plasma membrane channels and protrusions (fibripositors) specifies the parallelism of tendon. *The Journal of cell biology*, 165(4):553–63, may 2004.

[49] Daisaburo Fujimoto, Kin-ya Akiba, and Nobuo Nakamura. Isolation and characterization of a fluorescent material in bovine achilles tendon collagen. *Biochemical and Biophysical Research Communications*, 76(4):1124–1129, jun 1977.

[50] Paraskevi Gkogkolou and Markus Böhm. Advanced glycation end products: Key players in skin aging? *Dermato-endocrinology*, 4(3):259–70, jul 2012.

Die approbierte gedruckte Originalversion dieser Diplomarbeit ist an der TU Wien Bibliothek verfügbar.
The approved original version of this thesis is available in print at TU Wien Bibliothek.
TU Bibliothek WIEN Your knowledge hub

[51] Manuel Guizar-Sicairos, Giulia Carimati, Alfonso Gautieri, Matteo Moretti, Herbert Schoenhuber, Alberto Redaelli, Jess G. Snedeker, Martin Berli, Piero Volpi, Unai Silván, and Fabian S. Passini. Advanced glycation end-products: Mechanics of aged collagen from molecule to tissue. *Matrix Biology*, 59:95–108, 2016.

[52] S R Thorpe and J W Baynes. Maillard reaction products in tissue proteins: new products and new perspectives. *Amino acids*, 25(3-4):275–81, dec 2003.

[53] David R Sell, Klaus M Biemel, Oliver Reihl, Markus O Lederer, Christopher M Strauch, and Vincent M Monnier. Glucosepane is a major protein cross-link of the senescent human extracellular matrix. Relationship with diabetes. *The Journal of biological chemistry*, 280(13):12310–5, apr 2005.

[54] T.T. Andreassen, K. Seyer-Hansen, and A.J. Bailey. Thermal stability, mechanical properties and reducible cross-links of rat tail tendon in experimental diabetes. *Biochimica et Biophysica Acta (BBA) - General Subjects*, 677(2):313–317, oct 1981.

[55] Nicole Verzijl, Jeroen DeGroot, Zaken Chaya Ben, Orit Brau-Benjamin, Alice Maroudas, Ruud A Bank, Joe Mizrahi, Casper G Schalkwijk, Suzanne R Thorpe, John W Baynes, Johannes W J Bijlsma, Floris P J G Lafeber, and Johan M TeKoppele. Crosslinking by advanced glycation end products increases the stiffness of the collagen network in human articular cartilage: a possible mechanism through which age is a risk factor for osteoarthritis. *Arthritis and rheumatism*, 46(1):114–23, jan 2002.

[56] G. Binnig and H. Rohrer. Scanning tunneling microscopy. *Surface Science*, 126(1-3):236–244, mar 1983.

[57] Kunio Takayanagi, Yasumasa Tanishiro, Shigeki Takahashi, and Masaetsu Takahashi. Structure analysis of Si(111)-7 x 7 reconstructed surface by transmission electron diffraction. *Surface Science*, 164(2-3):367–392, dec 1985.

[58] J. Freund, J. Halbritter, and J. K.H. Hörber. How dry are dried samples? Water adsorption measured by STM. *Microscopy Research and Technique*, 44(5):327–338, 1999.

[59] G Binnig, C.F. Quate, and Ch Gerber. Atomi Force Microscope (invention). *Physical Review Letters*, 56(9), 1986.

[60] N. H. Thomson, S. Kasas, Smith, H. G. Hansma, and P. K. Hansma. Reversible Binding of DNA to Mica for AFM Imaging. *Langmuir*, 12(24):5905–5908, jan 1996.

[61] Hayato Yamashita, Azuma Taoka, Takayuki Uchihashi, Tomoya Asano, Toshio Ando, and Yoshihiro Fukumori. Single-Molecule Imaging on Living Bacterial Cell Surface by High-Speed AFM. *Journal of Molecular Biology*, 422(2):300–309, sep 2012.

[62] Constant A.J. Putman, Kees O. Van Der Werf, Bart G. De Grooth, Niek F. Van Hulst, and Jan Greve. Tapping mode atomic force microscopy in liquid. *Applied Physics Letters*, 64(18):2454–2456, 1994.

[63] Franz J. Giessibl. Advances in atomic force microscopy. *Reviews of Modern Physics*, 75(3):949–983, 2003.

[64] Iam M. Torrens. *Interatomic Potentials*. Elsevier, 2012, 2012.

[65] H. Balamane, T. Halicioglu, and W. A. Tiller. Comparative study of silicon empirical interatomic potentials. *Physical Review B*, 46(4):2250–2279, jul 1992.

[66] Frank H. Stillinger and Thomas A. Weber. Computer simulation of local order in condensed phases of silicon. *Physical Review B*, 31(8):5262–5271, 1985.

[67] B Y Philip M Morse. DIATOMICMOLECULESACCORDINGTOTHEWAVEMECHANICS.II.VIBRATIONALLEVELS. 457(1927), 1989.

Die approbierte gedruckte Originalversion dieser Diplomarbeit ist an der TU Wien Bibliothek verfügbar.
The approved original version of this thesis is available in print at TU Wien Bibliothek.
TU Bibliothek Your knowledge hub WIEN

[68] R. L.C. Vink, G. T. Barkema, W. F. Van der Weg, and Normand Mousseau. Fitting the Stillinger-Weber potential to amorphous silicon. *Journal of Non-Crystalline Solids*, 282(2-3):248–255, 2001.

[69] E. Generalic. LennardJonesPotential.

[70] Gordon Baym. *Lectures On Quantum Mechanics*. Westview Press, New York.

[71] H. C. Hamaker. The London-van der Waals attraction between spherical particles. *Physica*, 4(10):1058–1072, 1937.

[72] M Braus. The theory of electrolytes. I. Freezing point depression and related phenomena (Translation). 2019.

[73] Huseyin Yilmaz, Kimiyasu Sato, and Koji Watari. AFM interaction study of α-alumina particle and c-sapphire surfaces at high-ionic-strength electrolyte solutions. *Journal of Colloid and Interface Science*, 307(1):116–123, mar 2007.

[74] R.M Pashley and J.N Israelachvili. Dlvo and hydration forces between mica surfaces in Mg2+, Ca2+, Sr2+, and Ba2+ chloride solutions. *Journal of Colloid and Interface Science*, 97(2):446–455, feb 1984.

[75] O. Wolter. Micromachined silicon sensors for scanning force microscopy. *Journal of Vacuum Science & Technology B: Microelectronics and Nanometer Structures*, 9(2):1353, mar 1991.

[76] R. B. Marcus, T. S. Ravi, T. Gmitter, K. Chin, D. Liu, W. J. Orvis, D. R. Ciarlo, C. E. Hunt, and J. Trujillo. Formation of silicon tips with <1 nm radius. *Applied Physics Letters*, 56(3):236–238, jan 1990.

[77] NanoWorld AG. Contact Mode spring constant.

[78] NanoWorld AG. AC Mode cantilever constants.

[79] Peter Eaton and Paul West. Atomic Force Microscopy. *Atomic Force Microscopy*, 9780199570:1–256, 2010.

[80] M. Tortonese, H. Yamada, R.C. Barrett, and C.F. Quate. Atomic force microscopy using a piezoresistive cantilever. In *TRANSDUCERS '91: 1991 International Conference on Solid-State Sensors and Actuators. Digest of Technical Papers*, pages 448–451. IEEE, 1999.

[81] S. C. Minne, S. R. Manalis, and C. F. Quate. Parallel atomic force microscopy using cantilevers with integrated piezoresistive sensors and integrated piezoelectric actuators. *Applied Physics Letters*, 67(1995):3918, 1995.

[82] R. Erlandsson, G. M. McClelland, C. M. Mate, and S. Chiang. Atomic force microscopy using optical interferometry. *Journal of Vacuum Science & Technology A: Vacuum, Surfaces, and Films*, 6(2):266–270, mar 1988.

[83] D. Rugar, H. J. Mamin, R. Erlandsson, J. E. Stern, and B. D. Terris. Force microscope using a fiber-optic displacement sensor. *Review of Scientific Instruments*, 59(11):2337–2340, 1988.

[84] C. Schönenberger and S. F. Alvarado. A differential interferometer for force microscopy. *Review of Scientific Instruments*, 60(10):3131–3134, 1989.

[85] D. Rugar, H. J. Mamin, and P. Guethner. Improved fiber-optic interferometer for atomic force microscopy. *Applied Physics Letters*, 55(25):2588–2590, 1989.

[86] Nanosurf. AFM Modes Overview, 2020.

[87] Gernot Friedbacher and Harald Fuchs. Classification of Scanning Probe Microscopies. *Pure and Applied Chemistry*, 71(7):1337–1357, jul 1999.

Die approbierte gedruckte Originalversion dieser Diplomarbeit ist an der TU Wien Bibliothek verfügbar.
The approved original version of this thesis is available in print at TU Wien Bibliothek.
TU Bibliothek Your knowledge hub WIEN

[88] S. Herminghaus, A. Fery, and D. Reim. Imaging of droplets of aqueous solutions by tapping-mode scanning force microscopy. *Ultramicroscopy*, 69(3):211–217, oct 1997.

[89] M. Rief. Single Molecule Force Spectroscopy on Polysaccharides by Atomic Force Microscopy. *Science*, 275(5304):1295–1297, feb 1997.

[90] M Carrion-Vazquez. Mechanical design of proteins studied by single-molecule force spectroscopy and protein engineering. *Progress in Biophysics and Molecular Biology*, 74(1-2):63–91, aug 2000.

[91] Lorena Redondo-Morata, Marina I. Giannotti, and Fausto Sanz. Influence of Cholesterol on the Phase Transition of Lipid Bilayers: A Temperature-Controlled Force Spectroscopy Study. *Langmuir*, 28(35):12851–12860, sep 2012.

[92] W.C. Oliver and G.M. Pharr. Measurement of hardness and elastic modulus by instrumented indentation: Advances in understanding and refinements to methodology. *Journal of Materials Research*, 19(1):3–20, 2004.

[93] Jack C Hay. A critical examination of the fundamental relations used in the analysis of nanoindentation data. 14(6), 2008.

[94] David J. Keller and Fransiska S. Franke. Envelope reconstruction of probe microscope images. *Surface Science*, 294(3):409–419, 1993.

[95] John E. Sader, James W.M. Chon, and Paul Mulvaney. Calibration of rectangular atomic force microscope cantilevers. *Review of Scientific Instruments*, 70(10):3967–3969, 1999.

[96] H. J. Butt and M. Jaschke. Calculation of thermal noise in atomic force microscopy. *Nanotechnology*, 6(1):1–7, 1995.

[97] JPK Instruments. JPK Instruments AG- NanoWizard3 User Manual. SPM Software Release 4.2. 2012.

[98] D. T. Kirkendall and W. E. Garrett. Function and biomechanics of tendons. *Scandinavian Journal of Medicine and Science in Sports*, 7(2):62–66, 1997.

[99] Zhi-Ye Qiu, Yun Cui, Chun-Sheng Tao, Zi-Qiang Zhang, Pei-Fu Tang, Ke-Ya Mao, Xiu-Mei Wang, and Fu-Zhai Cui. Mineralized Collagen: Rationale, Current Status, and Clinical Applications. *Materials (Basel, Switzerland)*, 8(8):4733–4750, jul 2015.

Die approbierte gedruckte Originalversion dieser Diplomarbeit ist an der TU Wien Bibliothek verfügbar.
The approved original version of this thesis is available in print at TU Wien Bibliothek.
TU Bibliothek Your knowledge hub WIEN